Framework to research and design wrinkle free very large flexible offshore solar platforms by adding permeability

Eline Lavaerts

TU Delft

Framework to research and design wrinkle free very large flexible offshore solar platforms by adding permeability

by

Eline Lavaerts

to obtain the degree of Master of Science
at the Delft University of Technology,
to be defended publicly on Monday December 14, 2020 at 14:00 AM.

Student number:	4482794	
Project duration:	April 15, 2020 – December 14, 2020	
Thesis committee:	Dr. C. L. Walters,	TU Delft 3mE, chair
	Dr. ir. J. H. den Besten,	TU Delft 3mE, supervisor
	ir. H. M. Verhelst,	TU Delft 3mE, supervisor
	Dr. ir. S. Schreier,	TU Delft 3mE
	Dr. M. Pavlovic,	TU Delft CEG

This thesis is confidential and cannot be made public until December 14, 2020.

TU Delft

Preface

This thesis on wrinkling reduction in very large flexible floating solar platforms by adding permeability has been written for the fulfilment of the Master of Science degree in Marine Technology at the Delft University of Technology.

During the past months, I not did only learn about the wrinkling phenomenon, but also about planning and carrying out research as well as reviewing the results critically. Acquiring these skills would never have been possible without my supervisors ir. H.M. Verhelst and Dr. ir. J.H. den Besten. Hugo, thank you for inspiring me to research this topic, to always be available to answer any questions, for your positivity and thank you for your endless ideas on further research and possibilities to improve my research. Henk, thank you for teaching me to look further than theories and formulas, but teaching me a deeper understanding of structural behaviour, not only during this thesis but also during the courses you taught me over the past two years. Furthermore, I want to thank Dr. C.L. Walters, Dr. ir. S. Schreier and Dr. M. Pavlovic for being part of my graduation committee.

Besides my graduation committee, I want to thank everyone who was part of my five year long journey studying at the TU Delft. Five years ago, when I moved to Delft, I could never have imagined the academical as well as personal development I have achieved over these years. I want to thank my friends at the university, Karin, Thijs, Esmée, Koen and Brian for always stimulating each other to study together and discuss maritime topics but also enjoy lunch breaks. Thank you to my roommates, Wassenaar, Sylke, Meyers and Maaike. During the lock-down of the past months we have spend more time together than ever before. During these months, your encouragement, interest and understanding has been of great support. Lastly I especially want to thank my family. My brother for showing me that you can learn anything if you have a true passion and motivation for it. From learning the first 150 digits of the number pi and solving a Rubik's cube in less than a minute, to professional and academic skills. Lastly a very special thank you to my parents, for always being there and supporting me and to learn and show me how to make dreams come true, without any limitations or borders.

Eline Lavaerts
Delft, December 2020

Abstract

Offshore solar power installations can be increased in size and efficiency compared to land based installations due to the availability of space and the cooling effect of water. To increase survivability in large waves, very large floating solar platforms can be made flexible. However, a flexible structure is susceptible to wrinkling due to combinations of mooring loads, wave dynamics and the flexibility of the platform. Wrinkling is a limit state which is not commonly researched in maritime engineering, since generally structures are designed to be as stiff as possible. Wrinkling can lead to the global collapse of a very large flexible solar platform and should therefore be minimised. Very large floating platforms have an impact on the environment due to the shadow underneath. This problem can be diminished by adding holes to the platform. Furthermore, holes can be functional as manholes for maintenance of the bottom of the platform. Scientific research on the wrinkling behaviour of membranes has pointed out that wrinkling behaviour depends on the geometry of the membrane, which can for example be changed by adding holes to the membrane. The aim of this thesis is to set up a design and analysis framework for wrinkled membranes with permeability. In order to define this framework, (i) reliable computational indicators are developed; (ii) the influence of permeability on membrane wrinkling is investigated and; (iii) the framework is verified on a fictive case of an integrated stiff solar panel on a membrane.

The first objective in this thesis is to find reliable computational indicators to assess the wrinkling behaviour of a membrane. Current concepts of offshore solar platforms are flexible membranes including mooring systems based on concentrated tension loads. To study the wrinkling behaviour of a (subregion) of such a flexible floating solar platform, in this study, it is modelled as a rectangular membrane subjected to uniaxial tension; following the available literature on the wrinkling problem. Numerical analysis of the wrinkling behaviour is first done by non-linear post-buckling calculations. However, it appeared that the results of this calculation are highly dependent on the initial deformation which is used. An alternative method which does not depend on user defined input was found in studying the second principal stress field: when negative second principal stress is present in the membrane, wrinkling *can* occur. When no negative second principal stress is present in the membrane, wrinkling will not occur. Furthermore, the distribution and the area of the negative second principal stresses are indicators for the wrinkle distribution and amplitude. For a robust assessment of the susceptibility of a membrane to wrinkling, a study of the negative second principal stress field should thus be preferred over a post-buckling analysis.

The second goal of this thesis is to research the influence of permeability on membrane wrinkling. The effect of holes on the wrinkling behaviour is researched by studying their influence on the second principal stress field. The aim is to find wrinkle free configurations and study the mechanisms which minimise wrinkling behaviour. Therefore, the size, location and shape of holes are varied systematically in membranes of different sizes. It was found that holes should be chosen so that when the membrane is strained, they deform in a way so that they bring tension in the regions of the membrane which are subjected to negative second principal stress in the non-permeable configuration. Furthermore, holes should be chosen such that the load paths in the membrane are not interrupted.

The framework to research and design wrinkle free very large flexible solar platforms by adding permeability is verified and has proven to be effective by applying it on the configuration consisting of a stiff solar panel mounted on a flexible membrane. In this configuration, the framework has led to holes by which the wrinkling region is localised.

From the three parts of this thesis, it is concluded that a research framework for wrinkling of membranes with permeability was found in the analysis of the second principal stresses and the driving mechanisms were investigated and verified. To further develop this framework, research on the effect of stiffening the membrane and minimising wrinkling under load conditions other than tension are recommended.

Contents

1 Introduction

1.1. Motivation

This thesis will investigate the influence of permeability on the wrinkling behaviour of offshore solar platforms. Therefore, it combines the following three key-concepts:

- Offshore solar platforms
- Permeability
- Wrinkling

This section will give a motivation to research the combination of these key-concepts.

Offshore solar platforms

The worldwide energy demand has risen over the past years and will keep rising according to predictions [13, 54]. Renewable energy generation should follow this trend. A promising renewable energy source is solar energy, due to its high energy potential. Two improvements can be made to increase the utilisation of this potential: increase of the scale of solar power plants and increase of the efficiency of solar panels.
Both an increase of the scale of solar energy production and an increase of efficiency of solar panels can be realised by moving them offshore. Apart from the large surface availability offshore compared to onshore, floating solar plants have the advantage to be located further away from obstacles which block the sunlight, like buildings and trees. Furthermore, it is proven that the efficiency of floating solar panels can be higher than the efficiency of land based solar panels due to the cooling effect of water. Depending on the weather conditions, the location of the panel on the platform and the type of flotation structure the efficiency can be improved by 10% [35, 57, 58]. The most recently developed offshore solar power plant concepts are designed to be flexible [46, 62]. The survivability of flexible structures in high waves is larger compared to the survivability of a stiff structure because the structure will follow the waves and slamming can be avoided.

Permeability in offshore solar platforms

In the past, it was identified that very large floating structures in general have an influence on the environment. From experiments as well as models, the following influences on the environment became apparent: [28, 29, 38]

- Influence of current (current direction and speed) on: sediment transport, coastal hydrology, tidal flow, drifts and beach erosion. [6, 63]
- Influence on water quality [63]
- Influence on organisms living on the bottom of the sea and influence on organisms which attach to the platform [63].
- Influence on the ecological system due to obstruction of radiation of the sun through the surface, therefore hindering the photosynthesis of organisms. This leads to a reduced oxygen level in the water, and influences the water temperature underneath the platform. Furthermore this will influence fish because finding food will become more difficult when eyesight is limited [26, 43, 63]

The consequence of the obstruction of radiation of sun through the sea surface can be reduced by making holes in the platform, by adding permeability.

Wrinkling in offshore solar platforms as a consequence of flexibility

To survive in waves, offshore solar power plants are designed to be as flexible as possible. By making such structures flexible, water on deck and slamming loads will be minimised [51]. Making structures as flexible as possible is the exact opposite of what is generally done in maritime structures like ships and offshore structures. These are made as stiff as possible. Flexible structures are susceptible to wrinkling, a limit state which is not commonly researched in maritime engineering. Therefore, not all design principles which are generally applied in maritime engineering are applicable when designing a flexible offshore solar platform.

Figures 1.1a and 1.1b show two pictures of accidents with floating solar power plants. Left, a picture of a floating solar plant located in Friesland, the Netherlands is shown. In August of 2020, this platform was blown away during a storm. The platform was still under construction and only moored by a provisionally mooring system. [45] In the right picture, a floating solar power plant which caught fire during a typhoon in Japan is shown. [14] From these pictures it can be seen that the collapse of a platform can lead to a lot of damage. Therefore, research on all limit states of platforms is a necessity.

(a) (b)

Figure 1.1: Pictures of two damaged solar platforms. (a) A platform which was blown away during a storm in the Netherlands [45] and (b) a platform which caught fire after a storm in Japan, near the coastal city of Chiba [14].

Influence of permeability on the wrinkling behaviour of membranes

A multitude of papers on wrinkling of membranes exists. Figure 1.2 shows the results of one of them, written by Luo [37]. Both experimental and numerical results are shown. At the left, wrinkles in a non-permeable membrane can be seen. A rectangular membrane is clamped at two opposite sides and strained. Wrinkles can be observed in the middle of the membrane. The pictures in the middle show membranes with holes which are strained the same way. From these figures, it can be seen that these permeable membranes do not wrinkle. However, at the right, a membrane is shown in which holes are added at the free edges of the membrane, this membrane does wrinkle when it is strained. Not all holes will help to minimise wrinkling behaviour in membranes. The size, shape and location of holes have to be chosen correctly to obtain this result.

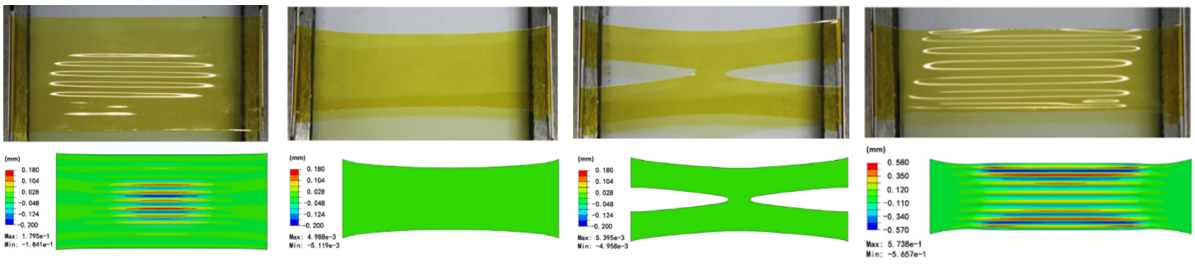

Figure 1.2: Experimental and numerical results on the wrinkling behaviour of membranes. All membranes are clamped at two sides and strained. The left membrane is non-permeable. Wrinkles can be observed when it is strained. In the middle, two permeable membranes can be seen which do not wrinkle when strained. Permeability is also added to the membrane at the right, at the free edges. However, this membrane still wrinkles when it is strained. [37] These observations lead to the conclusion that wrinkling of membranes can be avoided by adding permeability if the size, shape and location of the holes are chosen correctly.

1.2. Research goal

In literature, an example was presented which proves that wrinkles can be eliminated in a thin membrane by adding holes to it. This research has inspired the investigation of wrinkling reduction in very large flexible offshore solar platforms by adding permeability. However, in literature, only results are given for one specific design and no explanation on the underlying mechanism is discussed. Furthermore, wrinkling was not previously researched in the application of very large flexible offshore solar platforms. The goal of this thesis is to investigate the influence of permeability on the wrinkling behaviour of very large floating flexible solar platforms and to develop a design and analysis methodology to minimise the wrinkling behaviour. Therefore, this thesis will first focus on the method and investigate a method to research wrinkling behaviour in the application. Next, this method will be applied, to study the effect of permeability on wrinkling behaviour in very large flexible offshore solar platforms and understand the underlying mechanisms such that wrinkling can be prevented for by adding holes to the structure.

Literature exists on both offshore solar platforms as well as on wrinkling. However, these two concepts have never been combined. Previous research on wrinkling is of theoretical nature while research on offshore solar platforms is of rather industrial nature. The first challenge will be to model the industrial offshore solar platforms so that the theoretical knowledge on wrinkling of membranes can be applied to this application.

How can wrinkling be modelled keeping in mind flexible solar platforms as the application?

From literature on wrinkling of thin membranes, it appears that all methods can be classified into two categories: methods by which all details on the wrinkling behaviour are calculated (post-buckling calculations) and methods which only give approximations on the wrinkling behaviour. All methods will be researched and it will be investigated whether they are practically applicable when designing a very large flexible offshore solar platform:

What calculation method can be used to account for wrinkling behaviour in the design of very large flexible floating structures?
Is a post-buckling calculation adequate to research wrinkling behaviour of very large flexible offshore solar platforms?
By which indicators can the wrinkling behaviour of a membrane be approximated?

To be adequate for the application, the method should comply several criteria: it has to be applicable to a wide range of geometries to calculate whether or not wrinkling will occur and to discuss details on the wrinkling behaviour such as the wrinkling amplitude and the region of the structure in which wrinkling will happen. Furthermore, the method should not be computationally expensive so that it can be used to investigate different geometries fast and efficiently. Next to the investigation of post-buckling calculations, it will be investigated whether other methods exist to research wrinkling behaviour and whether these methods comply these criteria.
When a method to investigate the wrinkling behaviour is found, it will be applied to search for the influence of permeability on this behaviour with the goal to prevent for wrinkling.

How should holes be chosen such that wrinkling behaviour can be minimised?
In a membrane?
In a very large flexible floating solar platform?

1.3. Thesis outline

This thesis will be outlined in line with the research questions and sub-questions. First, all relevant literature will be discussed in chapter 2. Next every chapter will discuss a sub-question. Chapter 3 will discuss the use of a post-buckling calculation to study wrinkling behaviour of a membrane. In chapter 4, other indicators by which the wrinkling behaviour of a membrane can be approximated will be discussed. These indicators will be used to study the effect of permeability on the wrinkling behaviour in chapter 5. Practical implications of the results from chapter 5 will be discussed in chapter 6. Lastly, the main conclusions of this thesis will be summarised in chapter 7 and recommendations for further research are discussed in chapter 8.

2

Literature Review

This chapter will give an overview of all relevant literature to research wrinkling reduction in very large flexible offshore solar platforms. On the one hand, technical aspects of existing floating solar platforms will be researched. On the other hand an overview will be given of more theoretical literature which discusses wrinkling in membranes. The goal of this chapter is to conclude the current state-of-the art and relate the practical side of the research to the theoretical side:
How can wrinkling be modelled keeping in mind flexible solar platforms as the application?

Furthermore this chapter will make a start in answering the other two main research questions described in section 1.2. Calculation methods which are used to determine the wrinkling behaviour of a membrane will be discussed as well as what is known on the influence of the geometry of the membrane on the wrinkling behaviour.

2.1. Technical aspects of offshore solar platforms

This section will discuss technical aspects of offshore solar power plants and their development by the help of examples of existing solar power plants and concepts.

Figure 2.1: Picture of the first floating solar power plant, located in Aichi, Japan [42]

Aichi, Japan
The solar power plant which is considered as the first floating offshore solar power plant is the PV installation in Aichi Japan [66] which was build in 2007. This first floating photovoltaic installation was build by the National Institute of Advanced Industrial Science & Technology of Japan for research purposes. The capacity of this installation amounts 20 kW. The solar panels on this platform are positioned horizontally on interconnected floats which form a raft. [17]. A picture of this installation is shown in figure 2.1.

Floating Solar BV, the Netherlands
An offshore floating solar installation developed and build by Floating Solar BV is shown in figure 2.2. This floating solar power plant consists of interconnected frames which are kept afloat by cylindrical buoyancy tubes. The different frames are connected by hinges so that the platform can move more freely in waves. The platform is moored by a connection to three buoys. It is located on an inland water body in Rotterdam and has a commercial purpose. The platform is steered by a vertical-axis tracking system, a combination of winches and cables rotates the platform such that it is always oriented to the sun. [15, 17]

Figure 2.2: Picture of the floating solar installation from Floating solar BV [15]

Ocean Sun, Norway
Since 2017, Ocean Sun produces offshore power plants for commercial purposes. Their design, which is shown in figure 2.3, is inspired by the construction of fish cages. Its flotation system consists of a circular flotation tube. A thin, flexible membrane is tensioned between the tubes on which stiff solar panels are mounted. The membrane rests directly on the water surface. The cooling effect of the water has a positive influence on the efficiency of the solar panels. The membrane is flexible, and therefore moves with waves. The concept of Ocean Sun is therefore not only suited for inland water bodies, but can also be installed nearshore. Ocean Sun has produced two sizes of offshore solar platforms: a platform with a capacity of 200 kW which has a diameter of 50 meters and a platform with a capacity of 500 kW which has a diameter of 72 meters. A disadvantage of the system is that a pump is needed to pump out green water. [17, 46]

Figure 2.3: Pictures and sketch of the offshore solar power plant designed by Ocean Sun [46]

SUNdy, DNV GL concept

Figure 2.4 shows a concept proposed by DNV GL in 2012. This proposed solar power plant consists of a combination of thin film flexible floating solar panels mounted on flexible floating mattresses. The mattresses float directly on the water. Therefore the cooling effect of the sea water will lead to an improvement of the efficiency of the solar panels. Modules of flexible solar panels are combined in one hexagonal structure. Such a solar island would have a capacity of 2 MW. The conceptual island is moored by mooring cables to the seabed. All connections are based on tensional forces, the connection of the mattresses to the frame which connects all modules as well as the connection of the island to the seabed. This mooring system is usable in water depths from 20 up to 100 metres. Due to the flexibility of the thin film solar panels, the concept is resilient to waves and can thus be installed in offshore waters. [58, 66]

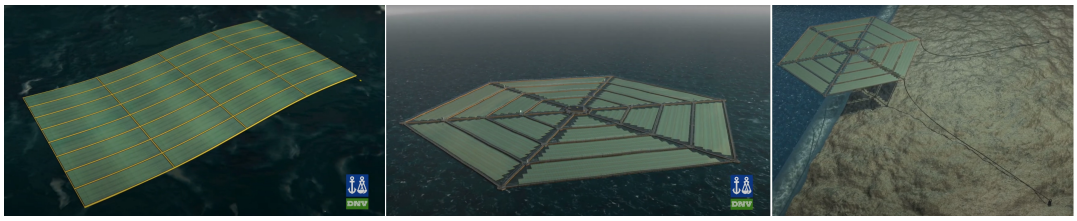

Figure 2.4: Sketches of the concept of a flexible floating solar power plant designed by DNV GL [62]

Oceans of Energy, North Sea

The first offshore solar plant in open water was realised in the North Sea. In 2019 the first solar power plant was installed with a capacity of 8.5 kW with the goal to research whether it would survive in rough sea conditions. Since than the capacity is already increased up to 17 kW. The aim is to further enlarge the platform to a capacity of 50 kW. The platform is constructed by a pontoon on which solar panels are mounted horizontally. In 2020, the platform survived in different storms, winds of 120 km/h and 5 meters high waves. The platform remained stable at all times and the mooring system and floaters remained intact. [47, 48]

Figure 2.5: Impression of the offshore solar energy installation developed by Oceans of Energy and installed at the North Sea [47, 48]

As a summary, the following technical developments of offshore solar platforms could be seen from the previously discussed examples:

- Location
    1. Inshore
    2. Nearshore
    3. Offshore
- Structure [17, 24]
    1. Interconnected floats to form rafts
    2. Interconnecting frames between buoyancy tanks or tubes
    3. Flexible membrane between flotation tubes
    4. Flexible thin film solar panels on a flexible floating mattresses
- Mooring system
    1. Mooring to buoys
    2. Mooring directly to the seabed
- Purpose
    1. Research
    2. Commercial
- Orientation [23]
    1. Fixed tilt
    2. Vertical axis tracking system
    3. Horizontal axis system

A general trend which can be seen is the use of "off-the-shelf" technology in the first concepts: simple pontoons with solar panels. Later developments of onshore solar installations are translated to offshore solar platforms (e.g. tilting the membrane towards the sun). The most recent concepts involve technology development specially for the application of offshore solar power plants (e.g. flexible solar panels on flexible floating mattresses in the SUNdy concept).

2.2. Wrinkling of membranes

An overview of literature on wrinkling behaviour of membranes will be given in this section. The first subsection will discuss which loads can lead to wrinkling of a membrane. Secondly, calculation methods to study wrinkling behaviour will be discussed. The final goal of this thesis is to research the influence of permeability on the wrinkling behaviour of membranes. Therefore this section will give necessary background information and focus on the influence of the intact geometry on wrinkles. Subsections 2.2.3 and 2.2.4 will give an overview of the influence of the intact geometry on the wrinkle onset and on wrinkle details respectively. The section will be concluded by reviewing literature on wrinkling of membranes with different topology, so including holes.

2.2.1. The wrinkling phenomenon

Wrinkling can be considered as a special form of buckling. Buckling can occur when a structure is subjected to compression. Wrinkling can happen as a consequence of different load conditions. When a structure is subjected to tension, shear or torsion on a global scale, compressive stresses can occur locally. These compressive stresses can lead to local buckling: *wrinkling*. This subsection will discuss wrinkling as a consequence of different loading conditions. All these global loading conditions have in common that they can lead to compressive stresses locally. These local compressive stresses are the cause of the occurrence of wrinkles.

Wrinkling under global torsion load

A common configuration which is used to study wrinkling as a consequence of torsion load is shown in figure 2.6. From the very beginning of wrinkling research, the wrinkling of a circular membrane wrinkled due to torsion load on the centre has been of interest. Already in one of the first papers on tension field theory [27], this configuration is described. Solving wrinkling analytically has only been successful for several boundary conditions. Kondo recognised the circular membrane loaded by torsion as one of these configurations which is suitable for an analytical solution [27]. Furthermore, experiments were performed which were in very good agreement with the results of the analytical calculations. [40] The circular membrane was used as a benchmark study during the development of finite element models for wrinkling in 1991 by Roddeman [56]. In the years following on that study the circular membrane was used for comparing tension field theory and bifurcation theory by Miyamura, Iwasa and Coman. [7–9, 20, 41] The results of the finite element calculations performed by Iwasa can be seen in figure 2.6, together with a schematic of a circular membrane loaded by torsion load. More experiments were performed by Miyamar and Wang. [41, 70]

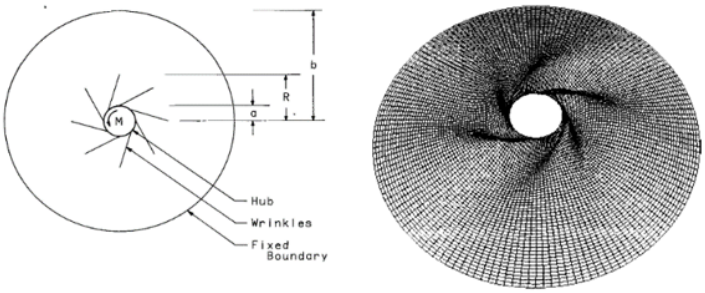

Figure 2.6: Schematic diagram of a circular membrane wrinkled by the rotation of the inner boundary (left) [40], and bird view of the wrinkled membrane calculated by finite element analysis. The membrane has an outer radius of 300 mm and an inner radius of 50 mm and is subjected to a rotation angle of 1.145° (right). [20]

Wrinkling under global shear load

The configuration which is used to investigate wrinkling under shear load is shown in figure 2.7. The configuration first appears in the research of Mansfield in 1969. [39] Mansfield derives an analytical formulation for the angle under which wrinkles appear in a sheared membrane, based on tension field theory. He compares his results with an experimental test. Jenkins takes the research of Mansfield a step further by applying non-contact measurements to be able to not only determine the angle of the wrinkles but also their amplitude from experiments. [22] The configuration of the sheared membranes returns in two papers of Wong and Pellegrino in 2002. They described the results of a finite element analysis. This analysis gives insight in the stress distribution in the sheared membrane. This insight is then used to derive a simple analytical solution of the problem which is compared with an experiment. [76, 77] The combination of experiments, analytical calculations and finite element calculations is again described by Wong and Pellegrino in a series of three papers on the wrinkling of sheared membranes in 2006. [72–74] An impression of the results of Wong and Pellegrino is given in figure 2.7, together with an illustration of the configuration.

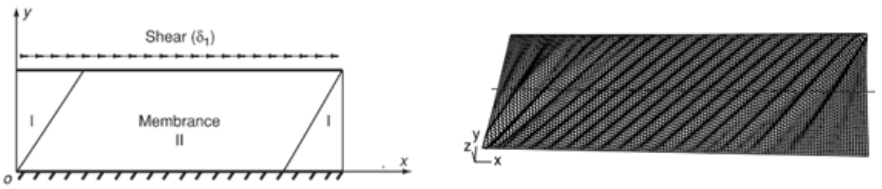

Figure 2.7: Schematic diagram of a rectangular membrane subjected to shear load (left) [80], and perspective view of the wrinkle pattern of a rectangular membrane with in plane dimensions of 380 mm and 128 mm, under a shear displacement of 3 mm, calculated by finite element analysis (right). [74]

Wrinkling under global tension load
Wrinkling as a consequence of global tension load is studied by two different configurations: square membranes loaded by tension in the four corners (figure 2.8) and rectangular membranes loaded by uniaxial tension (figure 2.9).

From 2000 until 2003, multiple papers are dedicated to the configuration of square membranes loaded by loads in the four corners. Both situations in which these four loads are equal, as well as situations in which only diagonally opposite pairs of the loads are equal were researched. This configuration is particularly of interest in the research field of space engineering. Solar sails, telescopes, radars and sunshields all experience corner loads. The tension field theory was used multiple times to determine the wrinkling regions in square membranes subjected to corner loads. [1, 3, 12, 75].
Also experiments, analytical methods and finite element calculations are performed during these years [72–74].

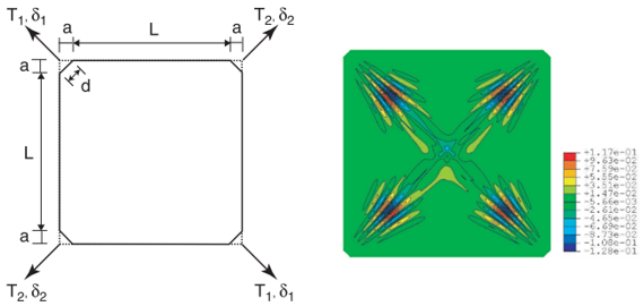

Figure 2.8: Schematic of a square membrane subject to corner loads (left), and contours of the out-of plane displacements ([mm]) for $T_1 = T_2 = 5N$ of a membrane with a length and width of 500 mm, calculated numerically. [73, 74]

A diagram and a contour plot of the wrinkle pattern of a rectangular membrane subjected to uniaxial strain are given in figure 2.9. Although this configuration already first appeared in the older papers, the uniaxially stretched membrane is still researched very often in recent literature. In 2000, Friedl discussed wrinkling in uniaxially stretched plates. [16]
Cerda explains wrinkling of elastic sheets under tension analytically from an energy point of view. He presents a method to obtain the wavelength and the amplitude of wrinkles by minimising the total energy, which is the sum of the bending energy and energy due to stretching. [4, 5]
In recent years, the stretching of thin films has become a benchmark study for development of finite element codes on wrinkling. [19, 53, 59, 60, 71] The wrinkle profile of a rectangular membrane subjected to uniaxial strain has also been studied by the use of commercial codes like ABAQUS. [44]. Furthermore in 2016, Sipos has performed tests on the uniaxial tension of thin films to verify numerical results.
Due to the fact that this configuration is frequently used as a benchmark, a lot of literature exists on this specific configuration and therefore the rest of this chapter will continue with the focus on rectangular membranes subjected to uniaxial tension.

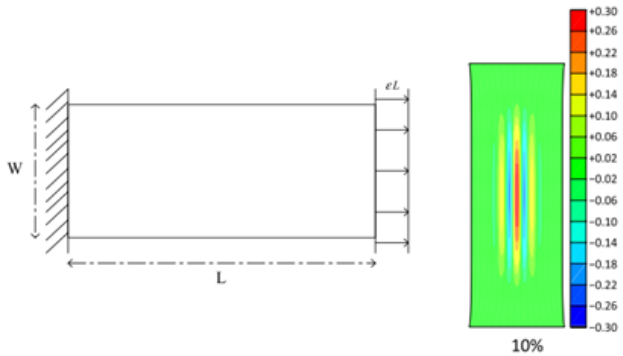

Figure 2.9: Schematic of a rectangular membrane subjected to uniaxial stretch (left) [19] and out-of-plane displacement ([mm]) of a rectangular membrane with dimensions 254 mm x 101.6 mm for a stretch of 10%. [81]

2.2.2. Calculation methods

As discussed in the previous section, wrinkling is discussed in literature as the consequence of three different loads: torsion, shear and tension. In the last 20 years, most focus went to one particular configuration: the rectangular membrane subjected to uniaxial strain. Since the year 2000, this configuration is researched in more detail to investigate the effect on wrinkling when the shape of the membrane is systematically varied. The first paper which initiated research on the influence of shape on wrinkling behaviour was written by Friedl [16]. Inspired by the fact that the critical buckling stress of plates under compression can be calculated by the use of critical buckling coefficients from diagrams, he developed a similar critical buckling diagram for plates under tension. More research on the topic followed by analytical, experimental and numerical analyses:

- **Analytical:** By minimisation of energy, Cerda [4, 5] proposed formulas for the critical buckling strain, wrinkle amplitude and wavelength of rectangular membranes under uniaxial stretch. This work was continued by Puntel [53]. Jacques and Portier-Ferry [21] compared analytical results with numerical analysis.
- **Experiments:** In 2009 Zheng [81] performed several experiments on rectangular, stretched membranes which are later frequently used as validation for numerical results. Later more experiments were performed by Panaitescu and Sipos [50, 60].
- **Numerical:** The advantage of investigating the problem numerically is the fact that the stress distribution can easily be obtained as well. Nayyar was the first to explain the influence of shape on wrinkling by looking at the stress distributions. [44] Other numerical studies on the influence of shape on wrinkling behaviour are the works of Healey [19] and Li & Haeley [33] who investigated the influence of different material models on the result. The most recent works on this topic are written by Wang [71], Panaitescu [50], Khalil [25] and Fu [18].

In general, all calculation methods to study wrinkling behaviour of membranes can be divided into two categories: wrinkling calculations by which all details of the wrinkling behaviour can be calculated (non-linear wrinkling calculations) and methods which do not provide all details but only give indications on the wrinkling region.

By the use of post-buckling calculations, the wave amplitude and wavelength of the wrinkles can be calculated. By applying non-linear wrinkling calculations, it is thus possible to calculate all details about the wrinkling pattern, but this comes at a price. The computational cost for these calculations is high. In literature, several papers can be found in which bifurcation theory is applied by the use of commercial finite element codes [20, 30, 64, 65, 74]. The membrane is modelled with shell elements. First buckling modes are searched and next, these are used as the initial imperfection for the wrinkling calculation in which the imperfect membrane is loaded in different load steps, load based or displacement based. Analytical applications of bifurcation theory are rather rare. It is only possible to find closed form analytical solutions for several specific configurations. [21, 53, 61, 73]

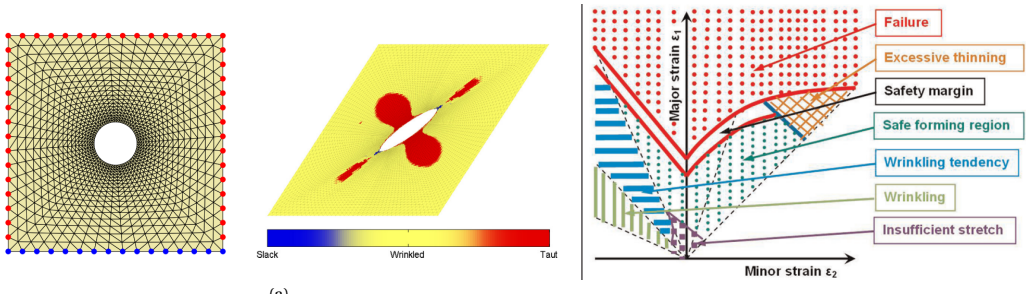

(a) (b)

Figure 2.10: (a) Illustration of results obtained using the tension field theory, calculated by de Rooij. [10] The left figure illustrates the undeformed geometry: a square membrane with a hole in the middle of the membrane. The membrane has a length and width of $L = W = 100mm$. The circular hole has a diameter of $D = 20mm$. The membrane is loaded by a shear load to a shear angle of $\gamma = 1/\sqrt{3} \approx 65°$. By the use of tension field theory, slack, taut and wrinkled regions can be distinguished in the membrane. The results of these calculations are shown at the right. (b) Schematic representation of the *forming limit diagram*. A diagram which indicates whether a metal can undergo a certain deformation without failure. [**?**]

Multiple estimation methods have been called 'tension field theory, however differences exist between these different methods [1, 7, 10, 27, 36, 39, 67–69]. In general, all of these methods are based on the assumption that the membrane has no bending stiffness and that compressive stresses are eliminated in membranes by forming wrinkles. All of these methods estimate the wrinkling region in a membrane by the principal stress or principal strains in the membrane. Three sets of such wrinkling criteria presented by Adler [1] are presented below. Also an example of results obtained by tension field are shown in figure 2.10a. Similar criteria to the wrinkling criteria can also be seen in other research fields. Figure 2.10b gives a schematic representation of the *forming limit diagram*. This diagram is used to evaluate whether a metal can be deformed without failure. Also wrinkling is indicated in this diagram as a failure mode.

$$\begin{cases} \sigma_2 > 0 & & \Rightarrow \text{Taut} \\ \sigma_1 \leq 0 & & \Rightarrow \text{Slack} \\ \sigma_1 > 0 & \sigma_2 \leq 0 & \Rightarrow \text{Wrinkled} \end{cases} \qquad \begin{cases} \varepsilon_1 > 0 & \varepsilon_2 > -\nu\varepsilon_1 & \Rightarrow \text{Taut} \\ \varepsilon_1 \leq 0 & & \Rightarrow \text{Slack} \\ \varepsilon_1 > 0 & \varepsilon_2 \leq -\nu\varepsilon_1 & \Rightarrow \text{Wrinkled} \end{cases} \qquad \begin{cases} \sigma_1 > 0 & \sigma_2 > 0 & \Rightarrow \text{Taut} \\ \sigma_1 \leq 0 & \sigma_2 \leq 0 & \Rightarrow \text{Slack} \\ \sigma_1 > 0 & \sigma_2 \leq 0 & \Rightarrow \text{Wrinkled} \end{cases}$$

with:

σ_1	The first principal stress
σ_2	The second principal stress
ε_1	The first principal strain
ε_2	The second principal strain
ν	The Poisson ratio

Next to tension field theory, also other suggestions are made in literature to make estimations on wrinkle details without having to perform a non-linear wrinkling calculation. [16, 34, 44, 71] Different suggestions are made, but the suggestions are not proven. Suggestions are made on what can be learned from the presence, the distribution, the magnitude and the orientation of compressive stresses. All suggestions are summarised in the following list:

What can we learn from...?

- **The presence of compressive stresses**
  - If there are no compressive stresses in the membrane, the membrane will not wrinkle. [16, 34, 44, 71]
  - If there are compressive stresses in the membrane, the membrane will possible wrinkle. Three reasons are mentioned which prevent the membrane from wrinkling even though there are negative compressive stresses present:
    → Clamped edges have a stabilising effect in their proximity. For membranes with small aspect ratios their influence is close enough to the compressive zone to prevent for wrinkling. [16]
    → The magnitude of the compressive stress must be large enough to cause wrinkling. [44]
    → The area of the compressive stress must be large enough to cause wrinkling. [44]

- **The distribution of compressive stresses**
  - The distribution of compressive stresses has a similar pattern as the distribution of wrinkles. [16, 34, 44, 71]
  - Buckling modes show their largest displacements in the regions with compressive stress. [16]
  - If the distribution of the compressive stresses is separated in two zones:
    → Two peaks in the stress pattern have to be sufficiently separated to result in two separated wrinkling packages.
    → When two peaks are not separated sufficiently, one wrinkling area can arise, or two wrinkling peaks which are still connected by smaller wrinkles in between. [16, 44]
  - From the aspect ratio of the region in which compressive stresses exist in the membrane, the number of wrinkles in the width direction can be estimated. [44]

- **The magnitude of compressive stresses**
  - Wrinkles restabilize at the critical strain. This is the strain for which the magnitude of the compressive stress is maximal. [71]
  - The critical strain from which the wrinkles originate and restabilise can be analytically estimated from the magnitude of the compressive stresses if the aspect ratio of the compressive region in the membrane is known. [44]
  - From the magnitude of the compressive stresses in the membrane as a function of the strain, the range of strains where wrinkling will occur can be calculated. [44]

- **The orientation of compressive stresses**
  - In anisotropic membranes, the orientation of wrinkles depends on the angle between the material orthotropy and the straining direction. [34]

2.2.3. Influence of shape on the wrinkle onset

This subsection will focus on wrinkle onset. The focus is on factors which influence whether or not wrinkles will form or not. From literature, it is apparent that wrinkling onset is influenced by the in-plane aspect ratio $\frac{L}{W} = \alpha$. Furthermore the thickness aspect ratio, $\frac{W}{t} = \beta$ (in which t indicates the thickness of the sheet) influences the wrinkling onset as well.

In-plane aspect ratio α

Critical buckling strain: lower boundary

In 2000, Friedl [16] presented a diagram of critical buckling coefficients as a function of the aspect ratio of the membrane. This diagram was set up by numerical buckling analysis performed in ABAQUS. This diagram is presented in figure 2.11a. From this diagram the critical buckling coefficient for every aspect ratio α can be determined. From that critical buckling coefficient, the critical tensile buckling stress can be determined by formula 2.1. The diagram is valid for materials with linear-elastic, isotropic behaviour with a Poisson ratio of 0.3.

$$\sigma_{crit} = k_c * E * (\frac{t}{W})^2 \tag{2.1}$$

σ_{crit}	is the critical buckling stress
k_c	is the critical buckling coëfficient
E	is the Young's modulus
t	is the thickness of the membrane
W	is the width of the membrane

From his diagram Friedl concludes that there are two driving factors influencing the graph: the compressive stresses as a result of the Poisson and the stabilising effect of the boundaries. He divides the diagram in three regions:

- $1.5 \leq \alpha < 2.1$
  The highest lateral compression can be found for an aspect ratio of 1.7. In this region, the effect of compressive stress on wrinkling can be seen at the left side of the interval. The stabilising effect of the boundaries can be seen at the right side of the interval.
- $2.1 \leq \alpha < 4.5$
  Both stabilising effects influence the sheet, this leads to an increase in the critical buckling factor.
- $4.5 \leq \alpha$
  The stabilising effect of the boundaries remains constant and the compressive stresses in the lateral direction become independent of the length, thus leading to convergence of the critical buckling factor to a constant value.

Zheng [81] dedicated a whole PhD thesis to the influence of geometrical parameters on wrinkling of thin membranes. He did both experimental tests and numerical calculations. Experimentally he investigated wrinkling of 27 samples with a thickness of 0.1 mm, widths between 30 mm and 100 mm, lengths between 25 and 250 mm and a Poisson ratio of 0.5. The numerically tested membranes have the same thickness and

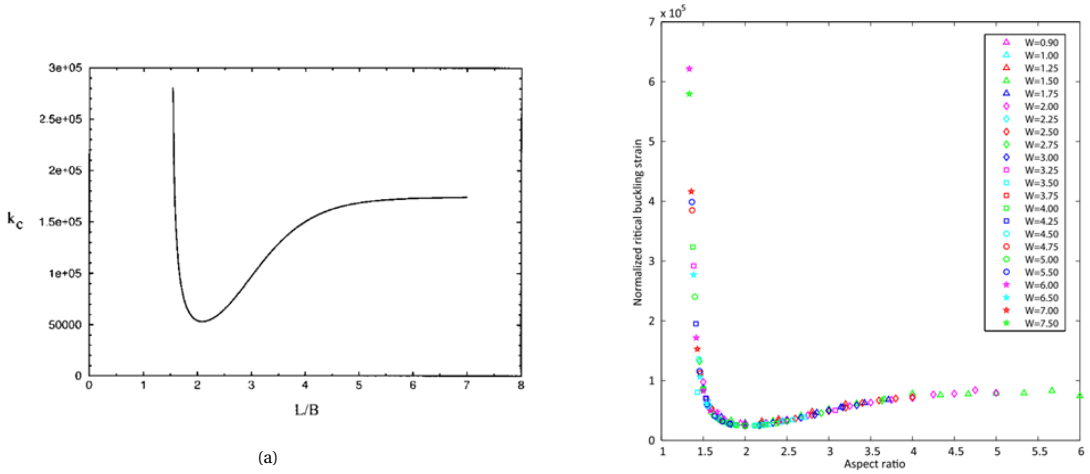

(a) (b)

Figure 2.11: (a) critical buckling coefficient as a function of the aspect ratio for a linear-elastic, isotropic material with a Poisson ratio of 0.3 [16] (b) Critical buckling strain, normalised by (β^{-2}) as a function of the aspect ratio. Determined by numerically determining the critical buckling strain of 144 membranes of different sizes with a Poisson ratio of 0.5 and a thickness of 0.1 mm. [81]

Poisson ratio. The lengths of these digital membranes range between 44.45 and 254 mm and have widths between 22.86 mm and 190.5 mm.
All experimental membranes were stretched until a strain of 100%. The result of these tests are summarised in figure 2.12a. In this graph, all tests are plotted in a length(width) axis system, in which the diagonals thus represent constant aspect ratios. The tests are indicated by a red cross to indicate that no wrinkling occurred during the test. Or by a green dot to indicate that wrinkling did occur during the test. The results of the 144 numerical tests are shown in a similar graph in figure 2.12b. In this length(width) graph, each black dot represents a tested membrane. For these membranes, the critical buckling strain is determined. These results are extrapolated to the contour plot as shown. From both the experimental and numerical tests, Zheng observes the following three conclusions:

- Membranes are more likely to wrinkle at intermediate aspect ratios ($1.5 \leq \alpha \leq 4$) than to wrinkle at extreme aspect ratios ($\alpha < 1.5$ and $\alpha > 4$).
- From a set of membranes which all have the same surface area, but different aspect ratio, the membrane with an aspect ratio equal to 2 will be the most susceptible to buckling.
- At fixed aspect ratio, membranes with larger sizes exhibit lower stability then those with smaller sizes.

Zheng also plots his 144 numerical results in a plot illustrating the critical buckling strain, normalised by $(\frac{t}{W})^2$ as a function of the aspect ratio. Zhengs plot is shown in figure 2.11b and shows the same trend as Friedls graph showing the critical buckling coefficient as a function of the aspect ratio.

Critical buckling strain: upper boundary
The results of Friedl and Zheng only included a lower boundary for the critical buckling stress and strain. A boundary which indicates that wrinkles will develop when it is exceeded. Zheng also mentions that there is an upper bound which marks the wrinkling region. In depth calculations on this upper bound are performed first by Nayyar [44] and results similar to those of Nayyar can also be found in the paper of Li and Haeley which was published in 2016. [33]
The critical wrinkling region in the strain - aspect ratio plane, calculated by Nayyar [44], is shown in figure 2.13a for two different thicknesses. This graph is obtained from numerical simulations of hyperelastic sheets. For low values of the aspect ratio α, a zone is indicated in which no compressive stresses can appear in the membrane, and thus no wrinkling will occur. This zone is in agreement with the conclusion of Zheng, who stated that no wrinkling occurs in membranes with an aspect ratio lower than 1.5.
Li and Haeley [33] use the strain - aspect ratio diagram to explain the difference between different material models. For membranes with a thickness of 0.01, they calculate the stability boundaries with four different models: neo-Hookean, Mooney-Rivlin, Saint Venant-Kirchoff and Föppl-von Kármán. The resulting graph of stability boundaries can be seen in figure 2.13b. For the neo-Hookean model, Mooney-Rivlin model and

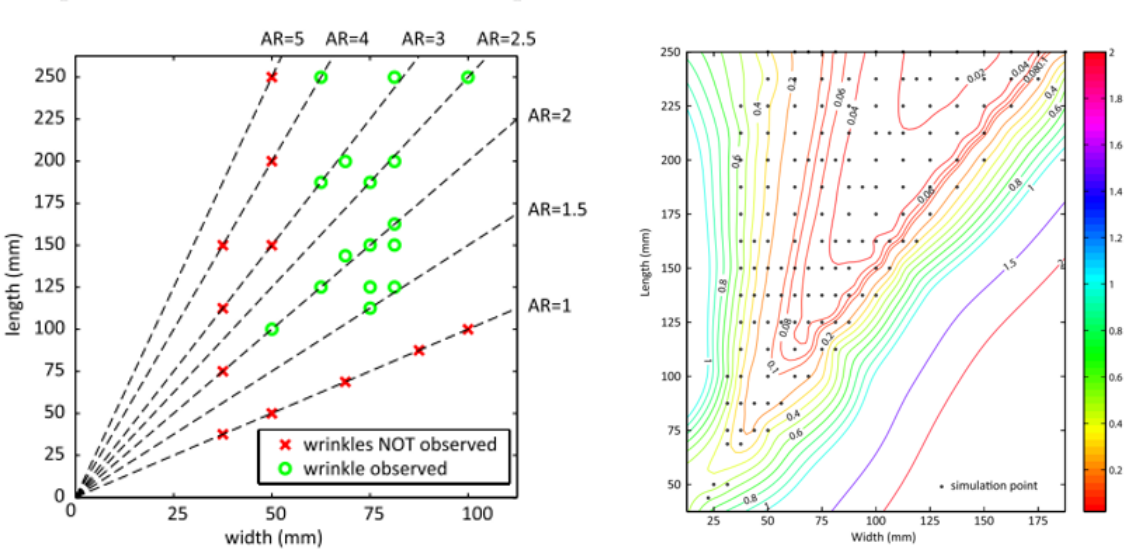

(a) (b)

Figure 2.12: (a) Results of the 27 experiments performed by Zheng [81]. 27 Membranes were stretched until a strain of 100%. Membranes which showed wrinkles during the experiment are indicated in the length(width) plane by a green circle. Membranes which did not show any wrinkles during the experiment are indicated with a red cross. All membranes have a thickness of 0.1 mm and a Poisson ratio of 0.5. [81] (b) Contour plot of the critical buckling strain as a function of the width and length of the membranes. Results obtained by the extrapolation of the results of calculations on 144 digital membranes of different in-plane sizes (indicated by the black dots), a thickness of 0.1 mm and a Poisson ratio of 0.5. [81]

Saint Venant-Kirchoff model, closed curves are found. Inside these closed curves wrinkling will occur. Outside these curves the membrane remains wrinkle free. The curve which is a result of the calculations using a Föppl-von Kármán model is open. The curve divides the strain - aspect ratio diagram in two regions. On the left side of the curve, no wrinkling will occur. On the right side, wrinkling will occur. From this result, it may be concluded that, according to the Föppl-von Kármán model, wrinkling will always occur for certain aspect ratios, without an upper bound of the critical strain. This is in contrast with the findings according to the other models and in contrast to the findings of Nayyar. Just like Nayyar and Zheng, Li & Healey's buckling diagram also shows the lower boundary for the critical buckling strain. They put this boundary at $\alpha = 1.25$, which is similar to the boundaries found by Nayyar and by Zheng.

Thickness aspect ratio β

Already in the plot on the wrinkling stability region by Nayyar [44], which was shown in figure 2.13a, it could be seen that, next to the influence of the in-plane aspect ratio, thickness has an influence on the critical buckling strain. A more systematic investigation of the effect of the thickness on the critical strain was already performed earlier by Zheng [81]. His findings are presented in figure 2.14a. As already discussed earlier, Zheng investigated the wrinkling behaviour of 144 different membranes by numerical calculations. In this plot he sorts all results by aspect ratio and plots the critical buckling strain as a function of the thickness to width ratio. For each value of the in-plane aspect ratio, quadratic dependence of the critical buckling strain on the dimensionless thickness was found.

Wrinkle packets

After his calculations on the critical wrinkling strain, Zheng performed post-buckling calculations to investigate the wrinkling pattern itself. From these calculations he found out that one packet of wrinkles forms for a length-to-width ratio smaller than, or equal to 2.8. But from that point on, the wrinkling packet splits into two packets which move away from each other with increasing length-to-width ratio. This is illustrated by a plot of the off-centre distance of the point of maximal wrinkle amplitude as a function of the membrane aspect ratio in figure 2.14b.

That wrinkles occur in one or two packets as a function of the aspect ratio was further researched by Wang [71]. He constructed a 3D phase diagram in which 3 regions are indicated: no wrinkles, one packet wrinkles and two packets wrinkles as a function of the strain, the length-to-width ratio and the thickness-to-width

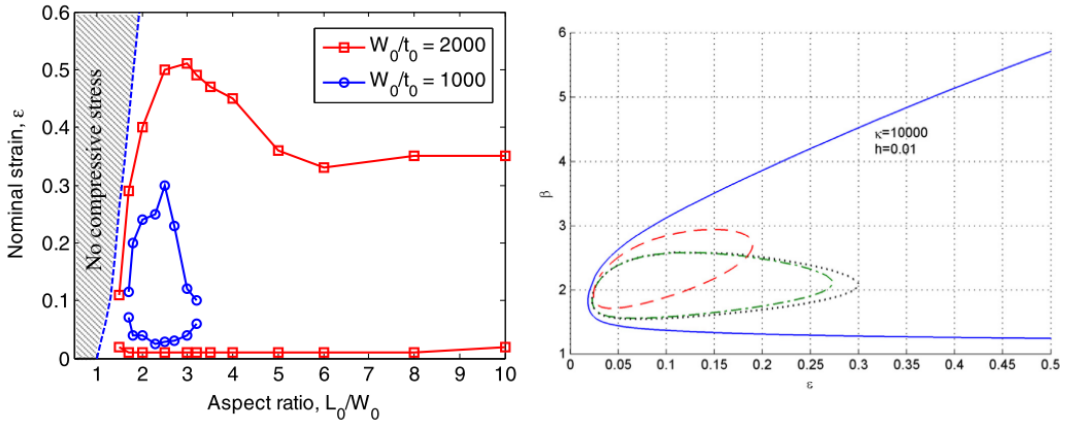

(a) (b)

Figure 2.13: (a) Wrinkling regions in the aspect ratio (α) - nominal strain plane for two different width-to-thickness ratios (t/W). The dashed line is the boundary for the region in which no compressive stresses will form during stretching, and therefore, no wrinkling will occur. [44] (b) Wrinkling stability boundaries in the length-to-with ratio - strain plane, calculated by four different models: neo-Hooken (dotdash), Mooney-Rivlin (dot), Saint Venant-Kirchoff (dash) and Föppl-von Kármán (solid). Wrinkling occurs inside of the closed curves, and at the right side of the open curve. No wrinkling occurs outside of the closed curves and at the left side of the open curve. [33]

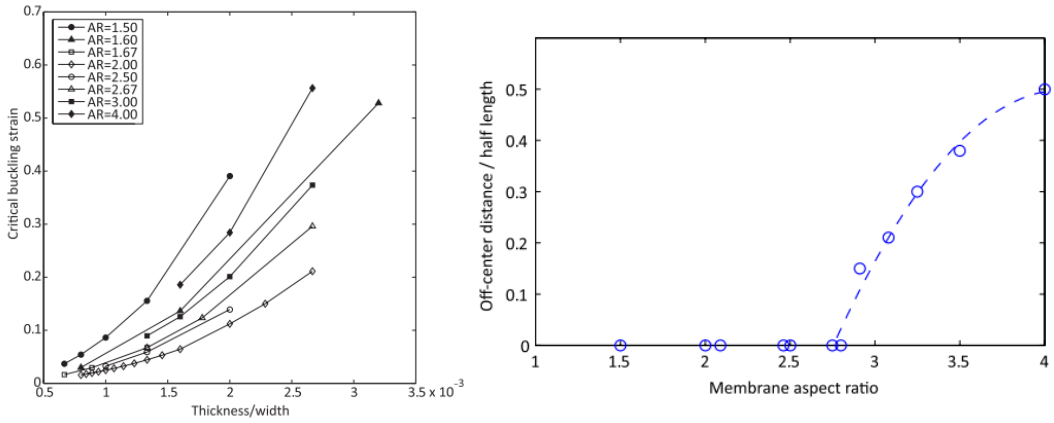

(a) (b)

Figure 2.14: (a) Critical buckling strain as a function of dimensionless membrane thickness (t/W), based on numerical results. [81] (b) The ratio of longitudinal off-centre distance of the point of the maximum wrinkle amplitude to the membrane half length $\frac{L}{2}$ as a function of the membrane aspect ratio. Results were obtained by numerical calculations. [81]

ratio. This diagram can be seen in figure 2.15. Furthermore two 2D intersections of the graph are given in this figure. From his diagram, Wang concludes that the boundary between the one packet wrinkle region and the two packet wrinkle region is found for an in-plane aspect ratio of 4, and is not influenced by the thickness-to-width ratio. Wang also briefly addresses ultra-long sheets. He states that for ultra long sheets, the aspect ratio has no longer influence on the bifurcation strains. For extremely long sheets ($\alpha = 30$ and $\beta = 2000$), the bifurcation strain is approximately the same as for a sheet with a length-to-width ratio of 5.

Wrinkling onset: summary
The 3D phase diagram of Wang in figure 2.15 also gives an overview of all conclusions on the wrinkle onset, which were discussed previously in this paragraph by the help of figures 2.11a, 2.11b, 2.12a, 2.12b, 2.13a, 2.13b, 2.14a and 2.14b:

- There exists a critical wrinkling strain. This is the strain which should minimally be applied on a uniaxially stretched membrane to wrinkle the membrane. [16, 81]
- The critical wrinkling strain depends on the in-plane aspect ratio of the membrane. Membranes with extreme aspect ratios ($\alpha \leq 1$ and $\alpha \geq 4$) are less susceptible to wrinkling compared to membranes with intermediate aspect ratios ($1 < \alpha < 4$). [16, 50, 71, 81]
- The critical wrinkling strain also depends on the width-to-thickness ratio of the membrane. For every length-to-width ratio, there exists a quadratic relation between the thickness and the critical buckling strain. [44, 81]
- There also exists an upper boundary to the strain above which no wrinkling will occur. Just like the lower boundary, this upper boundary depends on the length-to-width ratio and the width-to-thickness ratio of the membrane. [33, 44]
- Wrinkling can occur in one or two packets, depending on the length-to-with ratio of the membrane [71].

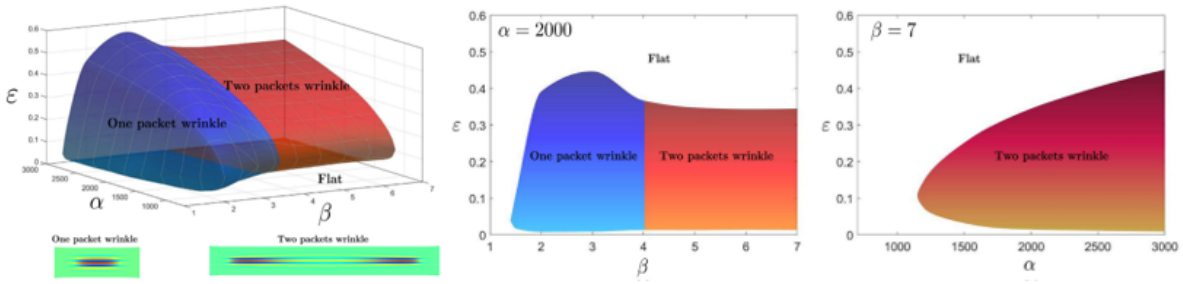

Figure 2.15: Three dimensional phase diagram showing the zones in which one and two package wrinkles will occur when stretching a rectangular uniaxial sheet as a function of the in-plane aspect ratio (indicated by $\beta = \frac{L}{W}$)) and the thickness aspect ratio (indicated by $\alpha = \frac{W}{t}$). Two dimensional cross sections of the phase diagram are given in the middle and at the right. [71]

2.2.4. Influence of shape on wrinkle details

After having discussed the onset of wrinkles in the previous section, the following section will focus on the wrinkle profile itself. The following paragraphs will discuss what influences the number of wrinkles, the wrinkle amplitude and wrinkle wavelength.
An impression of a wrinkle profile can be seen in figure 2.16. The wrinkle profile in longitudinal direction and transverse direction as well as a plot of the out-of plane displacement of a 254x101.6 mm membrane are given for a strain of 20%. This wrinkle profile was computed numerically by Zheng [81].

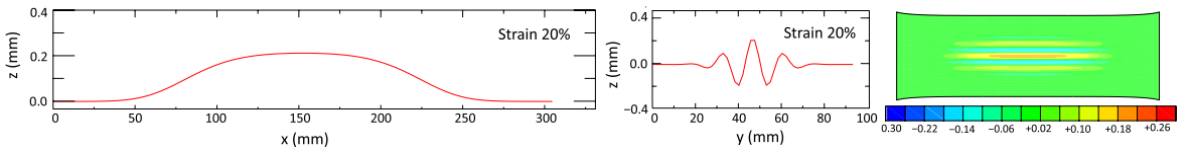

Figure 2.16: Wrinkle details of a 254 x 101.6 mm membrane with a strain of 20%, shown by the longitudinal wrinkle profile (left), the transverse wrinkle profile (middle) and a contour plot (right). Results are obtianed by numerical calculations performed by Zheng. [81]

Number of wrinkles
In 2011, Puntel [53] predicted a sequence of critical strains for increasing number of wrinkles. When a sheet is stretched by a strain larger then the first critical strain, the sheet would start to wrinkle. When it is stretched even further, and the next critical strain would be reached, the number of wrinkles would increase. He comes up with the following expression as an estimation for the number of wrinkles:

$$n_w \approx \frac{\varepsilon^{\frac{1}{4}}}{\alpha} + 1 \tag{2.2}$$

(2.3)

with:

n_w is the number of wrinkles
ϵ is the relative applied stretch
α is the in-plane aspect ratio of the sheet 2.9

However, in the same year, Nayyar [44] compares Puntels theory with his numerical results and concludes that the critical strain he finds is larger than the critical strain calculated by Puntels formula. Nayyar finds that the number of wrinkles stays constant with increasing strain, which is in contrast to the statement of Puntel that the number of wrinkles would increase with the applied strain. Unfortunately, a formulation which describes the dependency of the number of wrinkles on other factors like the aspect ratio of the sheet is not given by Nayyar.

Wavelength
The wavelength for a uniaxially stretched sheet was first investigated by Cerda. [4, 5] By minimising energy, Cerda derived a scaling law for the wavelength of the wrinkles as a function of the strain. This scaling law is shown in equation 2.4.

$$\lambda = \sqrt{tL} \cdot \left(\frac{4\pi^2}{3\gamma(1-\nu^2)}\right)^{\frac{1}{4}} \tag{2.4}$$

with:

λ is the wrinkle wavelength
t is the thickness of the membrane
L is the length of the free edges of the membrane
γ is the uniaxial tensile strain
ν is the Poisson ratio

Furthermore, Cerda performed experiments to verify his findings. The experimental results and the scaling law show similar results. Puntel [53] also derived a scaling law for the wavelength and came to the same formulation as Cerda. Nayyar performed a numerical version of the experiments of Cerda, but with a material with a Poisson ratio of 0.5. Furthermore he varied the in-plane aspect ratio of the membranes he tested and performed tests for membranes with width-to-length ratios of 1000 and 2000. His results are shown in figure 2.17a. Panaitescu [50] also made a graph to illustrate the influence of strain on the wavelength. This graph can be seen in figure 2.17b. He includes experimental results as well as numerical results and the scaling law of Cerda and concludes that the three show good agreement. But that the scaling law of cerda is only valid when $\varepsilon \gg \varepsilon_{critical}$.

Wrinkle amplitude
Next to the number of wrinkles and the wavelength, the wrinkle profile is characterised by the wrinkle amplitude. As was discussed previously in this literature review, literature indicates that there is an upper and lower boundary to the strain for which wrinkles occur. Outside of these boundaries, the wrinkle amplitude will thus be zero. This section will discuss how the wrinkle amplitude evolves in between these boundaries, and what parameters influence the wrinkle amplitude, next to the strain.

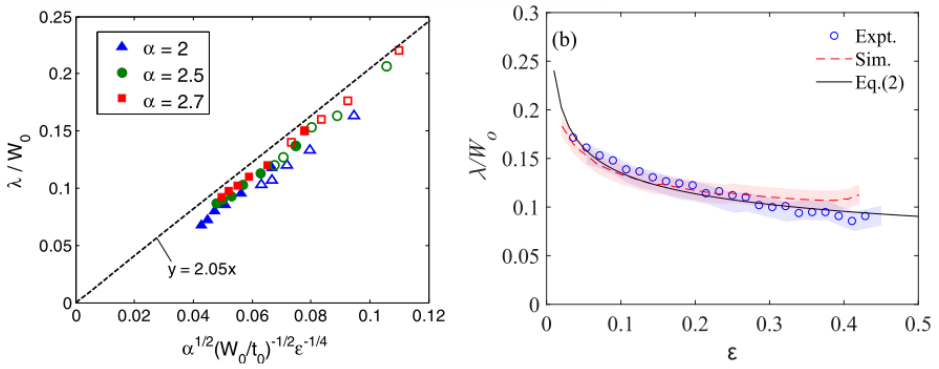

(a) (b)

Figure 2.17: (a) Normalised wrinkle wavelength $\frac{\lambda}{W}$ obtained by a post-buckling analysis, in comparison with the prediction by the scale analysis of Cerda (dashed line) [4]. The open symbols show numerical results for $W_0/t_0 = 1000$, the closed symbols show numerical results for $W_0/t_0) = 2000$. ($\alpha = \alpha$) (b) Non-dimensionalised wavelength as a function of strain for experimental membranes with dimensions $L_0/W_0 = 2$ and $t_0/W_0 = 10^{-3}$ plotted by blue dots. The shaded area corresponds to the experimental error. Results of similar numerical results by a Mooney-Rivlin model are plotted in red. The black curve indicates Cerda's scaling law, incorporating a Poisson ratio of 0.5 [50]

Cerda proposed a scaling law for the wrinkle amplitude as a function of the strain, the length of the membrane, the width of the membrane and the Poisson ratio. This formula was obtained by minimisation of energy. It is shown in equation 2.5.

$$A = \sqrt{\nu t L} \cdot \left(\frac{16\gamma}{3\pi^2(1-\nu^2)} \right)^{\frac{1}{4}} \tag{2.5}$$

with:

- A is the wrinkle amplitude
- ν is the Poisson ratio
- t is the thickness of the membrane
- L is the length of the free edges of the membrane
- γ is the uniaxial tensile strain

Cerdas formula was compared with numerical and experimental results by Nayyar and Panaitescu. However, they had to conclude that Cerdas formula does not match with their results. Panaitescu points out that the inextensibility assumption which was made by Cerda is the reason why the results don't agree with each other.

Panaitescu [50] summarises his experimental results in a graph of the non-dimensionalised wrinkle amplitude as a function of the strain. His plot is given in figure 2.18a. In this plot, Panaitescu compares the experimental results with the results of numerical simulations performed by himself, and by Nayyar. [44] For his own numerical simulations, Panaitescu uses a Mooney-Rivlin model. Nayyar made use of a hyperelastic neo-Hookean model. Panaitescu concludes that the experimental results and his own numerical results are in good agreement, both for the peak amplitude as well as for the critical wrinkling strain. He states that the Mooney-Rivlin model is an excellent descriptor of the elastic response of a latex sheet. But the difference with the results of Nayyar are significant. After also comparing his results with the results of Li and Healey [33], Panaitescu states that the material constants used in the different simulations might be different and that this comparison demonstrates that wrinkling at high strains is strongly affected by material nonlinearities.

The graph in figure 2.18a is a plot in which Fu [18] compares the wrinkling amplitude calculated according to different material models. He plots his own results together with the results of Li and Haeley [33]. In both the papers of Panaitescu and Li & Haeley, the conclusion is drawn that the neo-Hookean and the Mooney-Rivlin model are more accurate to simulate hyperelastic behaviour of rubber-like materials, compared to the Saint Venant-Kirchoff model, which predicts an early restabilisation of the material.

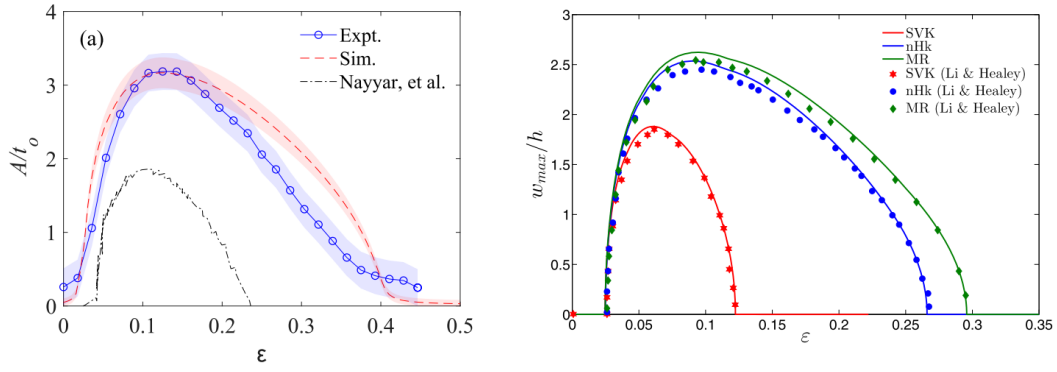

(a) (b)

Figure 2.18: (a) The measured amplitude versus applied strain (indicated with blue dots) compared with amplitudes determined using simulations of the Mooney-Rivlin model (indicated by red marks) and the neo-Hookean simulations of Nayyar (black line). The errors due to the material variation in the sheet thickness and the calibration of the profiles are shown by the shaded areas. Geometrical dimensions: $\frac{L_0}{W_0} = 2$ and $\frac{t_0}{W_0} = 10^{-3}$ [50] (b) Bifurcation diagrams according to different material models: Saint Venant-Kirchoff, neo-Hookean and Mooney-Rivlin. The solid lines represent simulation results of Fu himself [18]. The dots represent simulation results of Li and Haeley [33]. The geometric parameters of the tested sheet are: $\alpha = 2$ and $\beta = 1000$
[18]

Influence of the in-plane aspect ratio on the wrinkle amplitude

In the previous section, the influence of the in-plane aspect ratio on the critical wrinkling strain was already mentioned. Post-buckling analysis in several researches shows that the wrinkling amplitude is also influenced by the in-plane aspect ratio. An example of research which illustrates this phenomenon is the work of Wang [71], written in 2019. By numerical simulation he determines the maximal wrinkle amplitude as a function of the strain for systematically varying in-plane aspect ratios from three up to seven. Both the roots as well as the top of the wrinkle amplitude-strain curve are influenced by the aspect ratio. From Wangs graph one could conclude that the maximal wrinkling amplitude decreases for increasing values of the aspect ratio. This however, is not true over a larger range of in-plane aspect ratio values. Nayyar constructed a similar graph to the graph of Wang, giving the maximal wrinkling amplitude as a function of the strain. His graph is shown in figure 2.20a. [44] From the graph of Nayyar it can be seen that the maximal wrinkling amplitude indeed decreased for increasing aspect ratio, for aspect ratios larger than 2.5. For lower aspect ratios the maximal wrinkling amplitude increases for increasing aspect ratios.
Another phenomenon which was discussed earlier is the fact that there exists a value for the in-plane aspect ratio which forms the boundary between membranes in which one package wrinkles and two package wrinkles will form. This can also be seen from amplitude graphs. In figure 2.19b the wrinkle amplitude is plotted over the centre line of the membrane in longitudinal direction, so perpendicular to the clamped edges. In this graph it can be seen that for $\alpha = 3$, only one wrinkle forms over the length, but for increasing length-to-width ratios, two maxima arise. In other words, for increasing length-to-width ratios, the wrinkling package splits into two packets.

Influence of the thickness on the wrinkle amplitude

One last parameter which influences the critical buckling strain, which was discussed in the previous section, is the width to thickness ratio. This parameter also influences the wrinkle amplitude. Nayyar visualised this effect in a graph of the wrinkle amplitude as a function of the in-plane aspect ratio for two different width-to-thickness aspect ratios. This graph is shown in figure 2.20b. It can be seen that for a particular in-plane aspect ratio, the wrinkle amplitude is higher for $\beta = 2000$, than for a width-to-thickness ratio of 1000. For making a conclusion on the trend of the wrinkling amplitude as a function of the non-dimensional thickness, more data for different non-dimensional thickness values would be needed. However, to the best of our knowledge, no other thickness aspect ratios were previously studied.

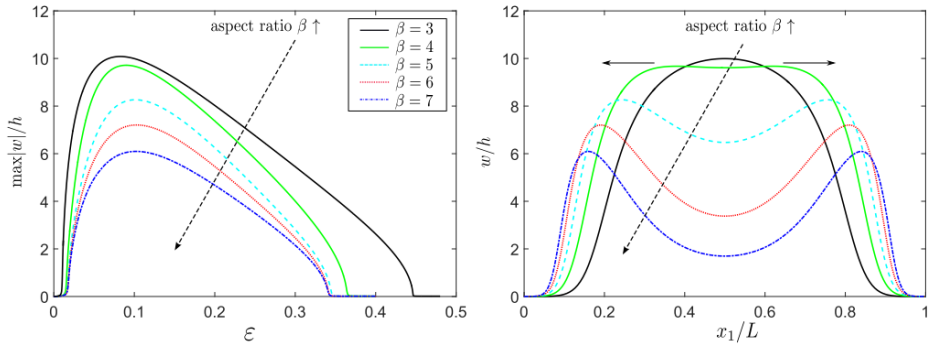

(a) (b)

Figure 2.19: (a) Bifurcation diagram of incompressible neo-Hookean model for $\frac{W_0}{t_0} = 2000$ and for various length-to-width ratios. [71] Right: Deflections along the centre line of the membrane, perpendicular to the clamped edges, for incompressible neo-Hookean model for $\frac{W_0}{t_0} = 2000$, and for the same length-to-width ratios ($\alpha = 3-7$). [71]

Influence of the material parameters on the wrinkle amplitude

A Mooney Rivlin material is described by two material constants: c_1 and c_2 (a complete description of the constitutive equation is given in equation 5.2). Fu [18] has studied the effect of parameter c_2. His results are shown in figure 2.21a. Fu concludes that the larger c_2, the later the wrinkles will disappear and the larger the deflections. The value of c_2 has no influence in the initial wrinkling stage.

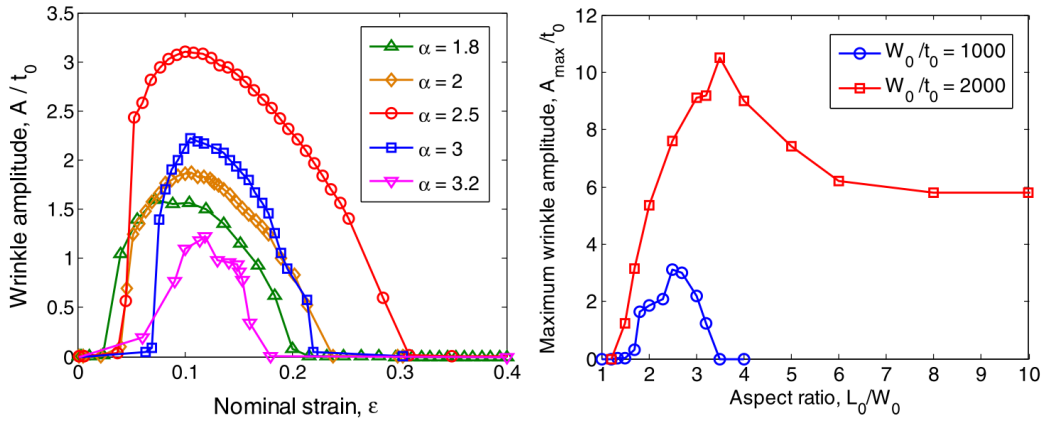

(a) (b)

Figure 2.20: (a) Stretch-induces wrinkle amplitude as a function of the nominal strain for the end-clamped rectangular sheets with different aspect ratios. The width-to-thickness ratio $\frac{W_0}{t_0}$ is 1000 for all cases. [44] (b) Maximum wrinkle amplitude as a function of the aspect ratio for a membrane with thickness aspect ratio $\beta = 1000$ and for a membrane with thickness aspect ratio $\beta = 2000$. [44]

Influence of (anti-)symmetry boundary condition on the wrinkle amplitude

To save computational time, often symmetry is used when performing calculations on wrinkled membranes. Two symmetry axis exist in rectangular membranes subjected to tension: one parallel to the clamped edges and one perpendicular to the clamped edges. On the symmetry axis parallel to the clamped edges, symmetric boundary conditions are applied. On the symmetry axis perpendicular to the clamped edges, both symmetric and anti-symmetric boundary conditions can be considered. Zheng [81] reported that the symmetric and anti-symmetric buckling modes arise at the same strain and are therefore equally likely to occur. Fu [18] investigated the effect of this boundary condition on the amplitudes-strain diagram. Results of his calculations are shown in figure 2.21b. From this graph it can be concluded that the strain for which wrinkles arise and decay are equal, but the maximal amplitude is higher when a symmetric boundary condition is used compared to when an anti-symmetric boundary condition is used.

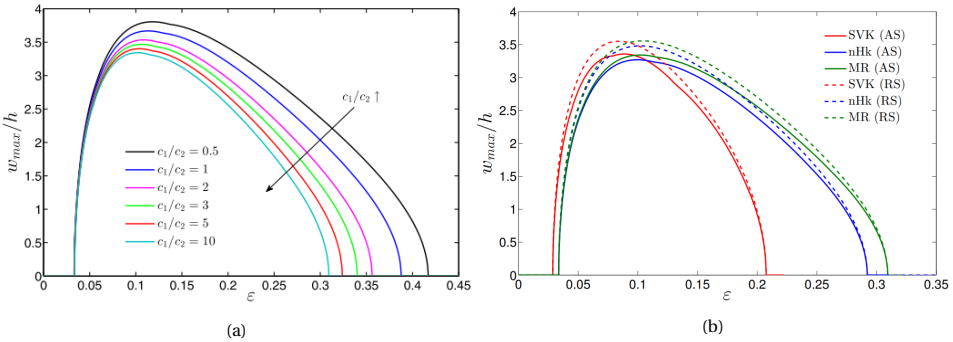

(a) (b)

Figure 2.21: (a) Amplitude-strain diagram of a membrane with aspect ratio $\alpha = 2.5$, thickness aspect ratio $\beta = 1000$ modelled by an incompressible Mooney-Rivlin material model for different values of c_2. (b) Amplitude strain diagram for a membrane of aspect ratio $\alpha = 2.5$ and thickness aspect ratio $\beta = 1000$ for three different material models (Saint Venant-Kirchoff, neo-Hookean and Mooney-Rivlin). Modelled using a symmetric (RS) and anti-symmetric (AS) boundary condition on the symmetry axis perpendicular to the clamped edges. [18]

2.2.5. Topology optimisation to minimise wrinkling

Previously, in sections 2.2.3 and 2.2.4, the influence of shape on the wrinkling behaviour of a membrane was researched. This section will go one step further in designing the membrane such that wrinkles are minimised by looking at topology optimisation.

The first to make the transition from shape optimisation to the more advanced topology optimisation was Yan, in 2014 [78]. He presents a method to control the wrinkle pattern of a uniaxially stretched membrane by the introduction of holes. In an experimental, numerical and analytical way, Yan researched the wrinkle pattern in a membrane with holes. Some of his experimental results are shown in figure 2.22. For the configuration with two holes, he researched the influence of the distance between the two holes and the diameter of the two holes. He observed that the critical buckling strain of a membrane with holes is significantly higher than that of a uniform membrane when the holes are placed close to the clamped boundary, but the diameter has an influence as well.
Yan also studies the influence of small reinforcements on the wrinkling behaviour of the membrane [79]. To conclude, Yan summarises the results of his two papers by stating that wrinkles in a membrane can be eliminated by punching holes along the horizontal centre line near the clamped edges, and by adding reinforcements on the vertical line near the free edges of the membrane.

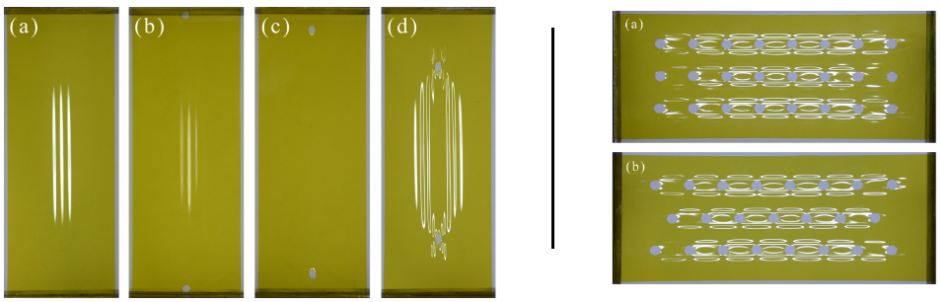

Figure 2.22: Left: Wrinkle patterns of a two-end clamped stretched membrane with a length-to-width ratio of 2.5 at 5% strain observed experimentally, for a membrane without holes (a), for a membrane with holes at $\frac{x_0}{L} = 0.05$ (b), $\frac{x_0}{L} = 0.15$ (c) and $\frac{x_0}{L} = 0.40$ (indicating the distance between the centre of the hole and the clamped side) (d) Right: Wrinkle patterns achieved by designing the distribution of holes with a radius of 2.0 mm, arranged in a square pattern (a) and in a hexagonal pattern (b) [78]

Luo [37] is the first to apply a topology optimisation algorithm to modify the topology of a membrane with the goal to reduce the wrinkling behaviour. For this, he starts from a topology optimisation method called 'Solid Isotropic Microstructure with Penalty', or SIMP in short, which was developed by Bendsøe and Sigmund [2]. In this method the structure is divided into smaller parts of which the density is changed iteratively to the material density or to zero. This change of density is changed based on multiple constraints. The constraints which were proposed originally by Bendsøe are maximisation of stiffness and a limitation to the

maximal area of the optimised structure. Luo adds stress-criteria to these constraints. These stress-criteria are based on the stress-criteria of tension field theory. He sets the restriction that both the first and the second principal stress should be positive everywhere. As was discussed in section 2.2.2, this implies that the constraint is set so that the full membrane is in the taut state, the slack state and wrinkled state are not allowed. Luo applies his method to multiple membranes to demonstrate its effectiveness. One of his results was already shown in the introduction, in figure 1.2. In this figure, a rectangular membrane with a length of 200 mm and a width of 100 mm is stretched. Both experimental and numerical results are shown. At the left, the wrinkled membrane without optimisation is shown. In the middle, two results of Luo's topology optimisation are shown. The difference between these two calculations is that the area constraint is set at different values. At the right, the result of topology optimisation without the stress constraint to minimise wrinkling is shown for comparison. From Luo's results, the conclusion can be drawn that the stress-criteria are necessary and effective to find the optimal topology for which wrinkles are minimised.

In 2017, a paper on wrinkling-suppression by topology optimisation of a membrane with a frozen zone was published by Li, with Luo as a co-author [32].
Li researches the effect of a frozen zone in membranes with different aspect ratios and investigates the effect of the dimensions of this frozen zone, in the different membranes in rectangular membranes with uniaxial stretch. From his research, Li concludes that wrinkling is the effect of three factors: the Poisson effect, the effect of the clamped edges and the influence of the frozen zone. To decrease the effect of all of these three different factors, three changes in the topology exist, each minimising the wrinkling initiation of one of the different factors. These topology changes are: concave edges, voids at the clamped ends and voids around the frozen zone, for minimising the effect of the Poisson contraction, the clamped edges and the influence of the frozen zone respectively. Figure 2.23 shows some of Li's results. The optimised designs for a membrane with aspect ratio 2, and a membrane with aspect ratio 1 are shown. Both having a frozen zone with a length of 20% of the initial length of the membrane and a width of 20% of the initial width of the membrane. In both optimised topologies, the concave edges and the voids at the frozen zone can be seen. In the membrane with an aspect ratio of 2, the topology optimisation also results in voids at the clamped edges. The right side of the figure shows the results of stretching the membranes. From these results it is clear that the topology optimisation is successful, no wrinkles occur for stretches up to 10%. An important side note is that Li performed his research for very thin graphene membranes (with a thickness of one atom), but he explicitly states that his results may also be useful as a guidance for optimisation of membranes of other scales.

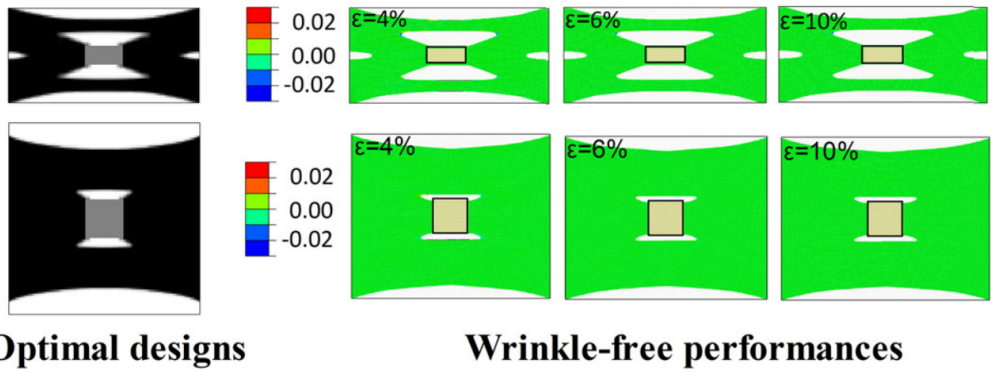

Figure 2.23: Optimal designs and wrinkle free capabilities for a membrane with aspect ratio 2 and a frozen zone with a length and width of 20% of the length and width of the total membrane (top) and for a membrane with aspect ratio 1 and a frozen zone with a length and width of 20% of the length and width of the total membrane (bottom) [31]

2.3. Conclusions

The main goal of this chapter was to answer the question: **'How can wrinkling be modelled keeping in mind flexible solar platforms as the application?'**. From section 2.1, it is clear that the most innovative concepts of offshore solar platforms consider the platforms to be flexible. The platforms should be as flexible as possible to follow the waves in rough weather conditions in order to avoid slamming and green water on the platform. Furthermore, it became apparent that tension is a dominant load due to the mooring system of the offshore solar platforms. [17, 46, 58, 66] From section 2.2, it became clear that tension is one of the loads which can cause wrinkling. [1, 3–5, 12, 16, 19, 44, 53, 59, 60, 71–75, 81] The flexible offshore solar platform subjected to tension from mooring forces will therefore be modelled as a rectangular thin membrane subjected to uniaxial tension. An impression of this configuration is given in figure 2.9.

This chapter also discussed how wrinkling behaviour of a membrane can be described. A wrinkled membrane can be described by: the wrinkle amplitude, the wrinkle wavelength and the number of wrinkles. Furthermore, for a rectangular membrane subjected to uniaxial tension, it appeared that wrinkles are only present for a limited amount of strains. The lower and upper critical strain define the range of strains for which wrinkling will occur. All details of the wrinkling behaviour can be calculated by the help of a non-linear wrinkling calculation [16, 18–20, 30, 44, 50, 53, 59, 60, 64, 65, 71, 74, 81]. Literature suggests that approximations on the presence of wrinkles can be made by studying the principal stress field of membranes [16, 33, 44, 71].

Wrinkling behaviour can be influenced by three geometrical parameters of the membrane: the in-plane aspect ratio of the membrane, the thickness aspect ratio of the membrane and by adding holes in the membrane:

- In-plane aspect ratio of the membrane:
  - Membranes with low aspect ratios ($\alpha \leq 1$) do not wrinkle [16, 44, 81].
  - Membranes with intermediate aspect ratios ($1 < \alpha < 4$) are most susceptible to wrinkling [16, 44, 81].
  - In membranes with large aspect ratios ($\alpha \geq 4$) two separate wrinkling packets will form [71].
- Thickness aspect ratio of the membrane:
  - Thick membranes ($\beta \leq 500$) do not wrinkle [71].
  - There exists a quadratic relationship between the lower critical strain of the membrane and the thickness of the membrane: the thinner the membrane, the lower the lower critical strain and thus the more susceptible to wrinkling [81].
- Adding holes to the membrane:
  - By adding holes to the membrane, wrinkles can be eliminated from the membrane. The underlying mechanisms are still unknown.

3

Non-linear Wrinkling calculations

This chapter will answer the question:
Is a post-buckling calculation adequate to research wrinkling behaviour of very large flexible offshore solar platforms?

To answer this question, first a model is constructed by which the wrinkling behaviour of a rectangular uniaxially stretched membrane will be researched. The model will be verified and validated by comparison to results from literature. The adequateness of the model to be used to investigate very large flexible offshore solar platforms will be judged by two criteria. The method should be convenient to be applied to membranes of different geometries and furthermore its computational cost should be small enough so that a wide range of geometries can be researched. Whether the model complies these two criteria will be discussed in the second half of this chapter.

3.1. Method

This section will give a step by step overview of the method to perform non-linear wrinkling calculations.

3.1.1. Approach

This section will discuss the details of the calculation model to determine the wrinkling pattern in a rectangular uniaxially stretched sheet. A sketch of this configuration is shown in figure 3.1. A rectangular membrane is considered, which is stretched from two opposite sides. These two sides are clamped, the other two sides are free. Symmetry is used to reduce the calculation time by modelling only one quarter of the membrane. In the rest of this report, all figures showing numerical results will only show this quarter of the membrane. Figure 3.1 gives an overview of the described boundary conditions. The model makes use of the program ANSYS APDL R2019.3.

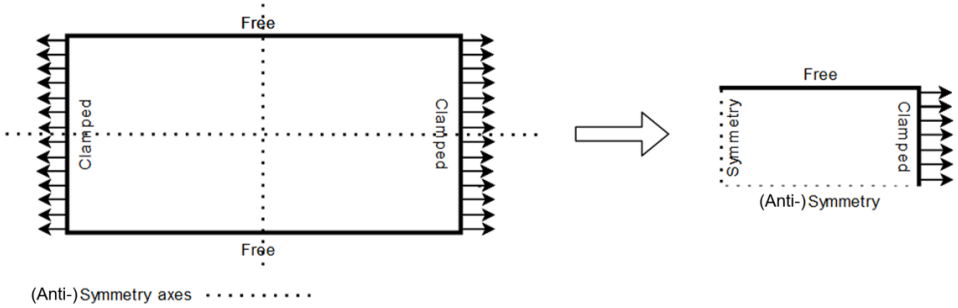

Figure 3.1: Sketch of a rectangular membrane under uniaxial tension. Symmetry is used to reduce the calculation time by modelling only one quarter of the membrane. This quarter is shown on the right. The right side of this quarter membrane is clamped, the upper side is free. On the lower and left side symmetry is guaranteed by setting the displacement along the symmetry axis to zero, and the rotation around the symmetry axis to zero as well. Furthermore, calculations were performed with anti-symmetric boundary conditions at this edge.

Wrinkling is a post-buckling phenomenon. To perform this post-buckling calculation, three steps have to be taken:

1. A pre-stressed static analysis
2. A buckling analysis
3. A non-linear static analysis

Wrinkling of a rectangular uniaxial stretched membrane can be considered as buckling under tension. To perform a post-buckling analysis numerically, initial deformations have to be imposed on the structure. Furthermore, non-linearities have to be taken into account. Both geometric non-linearity as well as material non-linearity are of importance.

Material non-linearity
Literature has confirmed that the material behaviour of membranes which are susceptible to wrinkling, like rubber, can be described best by hyperelastic material models [18, 33, 50]. The main characteristics of hyperelastic materials are that the materials can experience very large strains. All these strains are elastic and thus recoverable. Hyperelastic material models describe the non-linear relationship between stress and strain by the use of the energy density potential W. The stress in the material can be calculated by taking the derivative of this energy density potential with respect to the strain. The parameters in the energy density potential are the material properties. In the coming calculations, both the incompressible Neo-Hookean material model and the incompressible Mooney-Rivlin model will be used. The following formulae describe the energy density potential for these two material models:

$$\text{Neo-Hookean: } W = \frac{\mu}{2} \cdot (I_1 - 3) \tag{3.1}$$

$$\text{Mooney-Rivlin: } W = C_{10} \cdot (I_1 - 3) + C_{01} \cdot (I_2 - 3) \tag{3.2}$$

with:

W	the strain energy density potential
μ	the material property characterising an incompressible Neo-Hookean material
C_{10} and C_{01}	the material properties characterising an incompressible Mooney-Rivlin material
I_1 and I_2	invariants of C, the Cauchy-Green deformation tensor

3.1.2. Strain without initial imperfections

This subsection will focus on the verification and the validation of two hyperelastic models: the Neo-Hookean material model and the Mooney-Rivlin material model. It was chosen to focus on these two materials because literature indicates that these two models are most representative for calculations on wrinkling behaviour in rubber-like materials [33, 50]. The next two paragraphs will discuss verification and validation of these material models.

Verification of material models: Uniaxial tension test
For the verification of the material models, a uniaxial tension test was performed. In a uniaxial tension test, a material block is loaded by tension in one direction, while it is allowed to contract in the other two directions [11]. The uniaxial tension test is implemented in ANSYS using the SHELL181 element, with unity thickness, length and width. The analytical solution for the uniaxial tension test for the incompressible Neo-Hookean model and for the Mooney-Rivlin model respectively are as follows:

$$\text{Neo-Hookean: } \sigma = \mu \cdot (\lambda^2 - \lambda^{-1}) \tag{3.3}$$

$$\text{Mooney-Rivlin: } \sigma = c_1 \cdot (\lambda^2 - \lambda^{-1}) + c_2 \cdot (\lambda - \lambda^{-2}) \tag{3.4}$$

with:

σ	is the applied stress on the tensioned side
λ	is the stretch (stretched length/initial length)
μ	is the shear modulus of the material
c_1 and c_2	are the material properties for the Mooney-Rivlin material model

A plot which compares the analytical and numerical solution for the uniaxial tension test is shown in figure 3.2. The numerical and analytical solutions show excellent agreement. Therefore it is confirmed that the material model in ANSYS is implemented and used in the correct way.

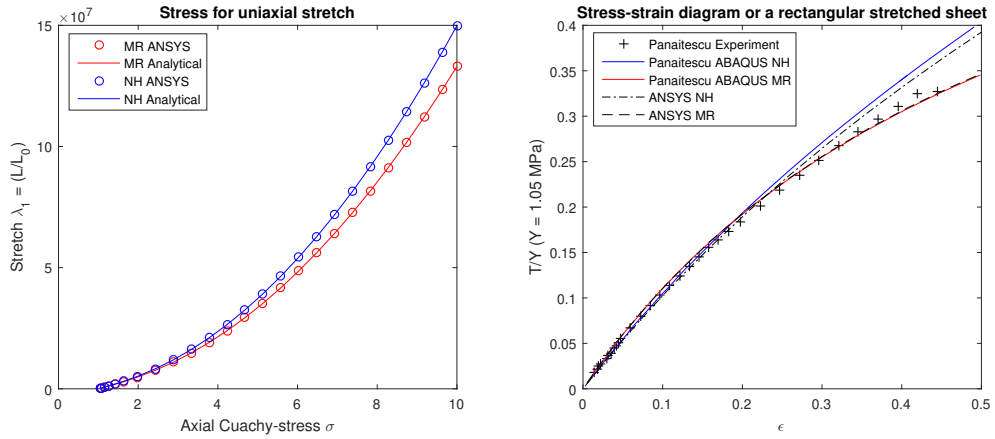

Figure 3.2: Left: Comparison of the analytical and numerical results of a uniaxial tension test for the Neo-Hookean model and for the Mooney-Rivlin model. Right: Stress-strain diagram for a rectangular stretched sheet. Experimental and numerical results published by Panaitescu [50] are compared with numerical results calculated by ANSYS.

Validation of material models: Comparison with experimental results

For validation of the material model, the results of the ANSYS calculations are compared to the experimental results of Panaitescu [50]. Panaitescu has researched the elastic properties of latex sheets by stretching them experimentally. The initial dimensions of these sheets are: $L_0 = 28$ cm, $W_0 = 14$ cm and $t_0 = 0.14$ mm. For a range of applied stresses Panaitescu has measured the consequential strain. His test results can be seen in figure 3.2.

The experiments were also used for validation of simulations by Panaitescu herself. Good agreement was found between the experimental stress-strain diagram and the stress-strain diagram calculated by Abaqus by Panaitescu for material parameters as described in table 3.1. The same parameters are used for the validation in ANSYS. The stress-strain diagram which was obtained by Panaitescu using Abaqus is plotted together with the stress-strain diagram obtained using ANSYS in figure 3.2. The difference between the results are within the error of Panaitescu's results.

Table 3.1: Material constants resulting from comparison between experimental results and calculations in ABAQUS performed by Panaitescu

	Mooney-Rivlin	neo-Hookean
D_1	0 Pa	0 Pa
C_{01}	$15.81 \cdot 10^4$ Pa	0 Pa
C_{10}	$6.21 \cdot 10^4$ Pa	$19.10 \cdot 10^4$ Pa

3.1.3. Buckling analysis

To obtain the initial deformation for the post-buckling analysis, buckling modes are calculated. In ANSYS, only a buckling solver for linear material models is implemented. Therefore, a linear isotropic material model is used when searching for buckling modes. The out-of-plane deformation for the first three buckling modes for a membrane of aspect ratio $\alpha = 2$ and a thickness aspect ratio of $\beta = 2000$ are shown in figure 3.3. The first buckling mode is used as the initial perturbation for the post-buckling calculation.

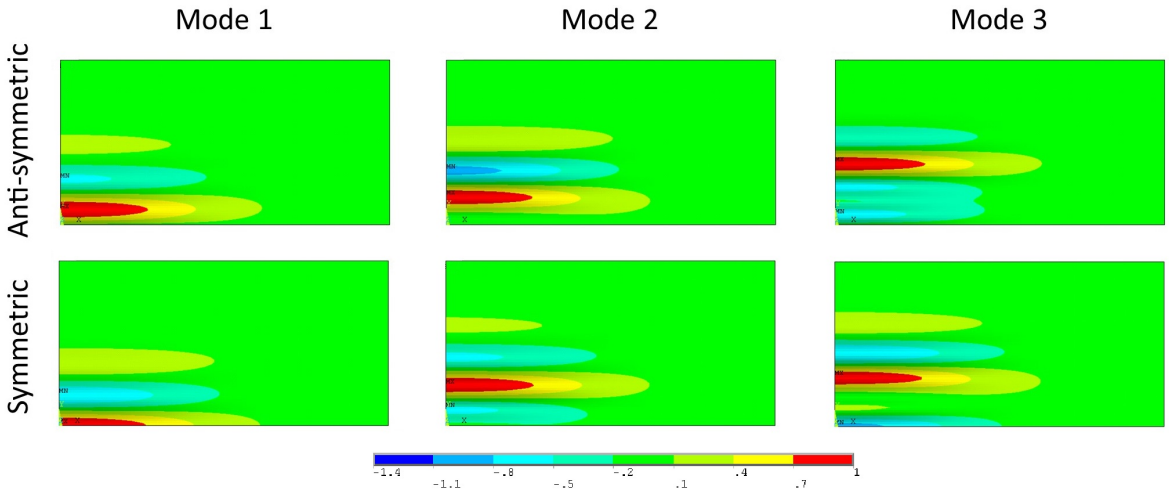

Figure 3.3: Buckling modes for membranes with symmetric and anti-symmetric boundary conditions along the horizontal axis for a membrane of aspect ratio $\alpha = 2$, thickness aspect ratio $\beta = 1000$ and a Neo-Hookean material model.

3.1.4. Wrinkling analysis

The previous two sections described the first two calculation steps which need to be taken in order to calculate the wrinkling behaviour of a membrane. This section will focus on the last step: straining the membrane with a buckling mode as the initial imperfection. The influence of this initial imperfection will be discussed. Validation of the results will be done by comparing the amplitude-strain diagram with experimental results from literature.

Verification

This paragraph will discuss the verification of the model. In order to verify the model, a range of settings are varied to examine their influence on the end result. The calculation is performed for varying values of the mesh density, the tolerance and the number of substeps. For all these settings, input values are found for which the end result is not influenced by their value, and for which the calculation time of the model is reasonable. Details on the mesh convergence study are discussed in appendix A.

Together with the mesh density, the tolerance and the number of substeps, also the initial deformation is verified. The first buckling mode is used as initial deformation, but the amplitude of the deformation is varied. The amplitude-strain diagram for different values of the initial deformation amplitude is shown in figure 3.4. From this plot, it can be seen that when the initial deformation is chosen too small ($\leq 1 \cdot 10^{-5}$), wrinkling is not initiated and the amplitude-strain curve remains flat. When the initial deformation is chosen too large ($\geq 1 \cdot 10^{-2}$), the result is influenced by the initial deformation. This influence can be seen over the full range of strains, but most clearly at the points of birth and decay of the wrinkles.

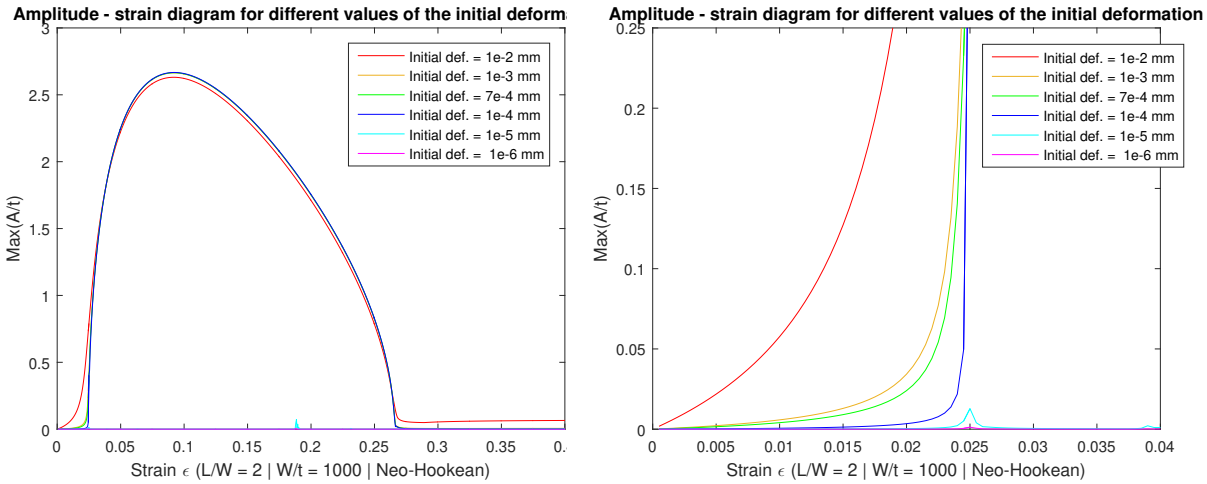

(a) (b)

Figure 3.4: Amplitude-strain diagram and a detail of this diagram, for different values of the initial deformation for a membrane of aspect ratio = 2, a thickness aspect ratio of $\beta = 1000$ and a Neo-Hookean material model.

Validation

After setting up the wrinkling model and performing verification, the results are compared with results from literature for validation. Figure 3.5 shows the comparison of results with experimental and simulation results obtained by Panaitescu [50]. The same maximal amplitude is found as the experimental amplitude reported by Panaitescu. The agreement between the results and the simulation results obtained by Panaitescu is very good.

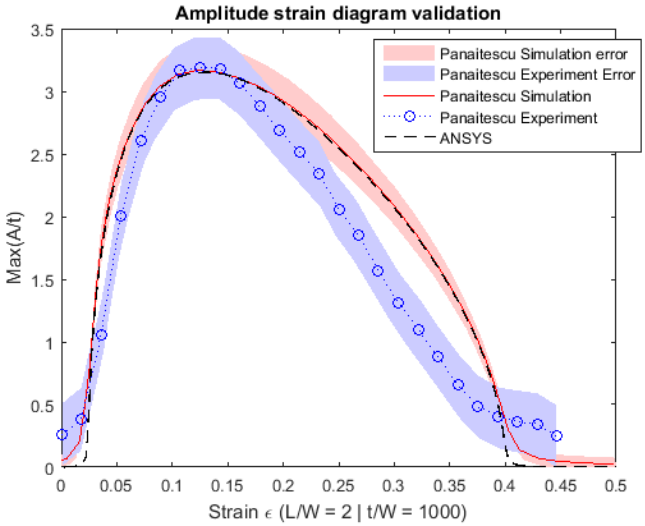

Figure 3.5: Validation of simulation resutls by comparison with experimental and simulation results from literature [50]. The amplitude strain diagram is shown for a membrane of aspect ratio $\alpha = 2$, a thickness apect ratio of $\beta = 1000$ and a Mooney-Rivlin material model.

3.2. Application

In this section, the method which was discussed in the previous chapter will be used to investigate the influence of material parameters on the wrinkle amplitude and investigate the influence of the membrane aspect ratio on the wrinkle amplitude.

3.2.1. The influence of the material parameters on the wrinkle amplitude

This subsection will discuss how the material parameters influence the wrinkle amplitude and how the material parameters influence the relation between the aspect ratio and the maximal wrinkle amplitude.

The influence of the material constants of the Mooney-Rivlin model were previously researched by Fu [18] for a membrane of aspect ratio $\alpha = 2.5$. This subsection will discuss this influence for membranes of other aspect ratios. In equation 3.4 it can be seen that the material parameters characterising the material for the Mooney-Rivlin material model are C_{10} and C_{01} (referred to as c_1 and c_2 by Fu himself). Figure 3.6a illustrates this research with an amplitude-strain diagram for different values of $\frac{c_1}{c_2}$ for a membrane with aspect ratio $\alpha = 2$.

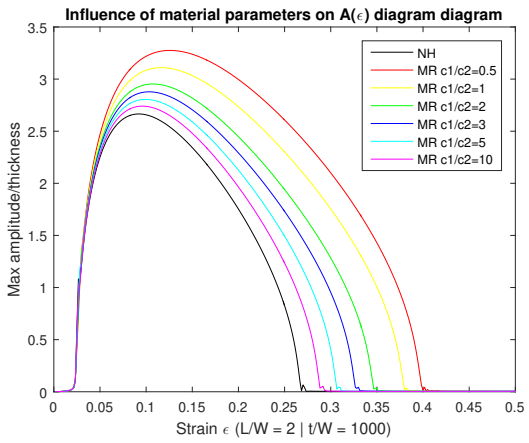

(a)

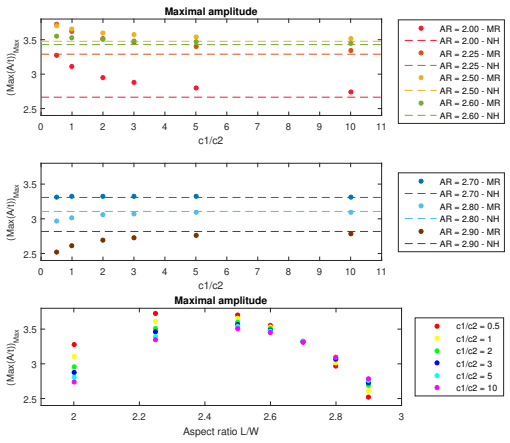

(b)

Figure 3.6: (a) Amplitude-strain diagram for a rectangular membrane with dimensions $\alpha = 2$ and $\beta = 1000$, for different material parameters. (b above and middle) maximal amplitude as a function of the material parameters $\frac{c_1}{c_2}$ for different membrane aspect ratios. (b below) Same data as two plots above, but plotted the other way around, showing the maxima amplitude as a function of the aspect ratio of the membrane, for different values of the material parameters.

The maxima of the amplitude - strain diagrams are plotted as a function of $\frac{c_1}{c_2}$ in figure 3.6b. This plot was extended by adding the relationship of the maxima amplitude as a function of $\frac{c_1}{c_2}$ for membranes with other aspect ratios. When varying the aspect ratios from 2 up to 2.9, it can be seen that the relation between the maximal amplitude and $\frac{c_1}{c_2}$ concluded by Fu is not valid for all aspect ratios. The same results are plotted in two graphs: the maximal amplitude as a function of $\frac{c_1}{c_2}$ for different aspect ratios from 2 to 2.6 (above), and for aspect ratios from 2.6 to 2.9 (middle) and the maximal amplitude as a function of the aspect ratio for different values of $\frac{c_1}{c_2}$ (below).

Given the results in figures 3.6a and 3.6b the following conclusions can be drawn. Firstly, the graph of the maximal amplitude as a function of the material parameters c_1/c_2 implies that:

- The higher $\frac{c_1}{c_2}$, the lower its influence on the maximal amplitude
- The results for the Neo-Hookean material model equal the results for the Mooney-Rivlin material model for $\frac{c_1}{c_2} \to \infty$.
- Low values of $\frac{c_1}{c_2}$ do have a significant influence on the maximal amplitude. The influence of $\frac{c_1}{c_2}$ on the maximum amplitude depends on the aspect ratio of the membrane. For low aspect ratios (AR = 2), the maximal amplitude increases rapidly for a decreasing $\frac{c_1}{c_2}$. A slower increase in maximal amplitude for decreasing $\frac{c_1}{c_2}$ is seen for higher aspect ratios (up to 2.6). For aspect ratios of 2.7 and higher this trend even changes in a decreasing trend of the maximum amplitude for decreasing values of $\frac{c_1}{c_2}$.

- For $\frac{c_1}{c_2} \leq 1$ the maximal amplitude is reached for an aspect ratio of 2.5. For $\frac{c_1}{c_2} = 0.5$, the maximal amplitude is reached for $\alpha = 2.25$. This change is due to the changing influence of the material parameters on the maximal amplitude for different aspect ratios.

Secondly, the graph of the maximum amplitude as a function of the aspect ratio for different values of $\frac{c_1}{c_2}$ shows the same results in another way. In this representation the change from a decreasing trend for the maximal amplitude for an increasing an $\frac{c_1}{c_2}$ ratio (AR $\leq$ 2.6) to an increasing trend for the maximal amplitude for an increasing $\frac{c_1}{c_2}$ ratio (AR $\geq$ 2.7) can be seen even more clearly.

3.2.2. Influence of aspect ratio on the wrinkle amplitude

This section will discuss the influence of the aspect ratio on the wrinkling amplitude. To isolate the effect of the aspect ratio, all other parameters will be kept constant. The thickness aspect ratio is set to $\beta = 1000$. The Neo-Hookean material model will be used for all calculations.
As discussed before, the first buckling mode of a membrane is used as initial displacement for the post-buckling analysis. Therefore, to study the post-buckling behaviour of membranes of different aspect ratios, the first buckling mode has to be found for all these membranes. The next paragraph will discuss the difficulties which were encountered while calculating these buckling modes. The second paragraph will discuss the post-buckling results for membranes of different lengths, thus with different aspect ratios α. This subsection will be concluded by discussing other methods which were researched to find the initial deformation with the goal to be able to perform a post-buckling calculation when the first buckling mode cannot be found.

Initial deformation for varying aspect ratios

Every buckling mode occurs for a specific critical buckling strain. In figure 3.7 the critical buckling strain is plotted as a function of the aspect ratio for aspect ratios ranging from 1.35 up to 2.95. From this figure, it can be seen that the critical buckling strain is lowest for an aspect ratio of 2. For lower aspect ratios, the critical buckling strain rises rapidly. Also for higher aspect ratios, the critical buckling strain increases, but at a lower rate. For an aspect ratio of 2.95 a sudden rise in critical buckling strain is noticed. For higher aspect ratios no buckling modes are found for the membrane subjected to uniaxial tension. The explanation for this result was not found.

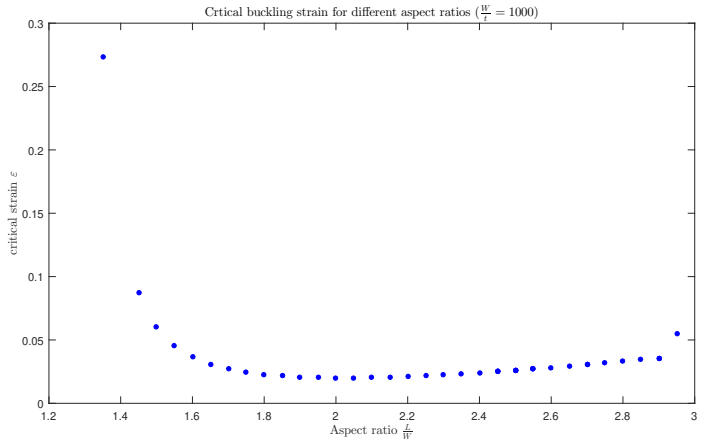

Figure 3.7: Critical buckling strain for the first buckling mode of a rectangular membrane loaded by uniaxial tension with aspect ratios between $\alpha = 1.35$ and $\beta = 2.95$ and a thickness-aspect ratio of $\beta = 1000$

Figure 3.8 gives an impression of the first mode shape for membranes of different aspect ratios.
In figure 3.8a the out-of-plane displacement along the longitudinal symmetry axis is given as a function of the normalised x-coordinate. When comparing the modeshapes for the different aspect ratios, it can be seen that for higher aspect ratios, the wrinkles in this first mode shape along the longitudinal symmetry axis spread over a longer range of the membrane than for the lower aspect ratios.
Figure 3.8b shows the out-of-plane displacements along the midline of the membrane in width direction. In this profile, wrinkles can be recognised. The number of wrinkles decreases for increasing aspect ratio. The degree by which the wrinkle amplitude decreases outwards along the different wrinkles increases with increasing aspect ratio. Furthermore, the higher the aspect ratio, the less influence the aspect ratio has on the mode shape. The mode shapes for aspect ratios 2.5 and 2.7 show more agreement compared to the mode shapes for aspect ratios 1.5 and 1.75.

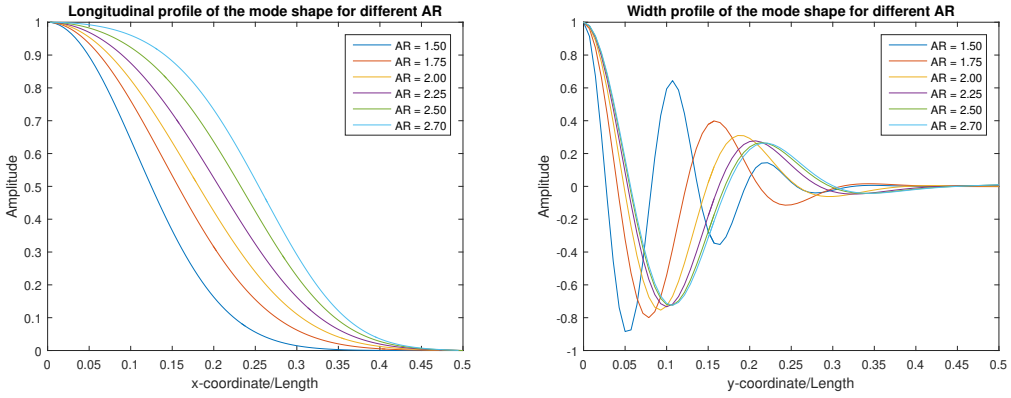

(a) (b)

Figure 3.8: out-of-plane displacement along the symmetry axes of the membrane for the first mode shape, for membranes of different aspect ratios.

Amplitude-strain diagram for varying aspect ratios
The amplitude-strain diagrams of the membranes for which the first buckling mode could be found can be seen in figure 3.9. For a thickness aspect ratio of 1000 and a Neo-Hookean material model, the wrinkle amplitude is maximal for a membrane with an aspect ratio of 2.5
The next to paragraphs will discuss the influence of the material parameters on this result.

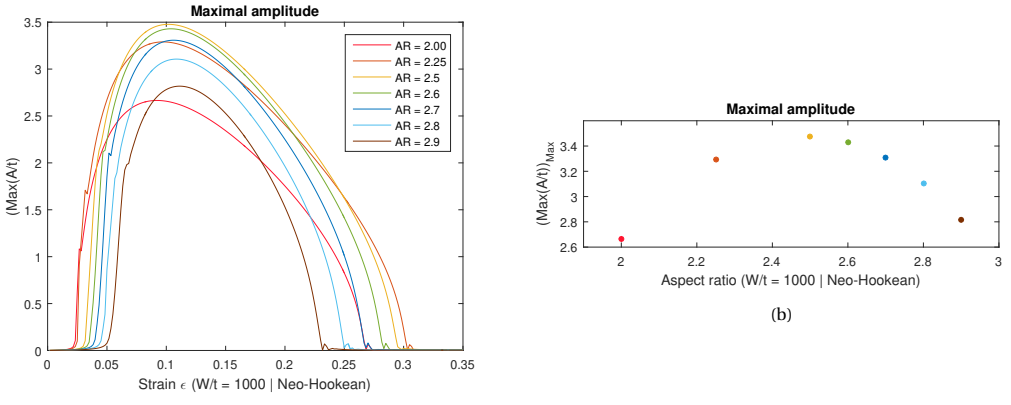

(a) (b)

Figure 3.9: (a) Amplitude-strain diagram for membranes with different aspect ratios α, a thickness aspect ratio of $\beta = 1000$ and a Neo-Hookean mateiral model. (b) Maximal aspect ratio as a function of the aspect ratio for membranes of different aspect ratios α, a thickness aspect ratio of $\beta = 1000$ and a Neo-Hookean material model.

Alternative methods to obtain the initial deformation of the membrane

As described before, the first buckling mode could not be found for all membranes. When comparing to results from literature, it appears that for some membranes no buckling mode could be found using the ANSYS model while wrinkling will occur [44, 50, 81].

This paragraph will discuss whether other deformations than the first buckling mode can be used as initial deformation in order to find the post-buckling behaviour of the membrane. Four options were researched:

1. A tensile buckling mode other than the first buckling mode
2. A compressive buckling mode
3. A deformation resulting from a post-buckling calculation with a compressive buckling mode
4. Out of plane deformation created by unbalancing forces

Figure 3.10 shows the first, second and third buckling modes and the amplitude-strain diagram which are obtained when these buckling modes are used as initial deformations. As discussed earlier, the correct amplitude-strain relation is obtained when the first buckling mode is used. The second and third buckling modes lead to very different results. When using buckling modes two or three as the initial deformation to calculate the post-buckling behaviour, the resulting amplitude is significantly lower than when buckling mode one is used.

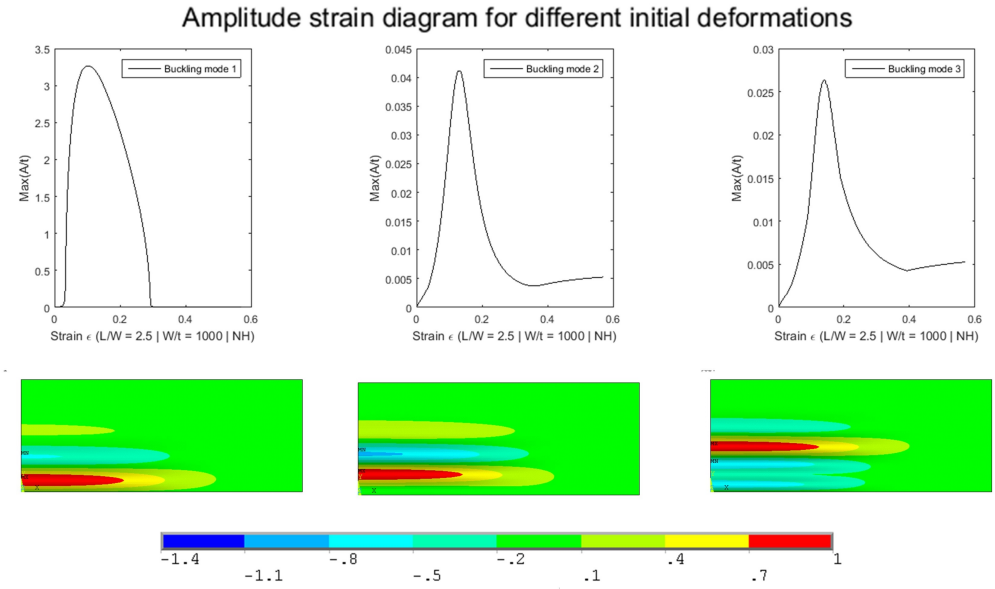

Figure 3.10: First, second and thirth anti-symmetric buckling modes of a membrane of aspect ratio $\alpha = 2.5$, thickness aspect ratio $\beta = 1000$ of a neo-Hookean material and the resulting amplitude-strain diagrams when using these as initial deformation

Figure 3.11 shows the amplitude-strain diagram which is obtained when a compressive buckling mode is used as the initial deformation. It can immediately be seen that this amplitude-strain diagram is different from the correct one. The obtained amplitudes are significantly higher than expected. However, when studying the deformations visually, wrinkles can be observed. An attempt was made to obtain the correct amplitude-strain relation by the use of this wrinkled geometry as initial deformation. However, as can be seen in figure 3.11 this attempt was not successful either. Larger amplitudes were found than there should be. Also, an attempt was done to create an initial deformation by performing a static analysis with unbalancing forces. The resulting perturbation as well as the post-buckling results can be seen in figure 3.11. It is clear that an initial deformation created by unbalancing forces will not necessarily lead to the correct post buckling results.

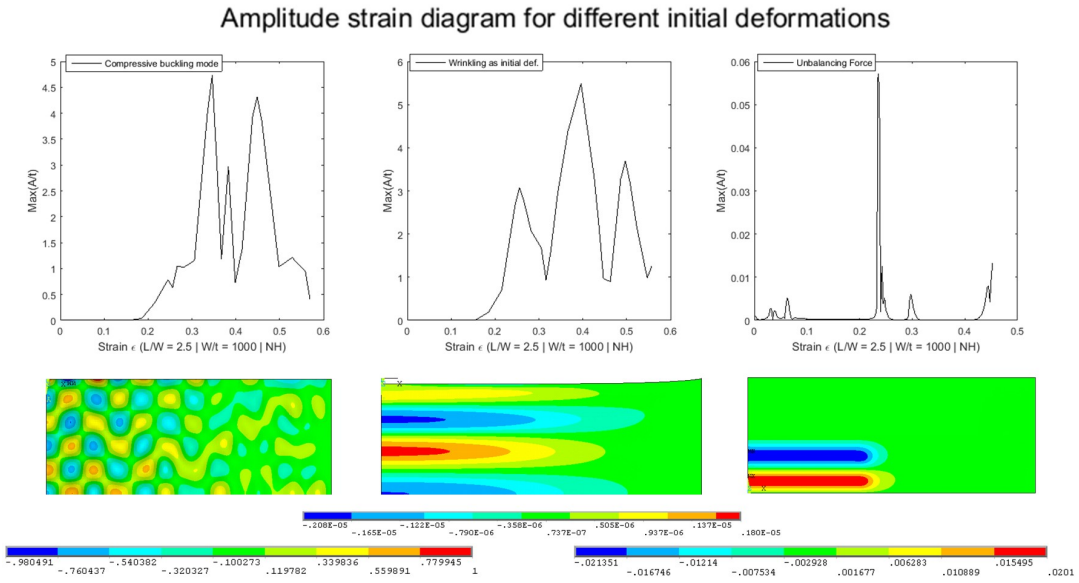

Figure 3.11: Buckling mode of a membrane of aspect ratio $\alpha = 2.5$, thickness aspect ratio $\beta = 1000$ in compression and the resulting deformation when this buckling mode is used as initial deformation for a post-buckling calculation in which the membrane is strained, which is again used as initial deformation. The graphs are the resulting amplitude-strain diagrams of the post-buckling calculations.

From this research to find the correct amplitude-strain diagram by using initial deformations other than the first buckling mode, it can be seen that the wrinkling calculation is very dependent on the geometry used as initial geometry. Using another buckling mode, a wrinkled geometry resulting from post-buckling such a buckling mode or using a geometry which is deformed by unbalancing loads does not lead to the reference amplitude-strain relation. This has very large consequences for researching the wrinkling behaviour of membranes with different geometries. Up to now no other method has been successful to perturbate the membrane other than using the first buckling mode as the initial membrane. Finding this first buckling mode is therefore a necessity to study the amplitude-strain relation of the membrane.

3.3. Conclusion

After successfully setting up a model for which wrinkling of a rectangular, stretched membrane can be calculated. It was used to study the influence of the aspect ratio of the membrane on the wrinkle amplitude and the influence of material parameters on the wrinkling amplitude. The next goal is to research the influence of permeability on the wrinkling behaviour of the membrane keeping in mind the application of very large flexible floating solar platforms. For the non-linear wrinkling calculation to be an adequate method for this application, two criteria were defined. The method should be applicable on a multitude of geometries and furthermore it should not be computationally expensive.

The main conclusion of this chapter is the influence of the initial deformation on the results of the post-buckling calculation to study wrinkling. The correct amplitude-strain relation is obtained for the post-buckling calculation when using the first buckling mode as the initial perturbation. However, when other buckling modes, or an initial deformation obtained by unbalancing forces is used, the correct result is not found. Due to the dependence of the results of the post-buckling calculation on user defined input, the result is not objective. This leads to the conclusion that the method is not adequate to be used to study the effect of changes in the geometry on the wrinkling behaviour of a membrane if the first buckling mode cannot be found for this geometry.

4

Wrinkling approximation indicators

In chapter 3, it was concluded that fully non-linear buckling analyses require accurate a priori selection of the initial perturbation to achieve reasonable results. To allow research on wrinkeld membranes with low computational costs and without the need for subjective inputs, this chapter will discuss the development of wrinkling indicators that are based on the principal stress distribution in the membrane without initial perturbation.

As discussed in section 2.3, wrinkles in a membrane can be measured by:

- The number of wrinkles
- The wrinkle amplitude
- The wrinkle wavelength
- The lower critical strain
- The upper critical strain
- The region of the membrane which wrinkles

By comparing the principal stress distribution in membranes with different aspect ratios with wrinkling details known from literature, four indicators were found by which the wrinkling behaviour of the membrane can be approximated. These wrinkling indicators will be discussed in the following sections.

Sections 2.2.3 and 2.2.4 discussed the influence of the thickness of the membrane on its wrinkling behaviour. It became clear that the thicker the membrane, the less susceptible it will be for wrinkling. Thin membranes are more susceptible to wrinkling. Thickness thus has a restraining effect on the wrinkling behaviour. In the membrane without initial perturbation with tension load at the clamped edges, all loads are working in-plane. The restraining effect of the thickness has no effect, the calculation only takes into account two dimensions, as if an infinitely thin membrane is strained. Therefore, in the search for indicators based on the principal stress distribution, the results of the indicators will be compared to wrinkling results from thin membranes. The thinnest membranes of which results are found in literature are membranes with a thickness aspect ratio of $\beta = 2000$.

4.1. The principal stress in membranes of different aspect ratios

As an introduction, before studying indicators based on the principal stress distribution, this section will give an overview of these principal stresses in membranes of different aspect ratios. The magnitude of the compressive stresses as well as the area of the membrane in which compressive stresses are present will be studied as a function of the strain.

From figure 4.1 it can be seen that for all membranes of the different aspect ratios which were taken into consideration, the graph of the most negative second principal stress as a function of the strain shows the same trend. No compressive stresses are present if the strain is zero. From that point onward, the magnitude of the compressive stresses increases up to a maximum, from which the magnitude decreases again to zero.

The trend of the compressive stress area as a function of the strain is different for membranes of small aspect ratios ($\alpha \leq 3.8$) than for large aspect ratios ($3.8 < \alpha \leq 6.7$) and very large aspect ratios ($\alpha > 6.7$). For membranes of small aspect ratios, the area of the membrane in which compressive stresses occur decreases

with increases strain. For large aspect ratios, first this area increases up to a maximum after which it also decreases with increasing strain. For the very large membranes which were calculated ($\alpha = 6.8$, $\alpha = 6.9$ and $\alpha = 7$), it can be seen that the opposite happens for the area in compression as a function of the strain. For small strains the area decreases to a minimum after which it increases again.

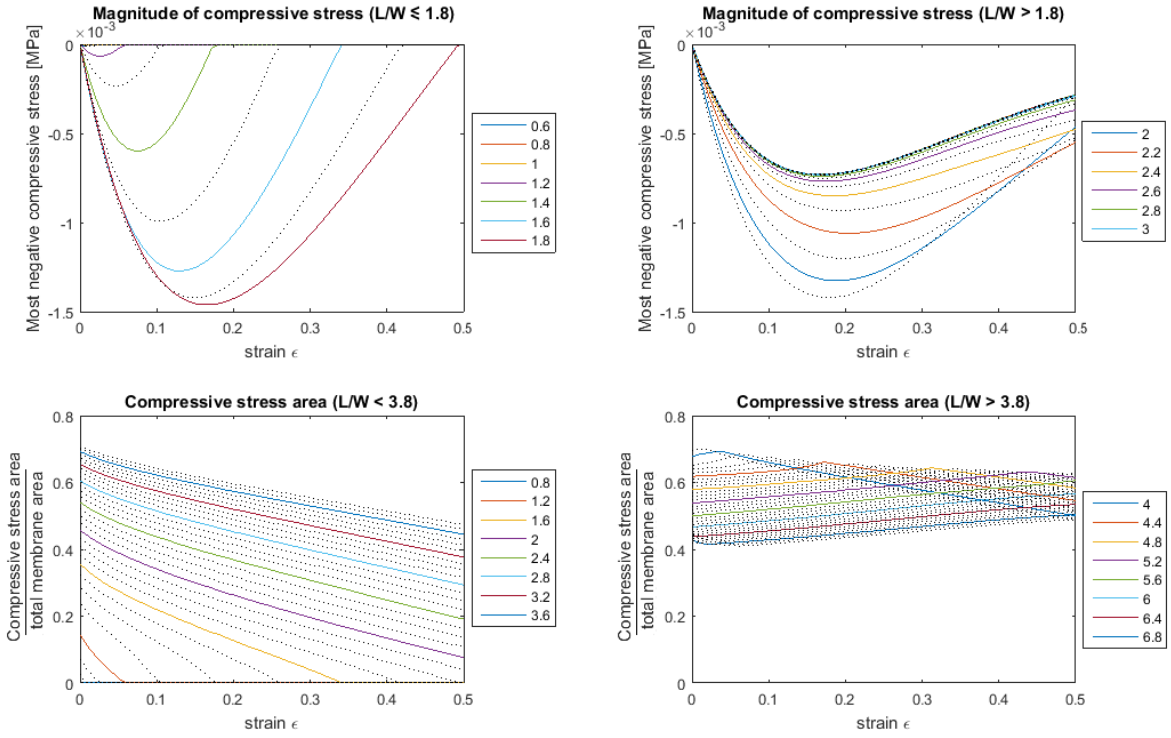

Figure 4.1: Magnitude of the maximal compressive stress and area of the compressive stress region as a function of the strain for membranes of different aspect ratios as a function of strain.

4.2. Compressive stresses as necessary condition for wrinkling

Compressive stresses are a necessary condition for wrinkling. The previous section discussed the magnitude of the compressive stresses and the area of compressive stresses as a function of strain for different aspect ratios (figure 4.1). From these results, it can be seen from a certain strain onward, the magnitude of the compressive stresses is zero. This boundary between compressive stresses and no compressive stresses is drawn in the stability boundary diagrams of Nayyar [44] and Wang [71] in figure 4.2. These stability boundary diagrams indicate the upper and lower critical strains, the strain from which wrinkling begins and at which the wrinkling decay, for membranes of different aspect ratios. By indicating these critical strains in an aspect ratio-strain diagram, a 'wrinkling region' can be separated from a 'no wrinkling region'. By adding the boundary which separates compressive stresses and no compressive stresses in figure 4.2, it can be seen that indeed, compressive stresses are present in all wrinkled situations.

It is important to note that compressive stress is thus a necessary condition for wrinkling, but not a sufficient condition. Situations exist in which compressive stresses are present in the membrane, but no wrinkling occurs.

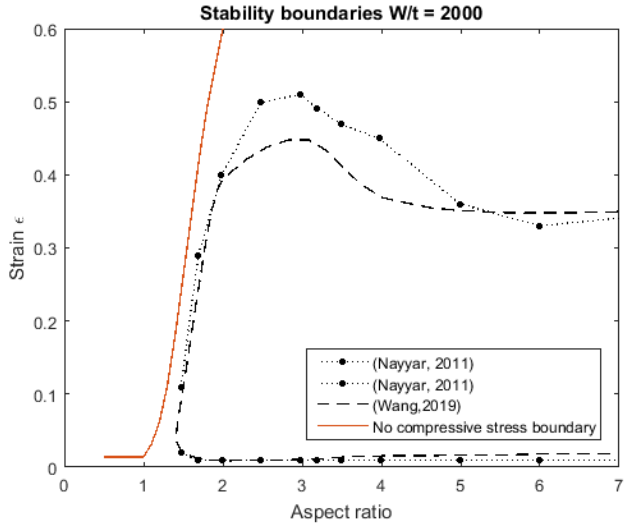

Figure 4.2: Stability boundary diagrams obtained by Nayyar [44] and Wang [71] obtained from non-linear wrinkling calculations. This stability boundary separates configurations which will wrinkle from configurations which will not wrinkle. No wrinkling will occur for membranes with an aspect ratio lower than $\alpha < 1.5$. For all other membranes the stability boundary indicates the lower and upper critical strain ε_1 and ε_2. The red boundary separates the region in which compressive stresses are present in the membrane (right from the red boundary) and the region in which no compressive stresses are present (left from the red boundary).

4.3. Isolated plate model

The previous section presented a binary indicator by which the susceptibility to wrinkling can be judged to be true or false. By considering the region of the membrane in which compressive stresses are presented as an isolated plate, a more precise indicator is searched for. The isolated plate is modelled as a rectangular plate subjected to biaxial stress.

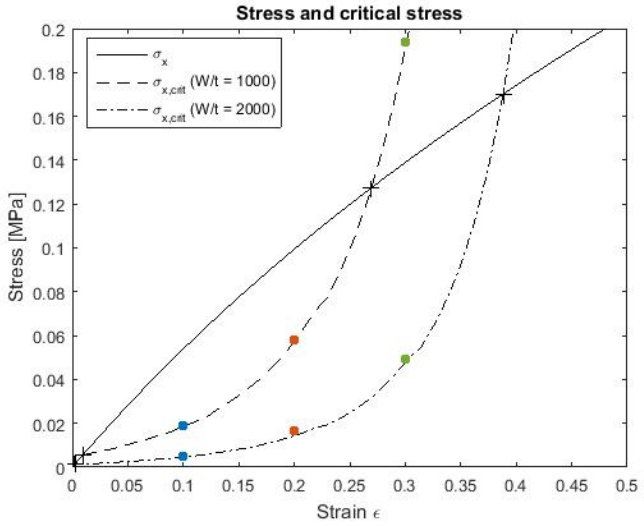

Figure 4.3: Stress-strain diagram and critical stress as a function of strain for $\beta = 1000$ and $\beta = 2000$ for a membrane of aspect ratio $\alpha = 2$. At a certain strain the membrane will wrinkle if the stress σ_x is higher than the critical stress $\sigma_{x,crit}$.

The critical stress for a rectangular plate subjected to biaxial stress can be estimated analytically. When modelling the compressive stress region as an isolated plate, the dimensions and loads on this isolated plate will depend on the strain. This leads to the fact that the calculated critical stress will depend on the strain as well. More details on this calculation are discussed in appendix A. Figure 4.3 shows the critical stress for two different plates. Also the actual stress is shown. For the strains for which the actual stress is larger than the critical stress, the plate will wrinkle. From the intersections between the actual stress and the critical stress, the critical strain can thus be estimated.

Figures 4.4a and 4.4b show the results which are obtained for different plates with different aspect ratios. This method can only be applied for plates in which the compressive stress region is clearly defined. That's why approximation of the critical strain is only indicated for a limited amount of plates.

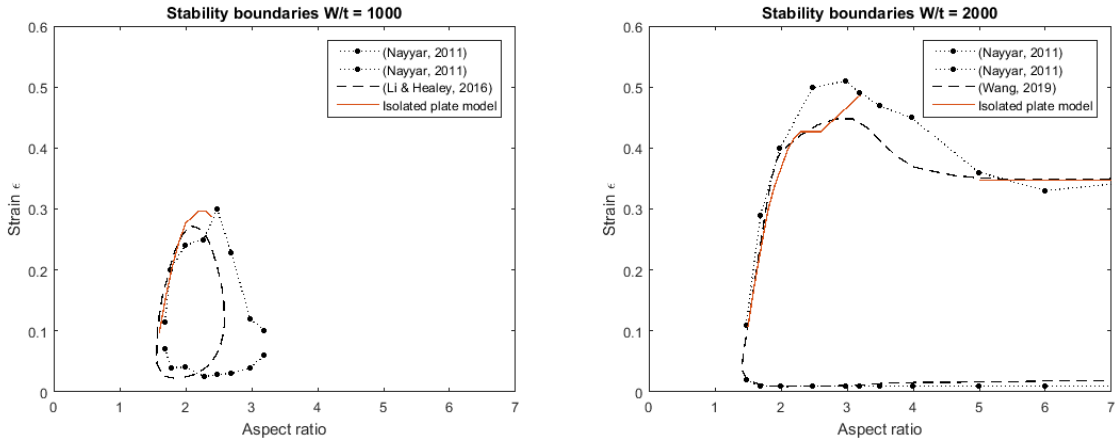

(a) (b)

Figure 4.4: Stability boundaries for membranes of thickness aspect ratio $\beta = 1000$ (a) and $\beta = 2000$ (b) from literature [33, 44, 71] togehter with the critical strain approximated by the isolated plate model for a limit number of aspect ratios.

4.4. Distribution of the compressive stresses

Literature suggests that the distribution of compressive stress can give insight in the location were wrinkles will form [16, 34, 44, 71]. To investigate this suggestion, figure 4.5 is made. This plot shows the most negative second principal stress for membranes of different aspect ratios, at different strains. By investigating the stress distribution, five different phases can be distinguished. In phase A, no compressive stresses are present in the membrane. This phase was already discussed in the previous section. Phases B-D give information on the location of the point with the most negative second principal stress and the stress distribution. In zone B the point with most negative second principal stress is located exactly in the middle of the membrane. Zone C indicates configurations for which the point with most negative second principal stress is located in the middle of the membrane longitudinally, but off centre in width direction. Zone D indicates membranes for which the point of most negative second principal stress is off-centre in the longitudinal direction.

Section 3.2.1. discussed wrinkle onset and concluded that the amount of wrinkle packets depends on the aspect ratio of the membrane. For membranes with an aspect ratio smaller than $\alpha = 4$, one packet of wrinkles will form. For larger membranes two separated wrinkle packets will form. Also at aspect ratio $\alpha = 4$, the compressive stress distribution splits from one zone to two separate zones which are in compression. This is in line with the suggestion that the compressive stress distribution is an indicator for the location were the membrane will wrinkle.

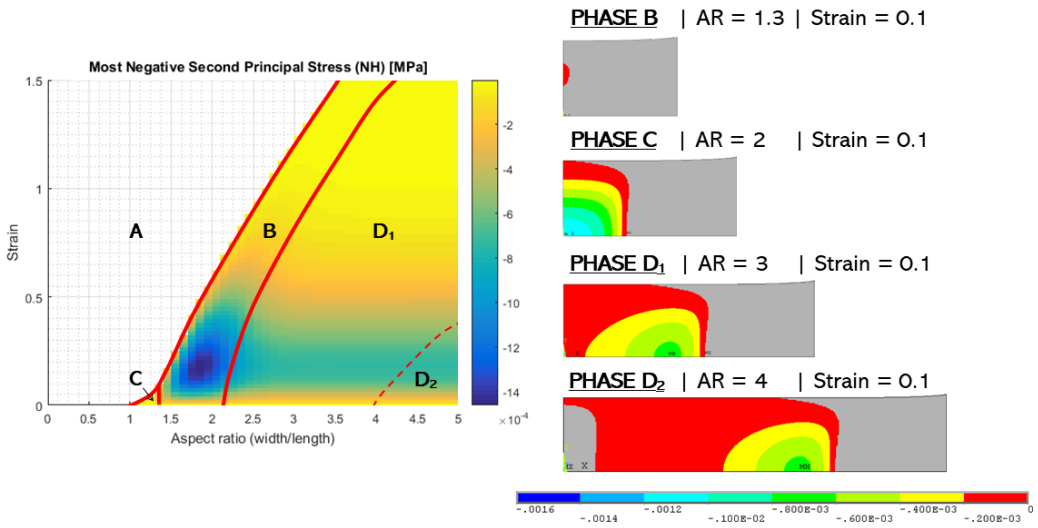

Figure 4.5: Phase diagram summarising the distribution of compressive stresses in membranes of different aspect ratios at different strains. The most negative second principal stress is shown in colour. In the white region, no compressive stresses are present (phase A). Phases B-D give information on the location of the point with the most negative second principal stress and the stress distribution. In zone B the point with most negative second principal stress is located exactly in the middle of the membrane. Zone C indicates configurations for which the point with most negative second principal stress is located in the middle of the membrane longitudinally, but off centre in width direction. Zone D indicates membranes for which the point of most negative second principal stress is off-centre in the longitudinal direction. The distribution of the second principal stress in zones B-D are illustrated at the right.

4.5. Conclusions

This chapter answered the question:
By which indicators can the wrinkling behaviour of a membrane be approximated?

This chapter discussed what we can learn about the wrinkling behaviour of a membrane with a certain aspect ratio without having to perform a non-linear wrinkling calculation, but on the basis of a calculation in which the membrane is strained without initial deformation. This calculation is easier and cheaper because no buckling modes have to be calculated. Furthermore, less elements are needed to calculate the distribution of the second principal stress than needed in a fully non-linear post-buckling calculation. This is discussed in appendix A. Therefore, in design and engineering practice, a study of the distribution of negative second principal stress will be more interesting than performing a fully non-linear wrinkling calculation.

Three *approximation* indicators were found:

- **Location of wrinkles on the membrane**
  The location of the compressive stress region in a flat, strained membrane is an indicator by which the location of the wrinkles in the membrane can be approximated.
- **Amplitude of the wrinkles**
  The size of the region on the membrane in which compressive stresses occur is an indicator by which the wrinkle amplitude can be approximated: the larger this area, the larger the wrinkle amplitude and vice versa.
- **Critical strains for which wrinkles occur and decay**
  By modeling the compressive stress region as an isolated simply supported plate subjected to uniform biaxial stress, the critical strains for which wrinkles occur and decay can be approximated.

Next to these three approximation indicators, it was found that compressive stresses are a necessity for wrinkling.
When there are no compressive stresses in the membrane, the membrane will not wrinkle.

5

Permeability

This section will answer the question:
How should holes be chosen such that wrinkling behaviour can be minimised in membranes?

As discussed previously (section 2.2.5), it is clear that wrinkling can be minimised or even be avoided by adding holes to the membrane. This section will investigate the underlying mechanisms with the goal of finding design rules by which wrinkle free permeable membranes can be created.

5.1. Approach

Previously the aim was expressed to minimise wrinkling behaviour of very large flexible floating structures. This is a necessity for safety and furthermore an improvement for the efficiency of very large flexible floating platforms. In this context, three different things can be considered which improve the safety and efficiency by wrinkling minimisation:

- The amplitude of the wrinkles in the improved membrane is lower than the amplitude of the wrinkles in the original membrane
- The area of the membrane which wrinkles is smaller for the improved membrane compared to the original membrane
- The range of strains for which wrinkling occurs $[\varepsilon_{crit,1}, \varepsilon_{crit,2}]$ is very small or is such that this range of strains can be avoided to occur as a loading in the application

The optimum in this minimisation process would be a membrane which does not wrinkle at all. So for all strains, the amplitude of the wrinkles is zero and the wrinkling area is zero.

As discussed before, a non-linear wrinkling calculation is computationally expensive, subjective and maybe not even working when no buckling modes can be found. Therefore, the previous chapter discussed alternative methods to make estimations on the wrinkling behaviour of a membrane without having to perform the non-linear wrinkling calculation. The main conclusion was that membranes in which no compressive stresses are present will never wrinkle. Therefore, membranes without compressive stresses are part of the optimal solution space. This is visualised in figure 5.1, to design right on the boundary of the solution space of wrinkle-free membranes, a non-linear wrinkling calculation is necessary. But since this calculation is expensive, membranes which are free of compressive stresses will be searched for. To guide this search, different candidate solutions will be compared to each other by the approximation methods which were discussed in chapter 4.

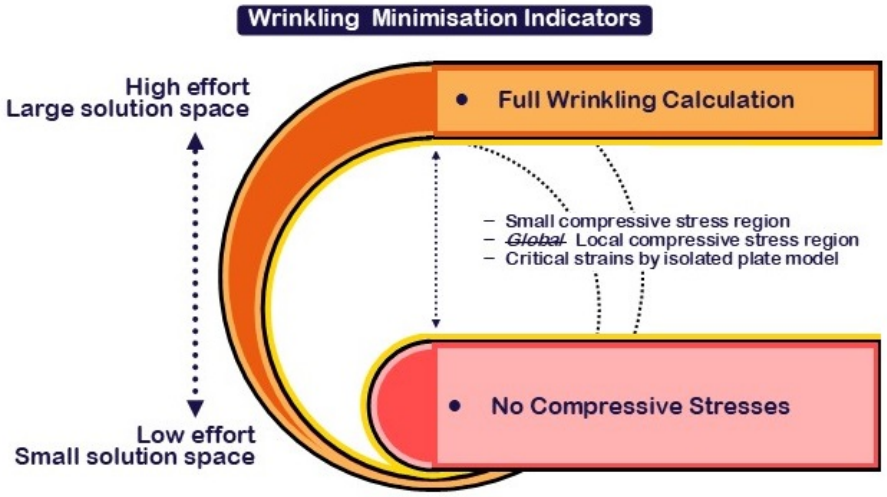

Figure 5.1: Wrinkling Minimisation Indicators

Optimisation of a rectangular uniaxially stretched membrane will be performed by adding permeability to the membrane. This permeability will exist of one or two holes in the membrane. To avoid searching for an optimal solution in an infinite domain, the design space is limited by the variation of the following parameters: the membrane aspect ratio, the permeability aspect ratio in width direction, the permeability aspect ratio in length direction, the location of the hole and the shape of the hole. Three different locations will be taken into account: a hole in the middle of the membrane, at the free edge of the membrane and at the clamped edge of the membrane. These three locations are chosen based on a wrinkle free membrane presented in literature and discussed in section 2.2.5 [31, 37]. The effect of two different shapes will be discussed: a circular hole and a hole formed by two parabola's (shown in figure 5.13). The permeability aspect ratio in width direction is defined as the ratio of the width of the hole to the width of the membrane. The permeability length aspect ratio is defined as the length of the hole to the length of the membrane. Note that these two parameters can be scaled separately for a hole shaped as a double parabola, but cannot be scaled separately for a circular hole. The effect of holes of different sizes, shapes and locations will be researched in three steps. All steps are summarised in table 5.1. For every step some of the variables will be varied, others will be kept constant.

Table 5.1: Three steps which will be taken to investigate the effect of the size, location and shape of a hole on the wrinkle behaviour of a membrane. Parameters which are varied are indicated by 'V', M/FE/CE indicated the middle, free edge and clamped edge of the membrane respectively.

	Step 1: Size	Step 2: Location	Step 3: Shape
Membrane aspect ratio	V	V	$\alpha = 2$
Permeability aspect ratio in width direction	V	V	V
Permeability aspect ratio in length direction	=	=	V
Location	M	FE / CE	M / FE / CE
Shape	Circle	Circle	Double Parabola

5.2. The influence of permeability on wrinkling

This section will discuss the effect of the size, location and shape of a hole in a membrane on the wrinkling behaviour of the membrane. The main goal is to find the mechanisms that can lead to minimisation or prevention of wrinkling behaviour.
The next subsection will discuss circular holes of different sizes in the middle of membranes with different aspect ratios. Subsection 5.2.2 will discuss the influence of the location of the permeability by investigating the effect of circular holes of different sizes at the clamped edge and at the free edge of membranes with different aspect ratios. In the thirth subsection, holes formed by two parabolas will be discussed. For these shapes, two permeability aspect ratios can be defined which will be varied separately.

5.2.1. Influence of the size of a hole on wrinkling

To start off the investigation of mechanisms which can lead to wrinkling minimisation by holes, the wrinkling behaviour of membranes of different aspect ratios with a circular hole in the middle of the membrane will be researched by the help of the wrinkling approximation indicators.
The design space for this first step is summarised in table 5.2. The shape of the permeability will not be varied in this step. The location of the permeability will not be varied either. All calculations will thus consider membranes with circular holes in the middle of the membrane. The aspect ratio of this membrane will be varied as well as the permeability aspect ratio. For a circular hole, this permeability aspect ratio is defined as the ratio of the diameter of the circle with respect to the width of the membrane. A small hole thus has a low permeability aspect ratio and a large hole in the same membrane has a higher permeability aspect ratio.

Table 5.2: Design space: aspect ratio and permeability aspect ratio

DESIGN SPACE	
Memrbane Aspect Ratio	$1 \leq \alpha \leq 5$
Permeability Aspect Ratio	$0.1 \leq D/W \leq 0.5$
Permeability Location	Constant (Middle)
Permeability Shape	Constant (Circle)

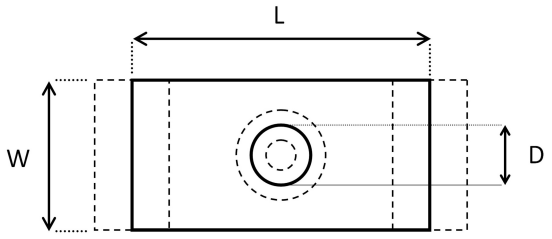

Figure 5.2: Design space: aspect ratio and permeability aspect ratio variable

The negative second principal stress regions for all membranes described in table 5.2 are summarised by the help of five different figures: figure 5.3a, figure 5.3b, figure 5.4, figure 5.5a and figure 5.5b.

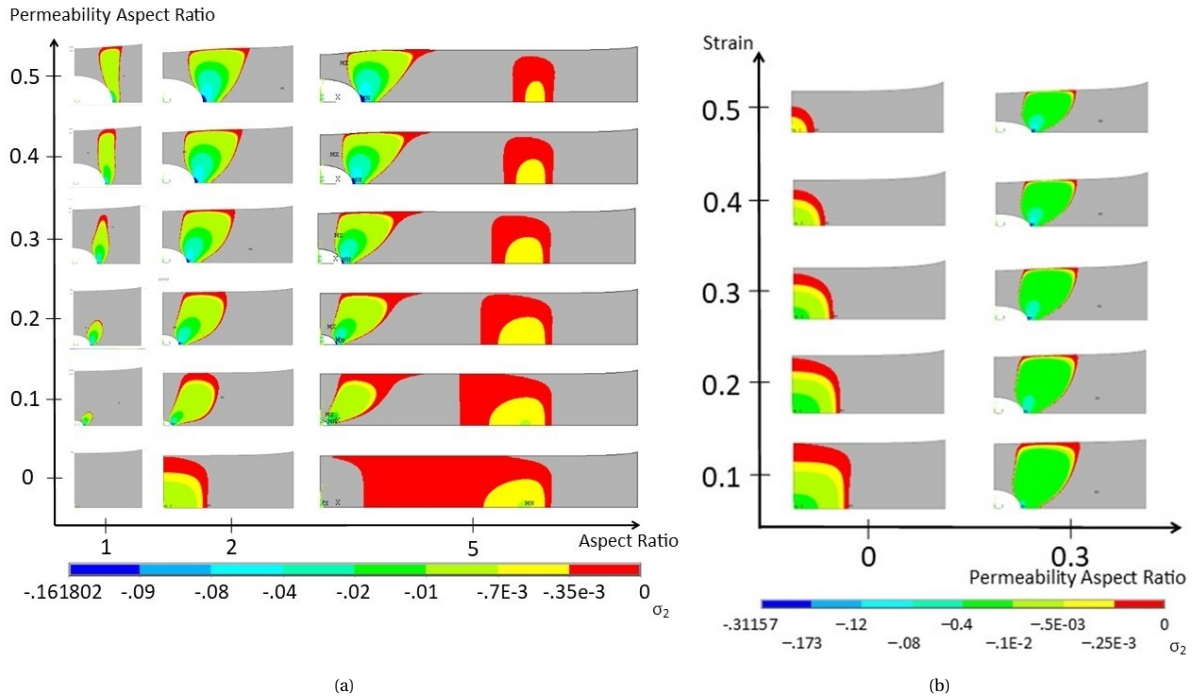

(a) (b)

Figure 5.3: (a) Overview of the negative second principal stress region for membranes of different aspect ratios with circular holes of different sizes at strain $\varepsilon = 0.15$. (b) Overview of the negative second principal stress region for membranes of aspect ratio $\alpha = 2$ for different strains.

Figure 5.3a gives a visual overview of the compressive stress distributions for membranes of aspect ratios $\alpha = 1$, $\alpha = 2$ and $\alpha = 5$, with circular holes in the middle of the membrane of permeability aspect ratio $D/W = 0.1$ up to $D/W = 0.5$. Also the compressive stress distributions of the non-permeable membranes are added.
To give an overview of the distribution of the compressive stress distribution in all membranes in the design space, a phase diagram is made. This phase diagram is shown in figure 5.4. From this phase diagram it can be seen that all compressive stress distributions can be categorised into four phases. In all of these phases, compressive stresses are present at the location of the hole. This compressive stress region can stretch all the way to the free edge of the membrane. Furthermore, a compressive stress region can occur in between the circular hole and the clamped edge.

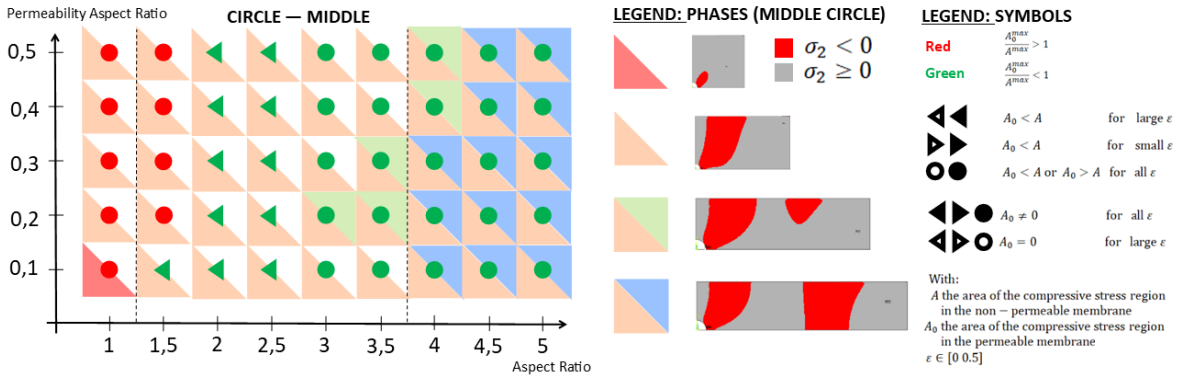

Figure 5.4: Overview of the shape and area of the negative second principal stress region region for membranes of different aspect ratios with a hole in the middle of the membrane.

Figure 5.3b gives a visual representation of the compressive stress region as a function of the strain for a membrane with aspect ratio $\alpha = 2$ and a permeability aspect ratio of $D/W = 0.3$, next to a non-permeable membrane. From this figure it can be seen that the area of the compressive stress region and the magnitude of the compressive stress as a function of strain behaves differently for the permeable and non-permeable membrane. To quantify this effect, figures 5.5a and 5.5b are made. In these figures, the area of the compressive stress region and the magnitude of the compressive stresses as a function of the strain are compared with the compressive stresses in the non-permeable membrane. The maximal area of the compressive stress region is an indicator for the wrinkle amplitude and when the area of compressive stresses is zero, no wrinkling will occur. Therefore, it is interesting to study the maximum of this graph and compare it to the non-permeable membrane. Also the trend of the area as a function of the strain is of interest. For the membrane of aspect ratio $\alpha = 2$, the indicator predicts that the amplitude of the wrinkles in the permeable membranes will be smaller than the wrinkle amplitude in the non-permeable membrane. It can also be seen that, for large strains, the non-permeable membrane will be wrinkle free while the permeable membrane might still be susceptible to wrinkling.

For membranes of other aspect ratios, the conclusions on the area of the compressive stress region as a function of the strain are summarised by a symbol in figure 5.4:

- The colour of the symbol indicates whether the maximal area of the compressive stress region as a function of the strain in the permeable membrane is larger than, or smaller than the maximal area of the compressive stress region in the non-permeable membrane.
- Open symbols indicate configurations for which all compressive stresses disappear before a strain of $\varepsilon = 0.5$. Configurations for which compressive stresses are present in the membrane for all strains up to $\varepsilon = 0.5$ are indicated with a closed symbol.
- Circles represent membranes for which the area of the compressive stress region is larger or smaller than the non-permeable version of the membrane for all strains up to $\varepsilon = 0.5$. Arrows indicate configurations for which the area of the compressive stress region is larger in the permeable membrane than in the non-permeable membrane for low strains, but smaller for low strains and vice versa.

The trend of the area of the compressive stress region as a function of the strain for a membrane of aspect ratio $\alpha = 2$ as shown in figure 5.5a can be recognised by a green, arrow shaped, closed symbol in figure 5.4. The maximal area of compressive stress is lower for the permeable membranes than for the non-permeable membrane (green). For small strains the area of compressive stress in the permeable membranes is smaller than for the non-permeable membrane, but for high strains this is the other way around (left pointing arrow). The area of the compressive stress region is non-zero for all permeable membranes for strains up to $\varepsilon = 0.5$ (closed symbol).

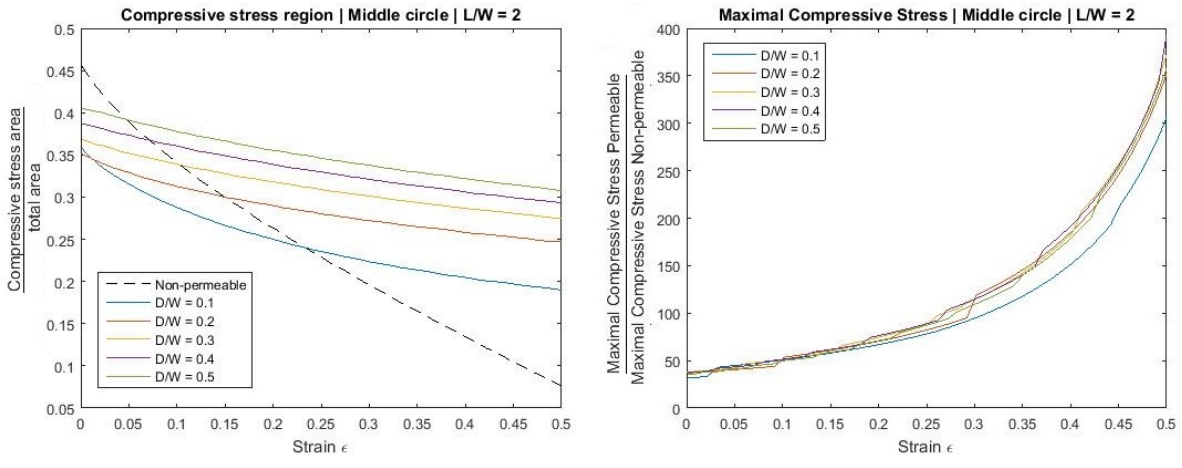

(a) (b)

Figure 5.5: (a) Area of the negative second principal stress region as a function of strain for membranes of aspect ratio $\alpha = 2$ with holes of different sizes in the middle of the membrane. (b) Magnitude of the most negative second principal stress region for the same membranes.

Observations on the influence of a circular hole in the middle of a membrane on the wrinkling behaviour
From studying the compressive stress distribution for membranes of different aspect ratios with circular holes of different sizes at the middle of the membrane, two conclusions can be made which hold for all studied configurations:

- From the phases which are shown 5.4, it can be seen that in all four observed stress distributions, compressive stresses will be present around the circular hole. This indicates that the region around the hole will be susceptible to wrinkling in all configurations.
- No open symbols can be seen in figure 5.4. The absence of open symbols indicates that the compressive stresses will be non-zero for all strains which are taken into consideration, for all configurations.

The presented results were obtained to study the influence of the size of a hole on wrinkling. It appeared that membranes of different sizes behave differently due to the presence of a hole, but the exact size of a hole is of less influence. From section 4.4 and figure 4.5 it was concluded that the compressive stress distribution in non-permeable membranes can be categorised in three different phases, depending on the strain and the aspect ratio. No compressive stresses are present in membranes with aspect ratios smaller than $\alpha = 1$. For membranes with aspect ratios from $\alpha = 1.5$ up to $\alpha = 4$, one central compressive stress region can be observed. For membranes with high aspect ratios, the initial compressive stress distribution is split into two regions. From the study on the influence of a circular hole in the middle of a membrane, it is observed that the effect of the hole depends on the distribution of the negative second principal stress in the non-permeable membrane:

- In membranes with small aspect ratios, no compressive stresses are present in the non-permeable membrane. However, compressive stresses are present in the permeable membranes of these small aspect ratios. The non-permeable membranes are therefore not susceptible to wrinkling while their permeable versions are. Wrinkling will occur in the region close to the hole.
- The compressive stress distribution of non-permeable membranes of intermediate aspect ratios is defined by one central compressive stress region. A central hole divides this compressive stress region into two smaller regions. Furthermore, for high strains, the compressive stress region has disappeared in the non-permeable membrane, while compressive stresses are still present in the permeable membrane. This indicates that the wrinkle amplitude in the permeable membrane will be lower than in the non-permeable membrane, but the permeable membrane will be susceptible for wrinkling for a larger range of strains than the non-permeable membrane.
- The two large compressive stress regions which exist in non-permeable membranes of large aspect ratios will each be split again in two when adding a hole in the middle of the membrane. The compressive stress regions have a smaller area which indicates that the maximal wrinkle amplitude will be smaller than in the non-permeable membrane. But potentially four wrinkle packets might appear instead of two packets as in the non-permeable membrane.

5.2.2. Influence of the location of a hole on wrinkling

Section 5.2.1 researched the influence of holes in the middle of a membrane. Both the permeability aspect ratio and the membrane aspect ratio were varied. To investigate the effect of the location of the hole, the research will be repeated for membranes with holes at the free edges and at the clamped edges of the membranes. A sketch of these configurations can be seen in figure 5.6. Again, not only the permeability aspect ratio will be varied. The membrane aspect ratio is varied as well, to study the influence of holes of different sizes in membranes of different sizes. All variations are summarised in table 5.3.

Table 5.3: Design space: Location

DESIGN SPACE	
Memrbane Aspect Ratio	$1 \leq \alpha \leq 5$
Permeability Aspect Ratio	$0.1 \leq D/W \leq 0.5$
Permeability Location	(Middle,) Clamped edge and Free edge
Permeability Shape	Constant (Circle)

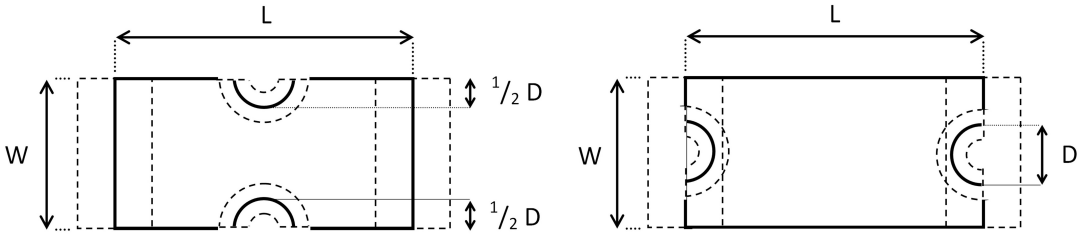

Figure 5.6: Sketch of the design space: location. Holes at the free edges of the membrane are shown at the left. Holes at the clamped edges of the memrbane are shown at the right.

Again, the influence of the permeability on the wrinkling behaviour of membranes will be studied by the help of the wrinkling indicators. For this study, similar figures as in section 5.2.1 are made which summarise the distribution of compressive stresses in the different membranes, the area of the compressive stress region in the different membranes and the magnitude of the compressive stress. For holes at the free edges of the membranes, visual representations of the compressive stress distribution for different configurations are shown in figures 5.7a and 5.8a. Also the change of the distribution of compressive stresses as a function of the strain is shown visually, in figures 5.7b and 5.8b. The change of the area of the compressive stress region and the magnitude of the compressive stresses as a function of the strain is quantified in figures 5.11a, 5.11b, 5.12a and 5.12b for membranes of aspect ratio $\alpha = 2$. A phase diagram which summarises the compressive stress distribution and the area of the compressive stress region as a function of the strain for all investigated configurations is shown in figure 5.9 for holes at the free edges of the membrane and in figure 5.10 for holes at the clamped edges of the membrane.

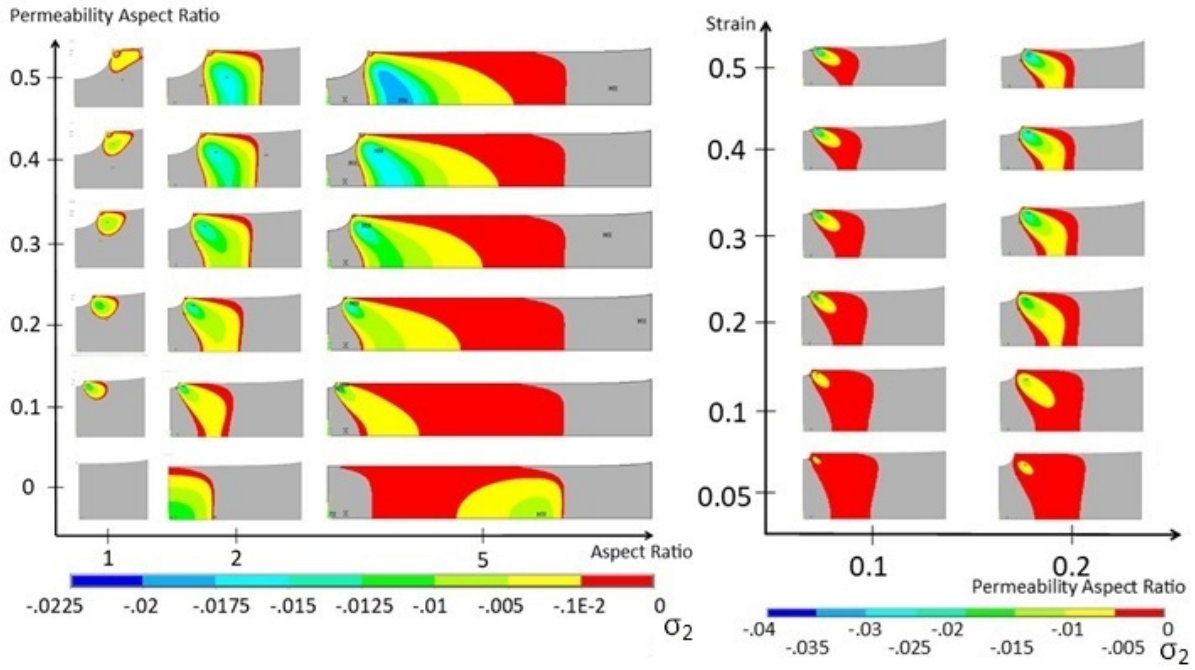

(a) (b)

Figure 5.7: (a) Overview of the negative second principal stress region for membranes of different aspect ratios with circular holes of different sizes located at the free edge at strain $\varepsilon = 0.15$. (b) Overview of negative second principal stress region for membranes of aspect ratio $\alpha = 2$ for different strains.

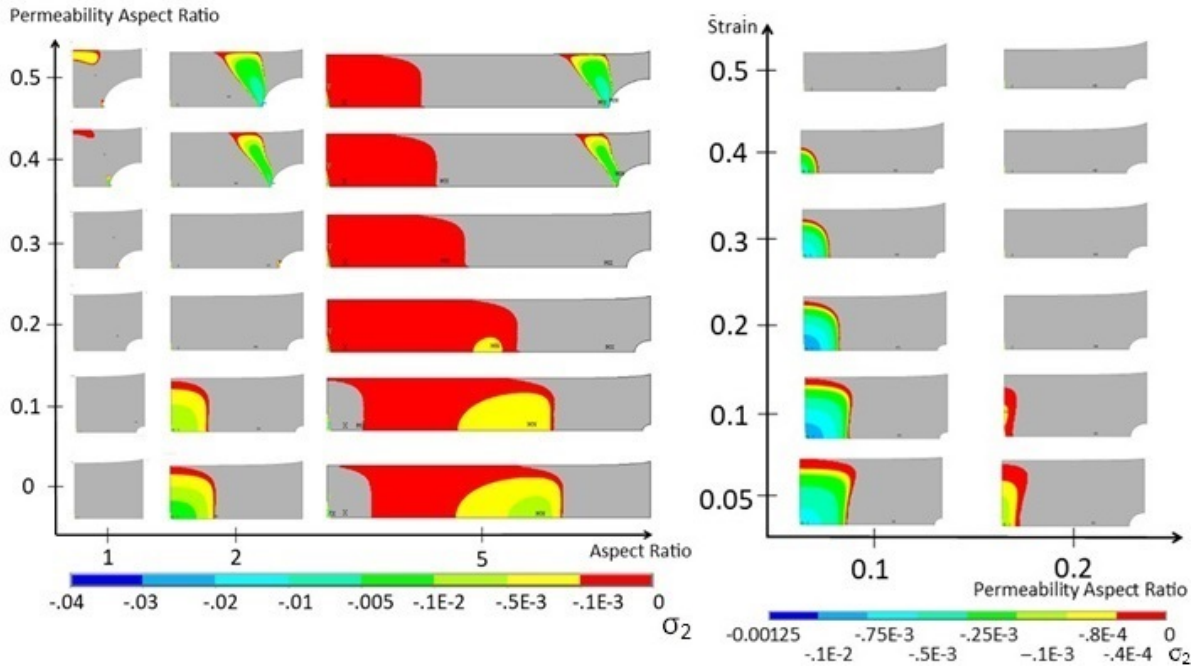

(a) (b)

Figure 5.8: (a) Overview of the negative second principal stress region for membranes of different aspect ratios with circular holes of different sizes located at the clamped edge at strain $\varepsilon = 0.15$. (b) Overview of negative second principal stress region for membranes of aspect ratio $\alpha = 2$ for different strains.

.

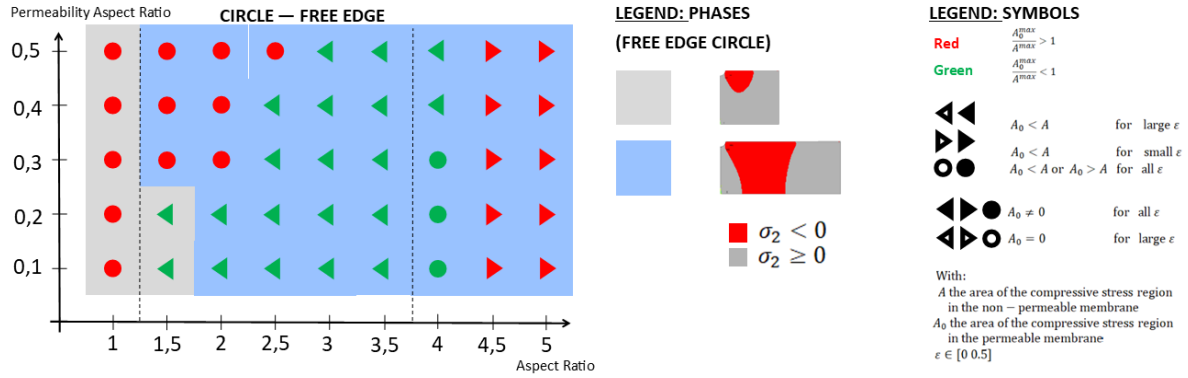

Figure 5.9: Overview of the shape and area of the negative second principal stress region for membranes of different aspect ratios with a hole at the free edges of the membrane.

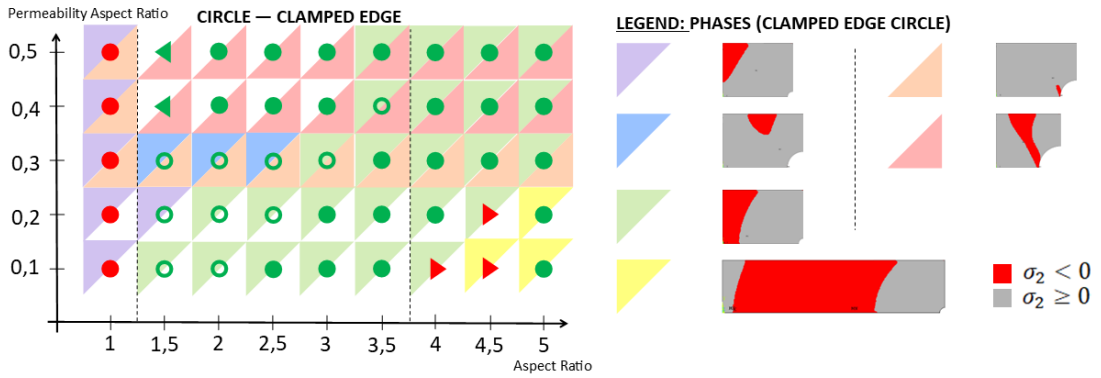

Figure 5.10: Overview of the shape and area of the negative second principal stress region for membranes of different aspect ratios with a hole at the clamped edges of the membrane. The legend of the symbols is identical to the legend of the symbols in figure 5.9

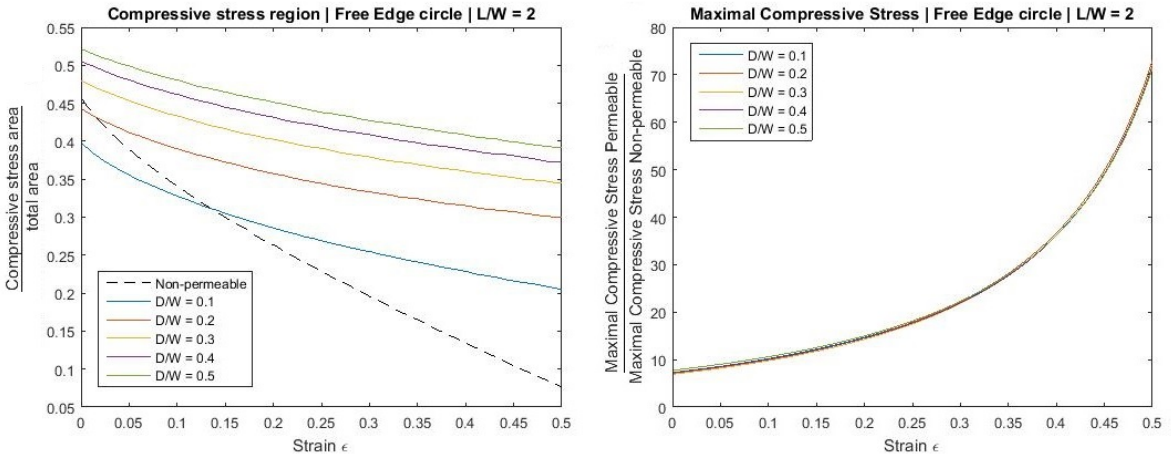

(a) (b)

Figure 5.11: (a) Area of the negative second principal stress region as a function of strain for membranes of aspect ratio $\alpha = 2$ with holes of different sizes at the free edge of the membrane. (b) Magnitude of the most negative second principal stress region for the same membranes

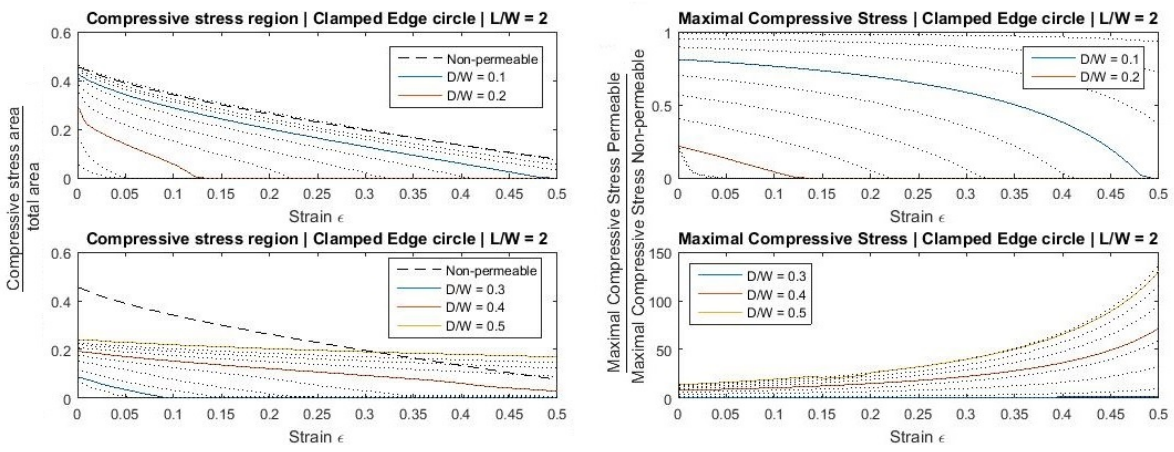

(a) (b)

Figure 5.12: (a) Area of the negative second principal stress region as a function of strain for membranes of aspect ratio $\alpha = 2$ with holes of different sizes at the clamped edge of the membrane. (b) Magnitude of the most negative second principal stress region for the same membranes

From the phase diagram in figure 5.9, it can be seen that when a hole is added at the free edges of the membrane, only two different phases of the stress distribution can be observed. In membranes of small aspect ratios, four regions of compressive stress will form. One in every quarter of the membrane, next to the hole. In membranes of large aspect ratios, two large compressive stress regions can be observed. One at every side of the hole in length direction, extending over the full width of the membrane.
Figure 5.10 shows that more different phases occur when the hole is located at the clamped edge of the membrane. In general it can be observed that the region of compressive stresses in the non-permeable membrane is reduced in size when a small hole is added at the clamped edge of the membrane. When a large hole is added however, an extra region of compressive stresses will occur around this hole.

Observations on the influence of a circular hole at the free edges of a membrane on the wrinkling behaviour
Based on the distribution of the compressive stresses as shown in figure 5.9 and the area of the compressive stress region as a function of strain, two conclusions can be drawn which hold for all studied membranes with a circular hole at the free edge:

- In all configurations, compressive stresses can be seen around at the circular hole. This implies that all membranes will be susceptible for wrinkling in this region.
- For all studied configurations, the stresses in the membranes are non-zero for strains up to at least $\varepsilon = 0.5$. This indicates that all configurations will be susceptible to wrinkling up to this strain.

Also, observations can be made which only hold for specific groups of membranes. Just as for the membranes with holes in the middle, the effect of holes at the free edges of the membrane depends on the distribution of the compressive stresses in the non-permeable membranes. Therefore, again conclusions will be drawn for memrbanes of small, intermediate and large aspect ratios separately.

- For small aspect ratios, no compressive stresses are present in non-permeable membranes. The presence of a hole however introduces a compressive stress region. In terms of wrinkling, this indicates that the permeable membranes will be susceptible to wrinkling while the non-permeable membranes are not.
- The compressive stress distribution in non-permeable membranes of intermediate aspect ratios consists of one central region. This region is split into two smaller regions by the addition of holes at the free edges of the membranes. The smaller size of the compressive stress region indicates that the wrinkle amplitude will be smaller as well. It is important to notice however, that for large strains, the compressive stresses in the non-permeable membranes have already disappeared while they are still present in the permeable membranes. This indicates that the upper critical strain ε_2 for the permeable membranes will be higher than for their non-permeable version.

- For membranes of large aspect ratios, the size of the compressive stress region in the permeable membrane is larger than in the non-permeable membrane. Also the magnitude of the compressive stress is larger than in the non-permeable membrane. A hole at the free edges will thus not lead to minimisation of the wrinkling behaviour.

Note that the conclusions which hold for all configurations with holes at the free edges of the membranes and the conclusions which hold for membranes of small aspect ratios are similar to the conclusions which were drawn for membranes with holes at the middle of the membrane. The effects of these holes are analogous.

Observations on the influence of a circular hole at the clamped edges of a membrane on the wrinkling behaviour

For the third time, the same conclusion can be drawn on the influence of holes in membranes of small aspect ratios. The non-permeable membranes of small aspect ratios are free of compressive stresses, while compressive stresses form in the permeable versions of the membrane. In terms of wrinkling this indicates that the non-permeable membranes are not susceptible to wrinkling while the permeable membranes are. Contrary to the situation in which holes are located at the free edge and in the middle of the membrane, it is not necessarily the region next to the hole which will be susceptible to wrinkling. The permeable membranes will be susceptible to wrinkling at the middle symmetry axis for small holes and also near the hole for large holes.

For membranes of intermediate and large aspect ratios, the influence of the hole on the wrinkling behaviour of the membrane not only depends on the aspect ratio of the membrane, but also on the size of the holes.

- When a small hole is added in a membrane with an intermediate aspect ratio, the size of the compressive stress region will be reduced. Furthermore, the stresses will disappear earlier than in non-permeable membranes as a function of the strain. In terms of wrinkling, this indicates that the amplitude of wrinkles in the permeable membranes will be smaller than the amplitude of the wrinkles in non-permeable membranes. The upper critical strain ε_2 for the permeable membrane will be smaller than for the non-permeable membrane.
- When a large hole is added in a membrane with an intermediate aspect ratio, the central region of compressive stresses which is present in the non-permeable membrane disappears completely. A smaller region with compressive stresses will be present around the hole at every side of the membrane. Wrinkling will thus take place at another location in the permeable membranes than in the non-permeable membranes. The size of the compressive stress region is smaller, indicating that the amplitude of the wrinkles will be smaller.
- For membranes with large aspect ratios, three different effects can be seen depending on the size of the hole. For a very small hole, the influence of the hole is very limited on the wrinkling behaviour. Intermediate holes will lead to the situation in which one central region of compressive stress is present in the membrane. In the non-permeable membrane, two wrinkle packets will be formed, in the permeable membrane only one, central wrinkle packet will form. Large holes will lead to an extra region of compressive stress, next to the hole. This indicates that multiple wrinkle packets can form because multiple regions in the membrane are susceptible to wrinkling.

5.2.3. Influence of the shape of a hole on wrinkling

The previous two subsections researched the influence of circular holes of different sizes on the wrinkling behaviour of membranes of different sizes. This section will focus on the shape of the hole. To limit the amount of variables which are varied, the aspect ratio of the membrane is set constant to $\alpha = 2$. A hole will be studied which is formed by two parabola's. This shape shape is illustrated in figure 5.13. The hole is scaled in length and width direction separately. Therefore, two aspect ratios are defined: the permeability aspect ratio in length direction l/L and the permeability aspect ratio in width direction w/W. Figure 5.13 illustrates holes for which these two aspect ratios are varied, one at a time. For holes at the middle of the membrane, the free edges and the clamped edges.

Table 5.4: Design space: shape

DESIGN SPACE	
Membrane Aspect Ratio	Constant ($\alpha = 2$)
Permeability Aspect Ratio in width direction	$0.1 \leq w/W \leq 0.5$
Permeability Aspect Ratio in length direction	$0.1 \leq l/L \leq 0.9$
Permeability Location	Middle, Clamped edge and Free edge
Permeability Shape	Constant (Double parabola)

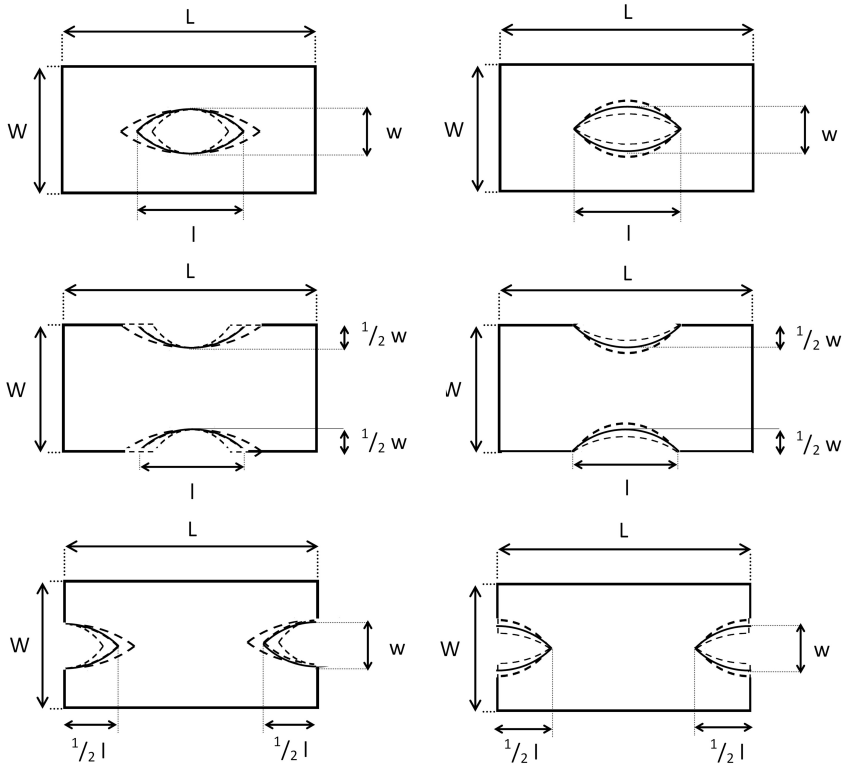

Figure 5.13: Sketch of the design space: shape

The same types of graphs as used to study the influence of the size and location of a hole will be used again. Visual representations of the influence of holes of different sizes are given in figures 5.14a, 5.17a and 5.21a. Also their behaviour as a function of the strain is visualised, in figures 5.14b, 5.17b and 5.21b. The exact area of the compressive stress region and the magnitude of the maximal compressive stress as a function of the strain for holes with a permeability aspect ratio in width direction of 0.2 and varying permeability aspect ratios in length direction are shown in figures 5.16a, 5.16b, 5.19a, 5.19b, 5.23a and 5.23b. A summary on the distribution of the compressive stresses and the area of the compressive stress region for all membranes is shown in figures 5.15, 5.18 and 5.22 by phase diagrams.

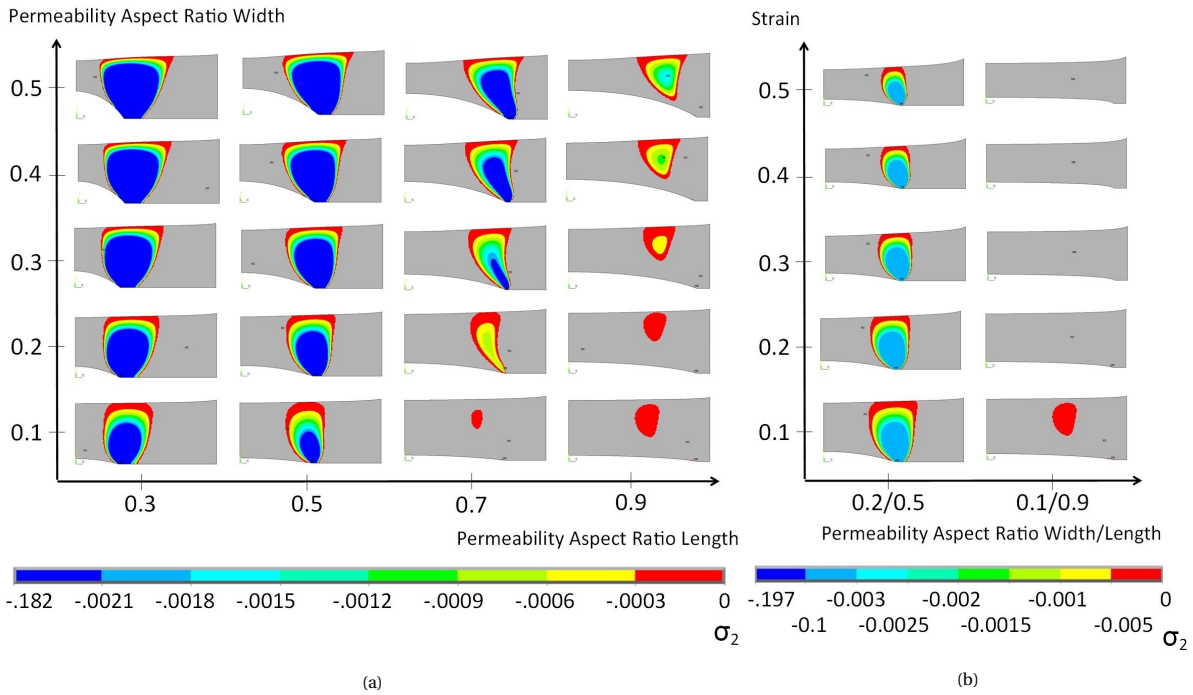

Figure 5.14: Distribution of the negative second principal stress for membranes of aspect ratio $\alpha = 2$ with holes in the shape of a double parabola of different sizes, at three different locations: in the middle of the membrane for a strain of $\varepsilon = 0.1$ (a) and for varying strain (b)

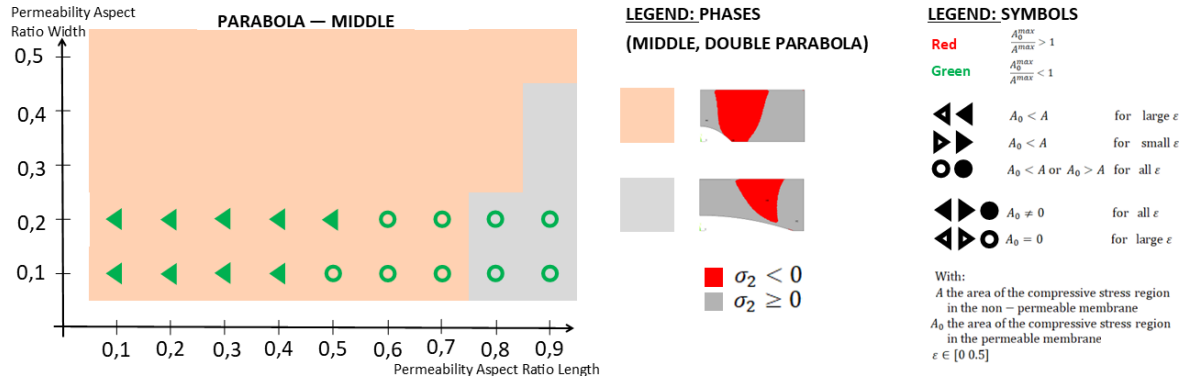

Figure 5.15: Phase diagram describing the distribution of the negative second principal stress in membranes of aspect ratio $\alpha = 2$ with a hole in the shape of a double parabola in the middle of the membrane, for different sizes of the hole. The symbols described the change of the area of the membrane in which the second principal stress is negative as a function of the strain. Due to convergence problems, no symbols are shown for permeability aspect ratio in width direction larger than 0.2.

.

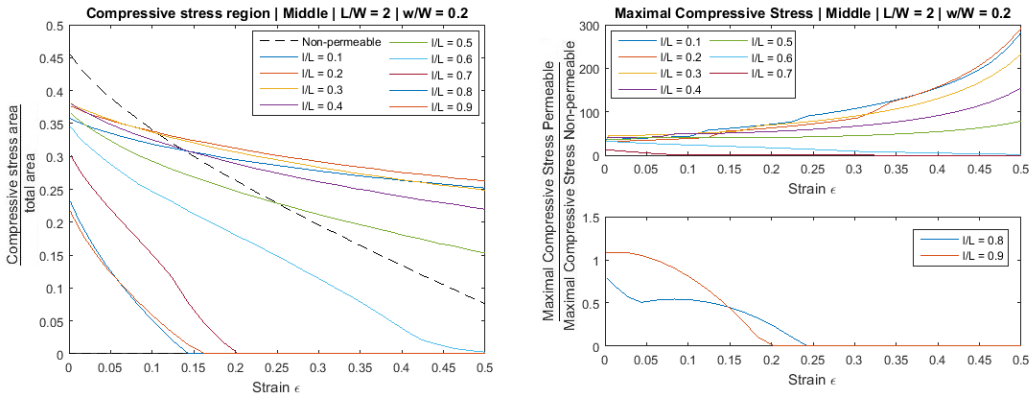

(a) (b)

Figure 5.16: (a) Size of the negative compressive stress region (a) and magnitude of the most negative compressive stress (b) as a function of strain in membranes with aspect ratio $\alpha = 2$ with holes in the shape of a double parabola in the middle of the membrane. All a permeability aspect ratio in width direction of $w/W = 0.2$ and varying sizes in length direction.

Observations on the influence of the shape of a hole at the middle of a membrane on the wrinkling behaviour

The influence of the shape of holes on the wrinkling behaviour of a membrane is studied by the help of the graphs in figures 5.14a, 5.14b, 5.15, 5.16a and 5.16b. From these figures, results are drawn on the influence of the permeability aspect ratio in length direction and the permeability aspect ratio in width direction:

- A hole in the middle of the membrane of aspect ratio $\alpha = 2$ will split the compressive stress region which occurs in the non-permeable membrane into two or four smaller regions. For holes with a small permeability aspect ratio in length direction, the compressive stress region is split into two regions which stretch over the full width of the membrane. A very long hole ($l/L = 0.9$) will split each of these two compressive stress regions into two leading to a total of four small compressive stress regions in the membrane. The area of these compressive stress regions is smaller than the area of the central compressive stress region in the non-permeable membrane, thus indicating that the amplitude of the wrinkles in the permeable membranes will be smaller compared to the amplitude of the wrinkles in the non-permeable membrane.
  From figures 5.16a and 5.16b and from the symbols in figure 5.15 it can furthermore be seen that, for membranes with holes of long permeability aspect ratios, the compressive stresses disappear as a function of the strain before they have disappeared in the non-permeable membrane. This indicates that the upper critical strain for membranes with a hole with a long permeability aspect ratio in the middle of the membrane will be lower than for non-permeable membranes.

- From figure 5.14a also the influence of the width of the hole can be studied. In general it can be concluded that the region with compressive stresses becomes smaller when the width becomes smaller. Also the magnitude of the compressive stresses becomes smaller when the width of the holes become smaller. In terms of wrinkling this indicates that a small hole should be preferred over a wide hole to minimise wrinkling.

- When the membrane of aspect ratio $\alpha = 2$ is cut into two in length direction, two membranes of aspect ratio $\alpha = 4$ will remain. For membranes of aspect ratio $\alpha = 4$ it is known that two separate compressive stress regions and two separate wrinkle packets will form (section 4.4). This limit case can be recognised when studying the membrane with a hole of aspect ratio 0.9 in length and 0.1 in width direction in figure 5.14a.

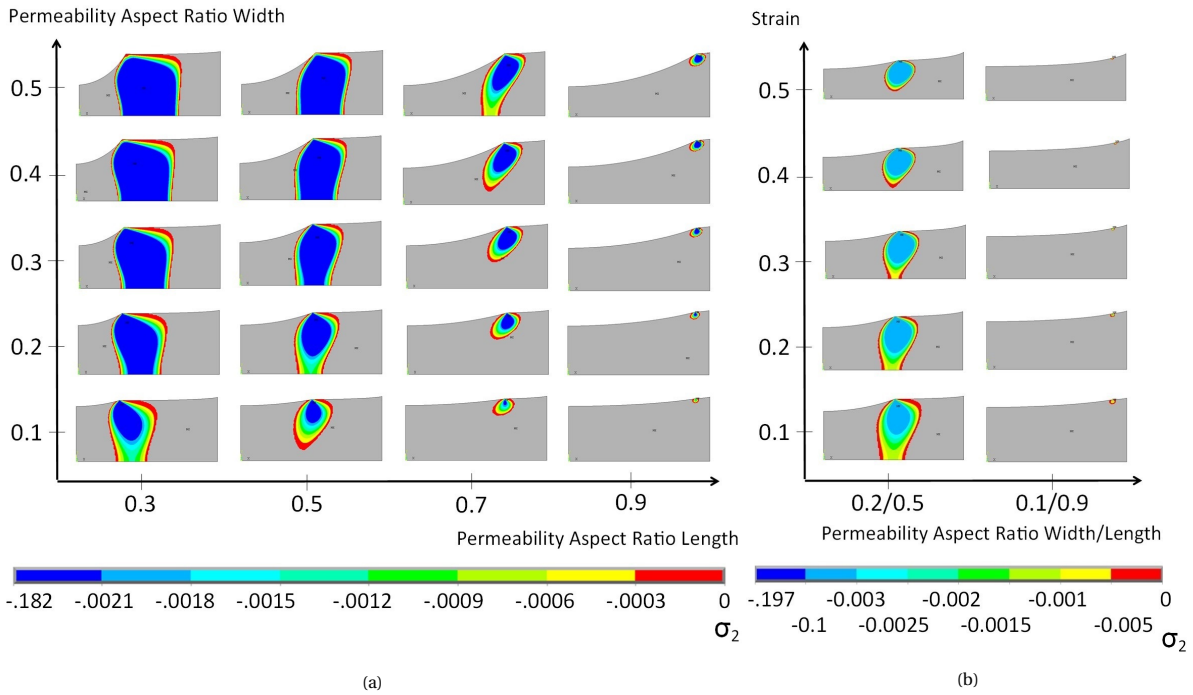

Figure 5.17: Distribution of the negative second principal stress for membranes of aspect ratio $\alpha = 2$ with holes in the shape of a double parabola of different sizes, at three different locations: in the middle of the membrane for a strain of $\varepsilon = 0.1$ (a) and for varying strain (b)

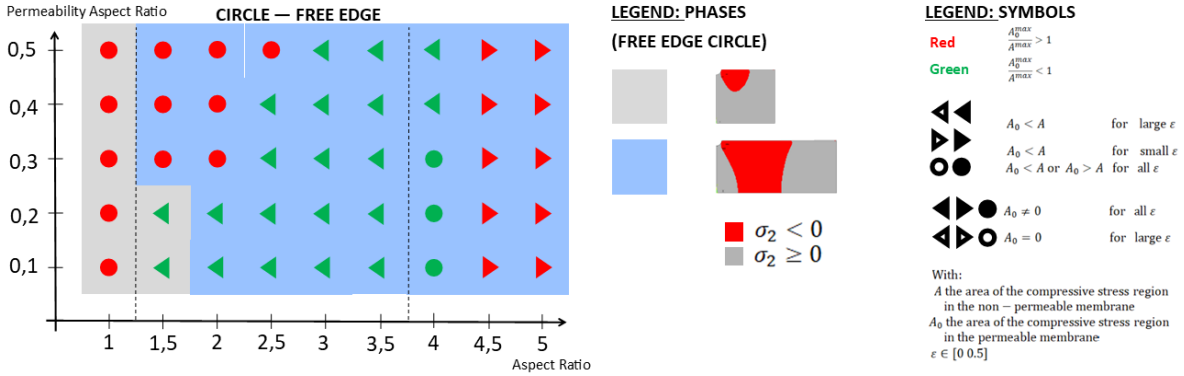

Figure 5.18: Phase diagram describing the distribution of the negative second principal stress in membranes of aspect ratio $\alpha = 2$ with a hole in the shape of a double parabola at the free edge of the membrane, for different sizes of the hole. The symbols described the change of the area of the membrane in which the second principal stress is negative as a function of the strain.

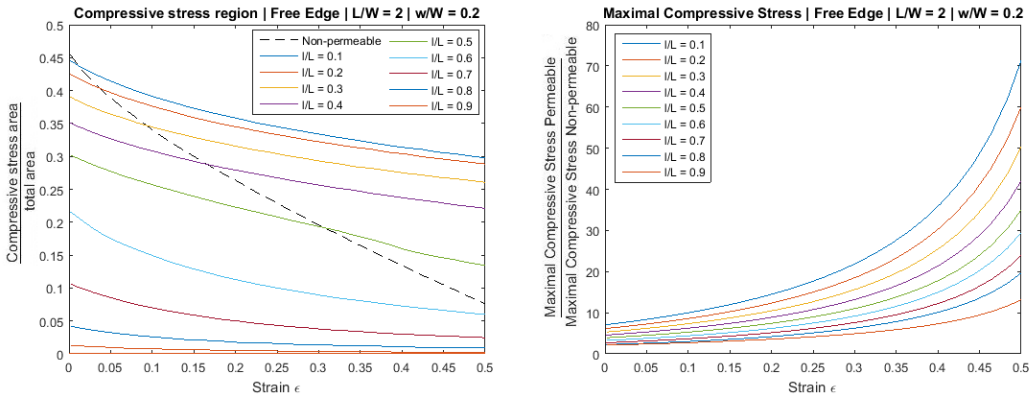

(a) (b)

Figure 5.19: (a) Size of the negative second principal stress region (a) and magnitude of the most negative second principal stress (b) as a function of strain in membranes with aspect ratio $\alpha = 2$ with holes in the shape of a double parabola at the free edge of the membrane. All having a permeability aspect ratio in width direction of $w/W = 0.2$ and varying sizes in length direction.

Observations on the influence of the shape of a hole at the free edges of a membrane on the wrinkling behaviour

An overview of the compressive stress distribution in membranes with holes of different sizes at the free edges are shown in figures 5.17a, 5.17b, 5.18, 5.19a and 5.19b. As was the case for circular holes, for parabolically shaped holes, the effect of holes at the free edges of the membrane and at the middle of the membrane is similar:

- By adding a parabolic hole at the free edges of the membrane, the central compressive stress region which is present in a non-permeable membrane of aspect ratio $\alpha = 2$ is split into two or four smaller regions. The compressive stress region is split into two smaller regions for holes with short and intermediate length. It is split into four regions when a long hole is present in the membrane. Smaller regions indicate that the wrinkle amplitude will be smaller.
  As can be seen from the graphs in figures 5.19a and 5.19b and from the symbols in figure 5.18, compressive stresses will remain in the membrane for high strains, at which the compressive stresses have already disappeared in the non-permeable version of the membrane. This indicates that the upper critical strain will be higher for the permeable membranes than for the non-permeable membranes.
- The influence of the width of the hole can be studied from figure 5.18. In general it can be concluded that the smaller the hole, the smaller the compressive stress region will be. Indicating that the wrinkle amplitude will be smaller as well.
- Figure 5.20 also shows a limit case: a membrane with a hole of permeability aspect ratio in length direction equal to one. When the full length of the free edge is parabolically shaped, it can be seen that no compressive stresses are present in the membrane. In terms of wrinkling, this means that the membrane will be wrinkle free for all strains.

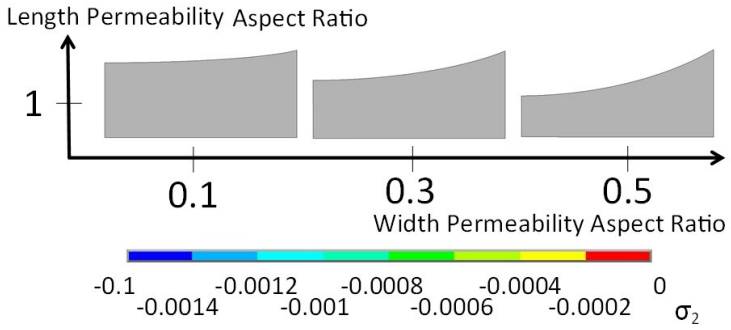

Figure 5.20: Distribution of the negative second principal stress for membranes of aspect ratio $\alpha = 2$ with parabolically shaped holes at the free edge of the membrane at a strain of $\varepsilon = 0.1$

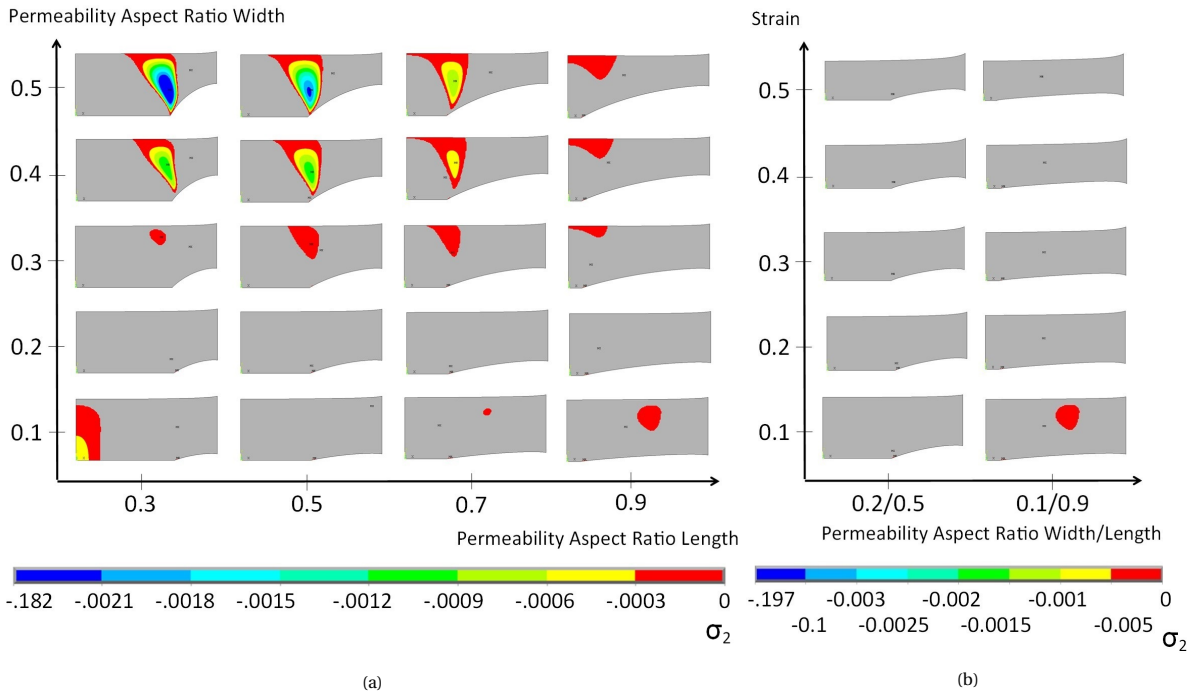

Figure 5.21: Distribution of the negative second principal stress for membranes of aspect ratio $\alpha = 2$ with holes in the shape of a double parabola of different sizes, at three different locations: in the middle of the membrane for a strain of $\varepsilon = 0.1$ (a) and for varying strain (b)

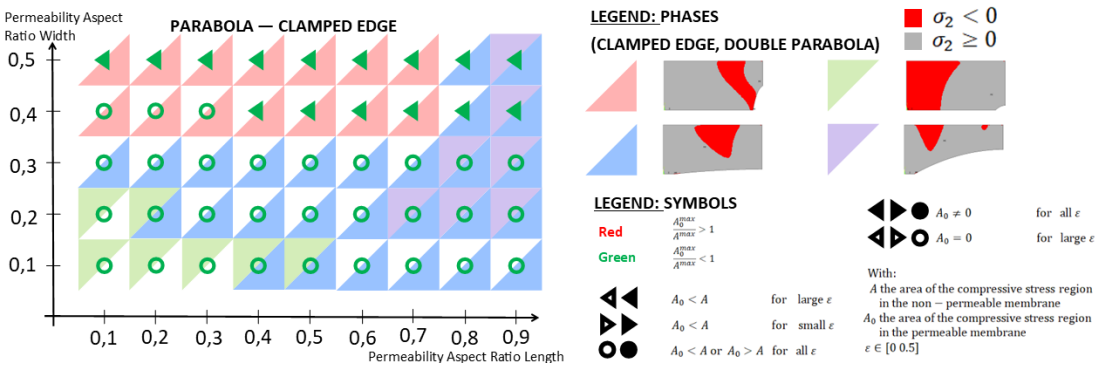

Figure 5.22: Phase diagram describing the distribution of the negative second principal stress in membranes of aspect ratio $\alpha = 2$ with a hole in the shape of a double parabola at the clamped edge of the membrane, for different sizes of the hole. The symbols described the change of the area of the membrane in which the second principal stress is negative as a function of the strain.

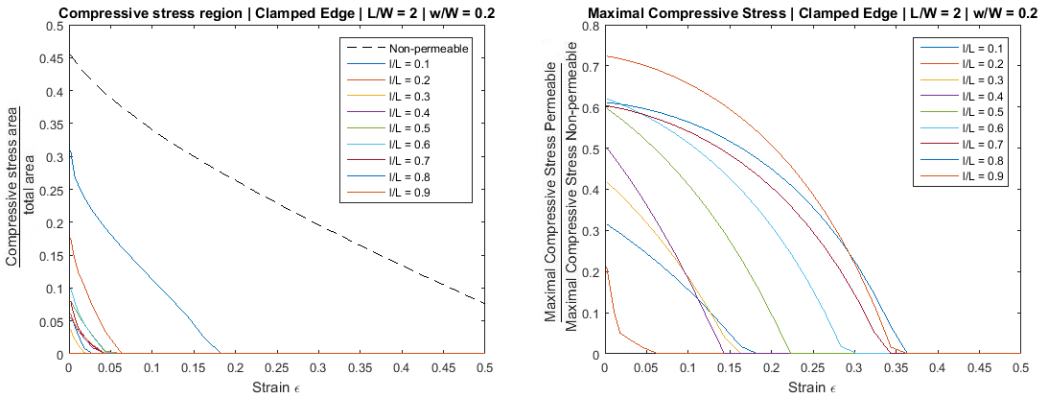

(a) (b)

Figure 5.23: (a) Size of the negative compressive stress region (a) and magnitude of the largest compressive stress (b) as a function of strain in membranes with aspect ratio $\alpha = 2$ with holes in the shape of a double parabola at the clamped edge of the membrane. All having a permeability aspect ratio in width direction of $w/W = 0.2$ and varying sizes in length direction.

Observations on the influence of the shape of a hole at the clamped edges of a membrane on the wrinkling behaviour

Based on figures 5.21a, 5.21b, 5.22, 5.23a and 5.23b, conclusions are drawn on the influence of the shape of a hole at the clamped edges of a membrane:

- When both the permeability aspect ratio in length and width direction are small, the compressive stress region decreases in size compared to the compressive stress region in the non-permeable membrane. The amplitude of the wrinkles in the permeable membrane will thus be smaller than the wrinkles in the non-permeable membrane. Furthermore, from figures 5.23a and 5.23b it can be seen that the upper critical strain will be lower for the permeable membrane than for the non-permeable membrane.
- When the permeability aspect ratio in width direction is high, the central compressive stress region disappears, but compressive stresses will form around the hole, indicating a change of the wrinkling location from the middle of the membrane to the clamped edges.
- For holes of intermediate permeability aspect ratios in width direction, the central region of compressive stress is divided into four smaller regions located at the four quarters of the membrane in between the middle and the clamped edge. In these smaller regions, wrinkles with smaller amplitudes will form compared to the wrinkles which form in the non-permeable membrane.
- If the width of the hole is intermediate or large, and furthermore, the hole has a high permeability aspect ratio in length direction, the four compressive stress regions will even be split up once again. Leading to a configuration with eight regions of compressive stress and thus eighth regions which are susceptible to wrinkling, two in every quarter of the membrane.

5.3. Conclusion

This chapter discussed the influence of holes on the wrinkling behaviour of a membrane. Wrinkle free membranes were found by searching for membranes in which no compressive stresses are present. The susceptibility of a membrane to wrinkling was judged by three indicators: the distribution of the compressive stresses, the magnitude of the compressive stresses and the area of the compressive stress region.
It was found that the influence of a hole on the wrinkling behaviour depends on the compressive stress distribution in the non-permeable membrane and thus on the aspect ratio of the membrane. The effect of holes on the wrinkling behaviour of a membrane was therefore investigated for membranes of small aspect ratios, intermediate aspect ratios and large aspect ratios separately.

Non-permeable membranes with small aspect ratios ($\alpha \leq 1.5$) do not wrinkle. No compressive stresses are present in these membranes. However, when a hole is added to the membrane, compressive stresses will be introduced. When a hole is added in the middle of the membrane or at the free edges of the membrane, compressive stresses will be present around the hole. When a hole is added at the clamped edges of the membrane, the compressive stress region will be located at the vertical symmetry axis close to the free edge of the membrane. For small holes at the clamped edge, the compressive stress region already disappears for low strains. Therefore, if a membrane with a small aspect ratio has to be permeable for some reason, and wrinkling should be minimised, a small hole at the clamped edge will be the best option.

A membrane of aspect ratio $\alpha = 2$ will be considered to be representative for all membranes of intermediate aspect ratios ($1.5 < \alpha < 4$) because the initial compressive stress distribution is similar for all of these membranes. It was discussed previously (section 2.2.3) that two causes can be identified of the wrinkling behaviour of these membranes: the Poisson effect which causes the contraction of the membrane in width direction and the clamped edges which restrain this contraction. At all three studied locations (in the middle, at the free edge and at the clamped edge of the membrane) a hole size and shape were found for which the indicators predict a decrease of the upper critical strain and of the wrinkle amplitude.
At the clamped edge of the membrane, a circular hole ($D/W < 0.4$) can lead to a minimisation of the wrinkling behaviour. This can be explained by the fact that the hole at the clamped edge limits the restraining effect of the clamped edge and allows for some contraction right next to the clamp.
When the free edge of the membrane is shaped parabolically instead of straight, the membrane will be free of compressive stresses for all strains. This permeability improves the wrinkling behaviour by influencing the first cause of wrinkling: the contraction in width direction due to the Poisson effect.
The wrinkling behaviour of a membrane of intermediate aspect ratio can be minimised by a hole in the middle of the membrane if this hole is chosen as long as possible in length direction and as small as possible in width direction. In this limiting case, the membrane will act like two membranes with an aspect ratio twice as high as the aspect ratio of the membrane. Membranes with high aspect ratios are less susceptible to wrinkling then membranes with intermediate aspect ratios (section 2.2.3).

For membranes of large aspect ratios, only the influence of circular holes was researched. No configuration was found for which such membranes are free of compressive stresses. A hole in the middle of the membrane will lead to an extra region which is susceptible to wrinkling at every side of the membrane. A hole at the free edge of the membrane increases both the area and the magnitude of the compressive stresses. By adding a circular hole of intermediate permeability aspect ratio ($0.2 < D/W \leq 0.3$) at the clamped edges of the membrane, the two separate compressive stress regions which are present in the non-permeable membrane will be merged into one central compressive stress region. The location of the wrinkling region can thus be influenced by adding holes at the clamped edges. Furthermore, the area of the compressive stress region as a function of the strain indicates that the upper critical strain for the permeable membrane will be lower than for the non-permeable membrane.

Combining all results discussed in this chapter leads to an answer on the question:
"How should holes be chosen such that wrinkling behaviour can be minimised in membranes?".
To eliminate wrinkles in membranes, holes should be added which comply to the following two design rules:

1. Holes should be chosen so that when the membrane is strained, they deform in a way so that they bring tension in the regions of the membrane which are subjected to negative second principal stress in the non-permeable configuration.
2. Holes should be chosen such that load paths in the membrane are not interrupted

6

Practical Implications

This thesis started with a study on existing designs of very large floating solar platforms (section 2.1). These very large floating solar platforms were modelled as membranes to search for a framework to research and design permeability in these structures so that they are wrinkle free. This chapter will close the circle by reflecting on the applicability of the lessons learned from the investigation of wrinkling in membranes. Furthermore, the influence of the choice to neglect the effect of water under the platform when modelling it as a membrane is discussed.

6.1. Flexible membrane with one stiff solar panel

As discussed in section 2.1, flexible floating solar platforms are only described in concepts but are not realised yet. The construction closest to this concept which is realised is the floating solar platform of Ocean Sun. This platform consists of a flexible membrane with stiff solar panels mounted on top. The conclusions of chapter 5 will be applied to such a configuration to illustrate the applicability of the research.
A stiff zone is added to the membrane. This is illustrated in figure 6.1. The stiff zone is modelled by a hole of which the edges are clamped. Therefore, the solar panel is modelled to be infinitely stiff. The solar panel is scaled in length and width direction by varying the ratio of its length and width with respect to the length and width of the membrane as described in equation 6.1.

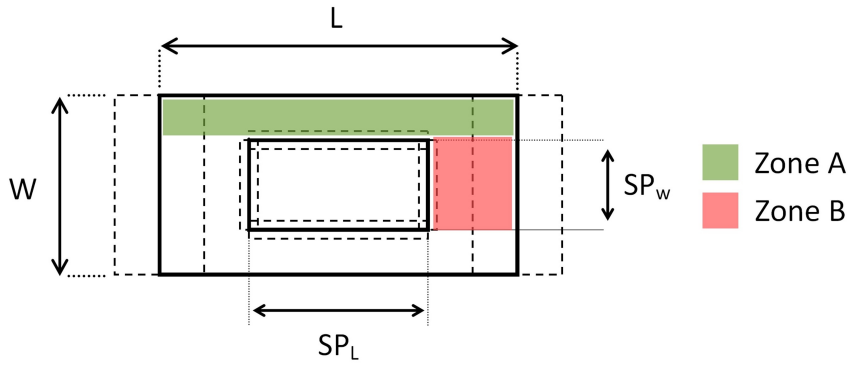

Figure 6.1: Sketch of a permeable membrane with a stiffened region in the middle which represents a solar panel. The wrinkling behaviour of this configuration is studied by focusing on two regions, indicated as 'zone A' and 'zone B' in this sketch.

$$SPAR_l = \frac{SP_l}{L} \quad SPAR_w = \frac{SP_w}{W} \tag{6.1}$$

with:

$SPAR_l$	and	$SPAR_w$	The solar panel aspect ratio in length and width direction
SP_l	and	SP_w	Te length and the width of the solar panel
L	and	W	The length and the width of the membrane

The wrinkling behaviour of a membrane with a stiff region will be investigated by a study of the second principal stress distribution. The distribution of the negative second principal stresses in membranes of aspect ratio $\alpha = 4$ with stiffened regions of different dimensions are shown in figure 6.2. Two regions will be investigated separately: the region between the stiffened region and the free edge and, the region between the stiffened region and the clamped edge, as indicated in figure 6.1 and referred to as zone A and zone B respectively. In figure 6.2 the aspect ratios of these zones are shown. All of the configurations in figure 6.2 show a region with negative second principal stress in zone A. Zone B is only subjected to negative second principal stress when the aspect ratio of this zone is intermediate or large. When the aspect ratio of zone B is small, no negative second principal stresses are present in this region. This is in line with the theory discussed in literature in chapter 2. Zone B can be considered as a rectangular sheet which uniaxially strained. These sheets do not wrinkle when their aspect ratio is small ($\alpha \leq 1.5$) [16, 44, 81].

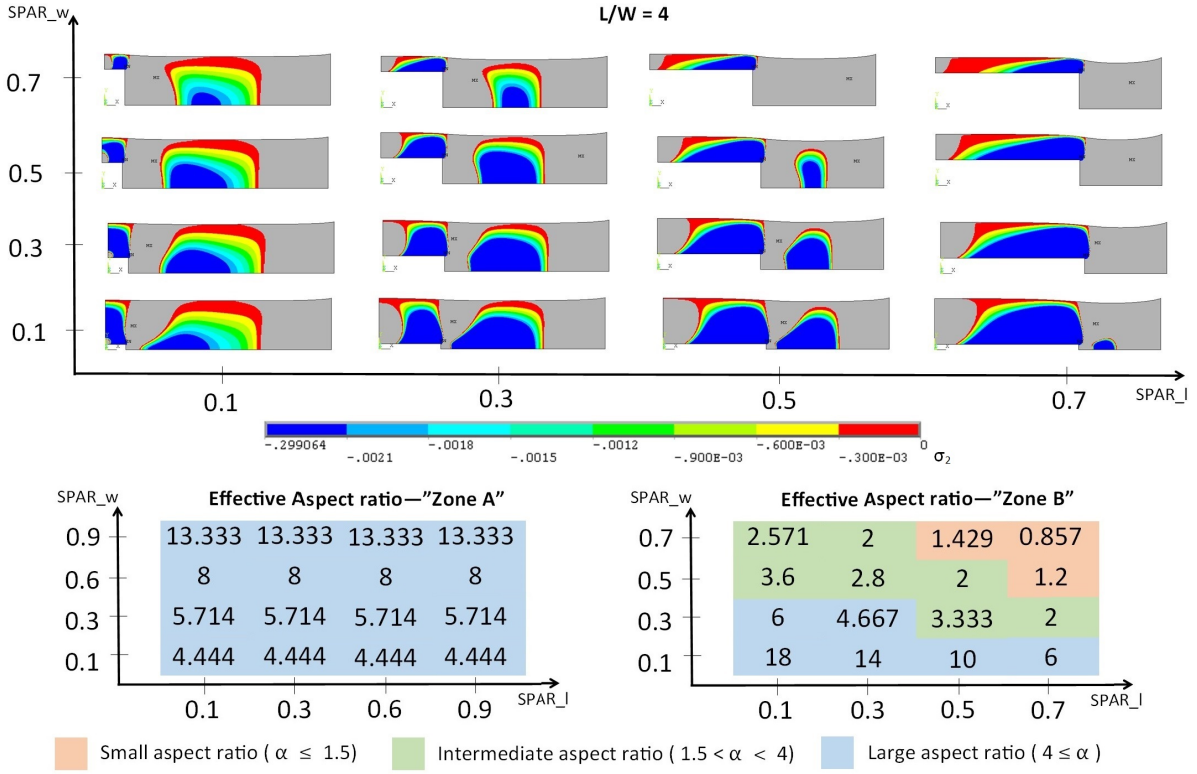

Figure 6.2: The negative second principal stress distribution in membranes of aspect ratio α with stiffened regions of different dimensions for a strain of $\epsilon = 0.1$. Furthermore an overview is given of the aspect ratios of zones A and B as indicated in figure 6.1 for the different configurations.

To show the effect of adding permeability in this application, permeability will be added step by step. A membrane of aspect ratio $\alpha = 4$ and a stiffened region with aspect ratios $SPAR_l = 0.3$ and $SPAR_w = 0.3$ will be used in this example. Results are shown in figure 6.3. First, the region of compressive second principal stress in zone B is decreased in size due to the addition of parabolically shaped holes at the clamped edges and at the stiffened region.

Region A behaves differently than region B. Due to the horizontally clamped edge in this region, the previously researched design rules are not valid in this region. By cutting this edge from the horizontal clamped edge, region A is subjected to uniaxial tension. A compressive stress region can be seen similar to the compressive stress distribution in membranes of large aspect ratios in which two wrinkle packets will form. A region which is susceptible to wrinkling is still present in the membrane due to the interruption of the load paths by the holes, this is line with the conclusions drawn in section 5.2 .

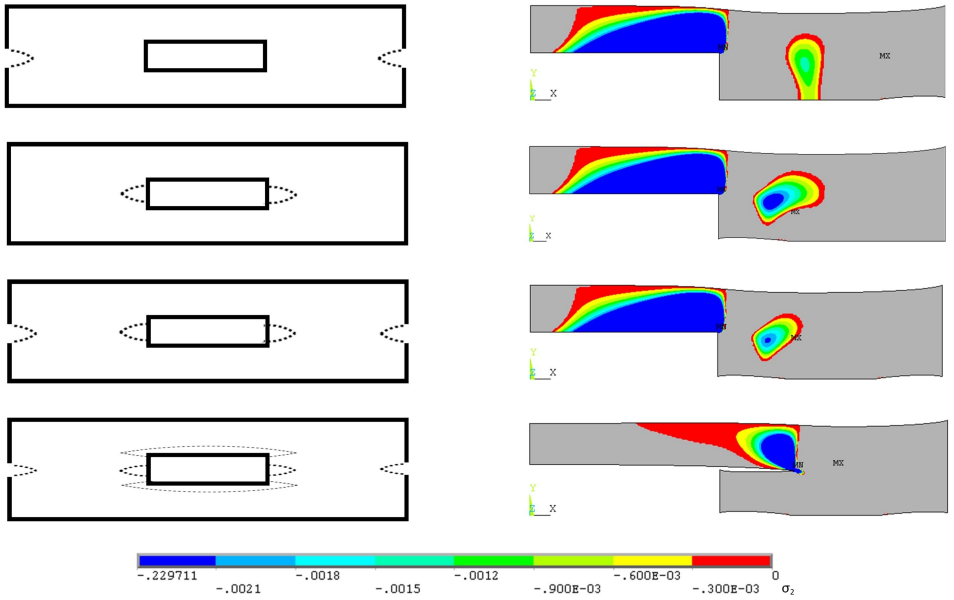

Figure 6.3: Distribution of the negative second principal stress in a membrane of aspect ratio $\alpha = 4$ with a stiffened region of dimensions $SPAR_l = 0.3$ and $SPAR_w = 0.3$ shown for a strain of $\varepsilon = 0.1$. Permeability is added at different locations to show its influence on the distribution of the compressive stresses.

To further investigate the use of permeability to minimise wrinkling behaviour in zone A, a membrane of aspect ratio $\alpha = 0.5$ is researched in which the stiffened region has aspect ratios $SPAR_l = 0.5$ and $SPAR_w = 0.5$. The distribution of the negative second principal stress in this configuration is shown in figure 6.4. The aspect ratio of zone A and B in this region are 2 and 0.25 respectively. The aspect ratio in region B is small and therefore no negative second principal stresses are present in this region. When the horizontal clamped edge in region A is cut loose by adding a long parabolic hole around this edge, it can be seen that one central region with compressive stress is present in region A of the membrane. This is in line with the stress distribution in a rectangular unaixially stretched membrane of aspect ratio $\alpha = 2$. As discussed in section 5.2, wrinkling in a rectangular membrane subjected to uniaxial strain in a membrane of aspect ratio $\alpha = 2$ can be minimised by adding permeability at the free edge so that this edge is parabolicaly shaped instead of straight. In figure 6.4 it can be seen that this conclusion was also a satisfactory solution in this application.

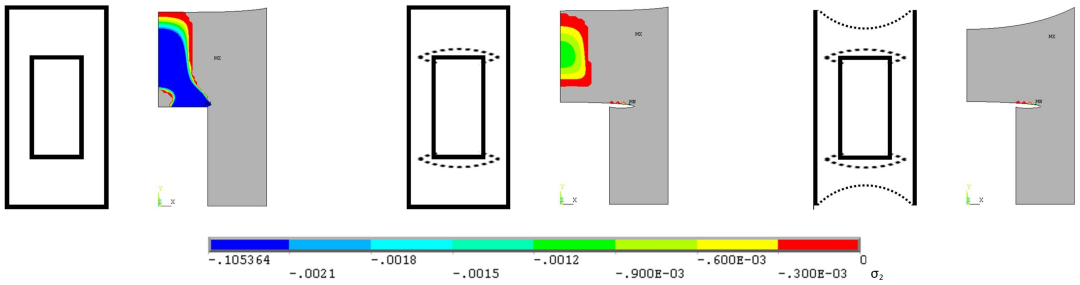

Figure 6.4: Distribution of the negative second principal stress in a membrane of aspect ratio $\alpha = 0.5$ with a stiffened region of dimensions $SPAR_l = 0.5$ and $SPAR_w = 0.5$ shown for a strain of $\varepsilon = 0.1$. Permeability is added around the stiffened region and at the free edge to show its influence on the distribution of the compressive stresses.

6.2. Flexible platform with stiff solar panels

This section will discuss susceptibility to wrinkling of a very large flexible solar platform inspired by the concept of ocean sun which was discussed in section 2.1. Figure 6.5 shows a sketch of this configuration together with sketches of deformed shapes of the platform. One part in the middle of the platform is investigated, indicated in red. The geometry and boundary conditions used for the numerical calculations are also shown in figure 6.5.

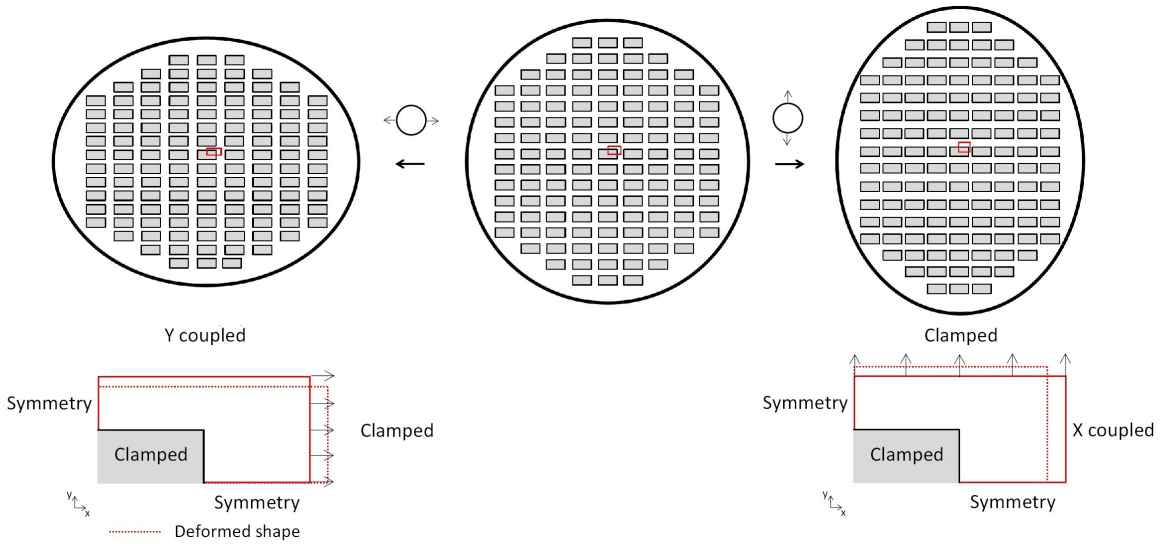

Figure 6.5: Schematic representation of a very large flexible solar platform and its deformed shape due to loads in two different directions. The wrinkling behaviour at the middle of the platform is researched, indicated in red. The geometry and boundary conditions are shown for the two different load directions.

The wrinkling behaviour of the platform is investigated by a study of the distribution of the negative second principal stresses present in the membrane. Results are shown in figure 6.6. Contrary to the configurations which were researched previously in this report, this configuration does not have any free edges. When studying the second principal stress field for the non-permeable configuration, it can be seen that this membrane therefore behaves differently. No region of uniaxial tension is presented in the membrane, but shear will be the cause of wrinkling.
From figure 6.5, it is clear that it is a necessity to study the effect of loads in different directions. Keeping this in mind, holes are chosen such that they are symmetric and therefore deform the same way when the load direction changes. The effect of two differently shaped holes at the corner of the stiff solar panel are investigated, for two different sizes of these holes. Results can be seen in figure 6.6. However, it can be seen that these holes do not lead to a minimisation of the area of the compressive stress region or a decrease in the magnitude of the compressive stresses. This leads to the conclusion that further research is necessary to investigate the effect of holes on wrinkling behaviour of membranes subjected to shear load. This observation will be described further in chapter 8: recommendations.

6.3. The effect of water

When the membrane rests directly on the water surface and is subjected to a load which causes wrinkling, a competition starts between the tendency of the membrane to wrinkle and the foundation in which the potential energy due to the displacement of the water would have to increase to allow for the wrinkles [52, 55]. Therefore, in a membrane resting on water, the number of wrinkles will be larger and the wrinkle amplitude will be smaller than in a membrane which does not rest on water. Neglecting the effect of water has no influence on the wrinkle region and leads to an overestimation of the wrinkle amplitude. Therefore, the research in this thesis is conservative by not taking into account the water under the solar platform.

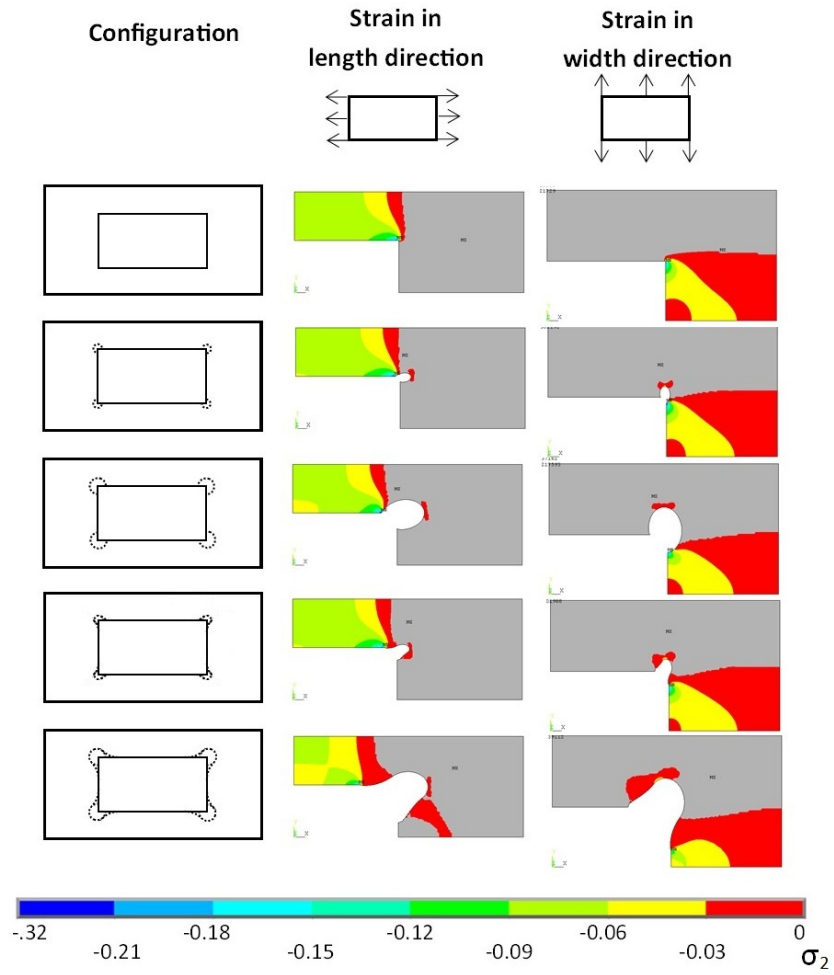

Figure 6.6: Distribution of the negative second principal stress in a membrane of aspect ratio $\alpha = 2$ with a stiff solar panel of half the length and half the width of the membrane, subjected to loads in two different directions. The distribution of the negative second principal stress is shown for a strain of $\varepsilon = 0.1$. Holes of different shapes and sizes are added to investigate their effect on the wrinkling behaviour of the membrane by a study on their influence on the second principal stress distribution. All boundary conditions are discussed in figure 6.5.

6.4. Conclusion

After discussing wrinkling in fully flexible membranes in the previous chapters, this chapter aimed to investigate a more practical case by adding a stiff solar panel to the flexible membrane. It was observed that different regions can be distinguished. In regions with a free edge, at the free edge of the membrane or created due to a long cut, the design rules concluded from chapter 5 were successfully applied. However, it could also be seen that there is need for a second set of design rules, specifically for regions subjected to shear load.
Furthermore, this chapter discussed the effect of water on the wrinkling behaviour of membranes. It was concluded that the wrinkling behaviour of a membrane is reduced due to the presence of water underneath. Therefore, this thesis designed on the safe side by leaving water out of consideration.

7

Conclusions

In this thesis, a framework to research and design wrinkle free very large flexible offshore solar platforms by adding permeability was developed. Wrinkling of very large flexible offshore solar platforms was never studied before, and therefore the following research question was formulated:

How can wrinkling be modelled keeping in mind flexible solar platforms as the application?

A framework to research wrinkle behaviour of very large flexible offshore solar platforms was searched for. Two criteria were set for this framework: the calculation method should be applicable to a wide range of geometries to calculate at least whether the membrane will or will not wrinkle. Additionally, it would be valuable if the method also gives indications on wrinkle details like the wrinkle amplitude and wrinkle region. Secondly, the method should be as computationally cheap as possible. To find a framework to research wrinkle behaviour, the following research questions were defined:

What calculation method can be used to account for wrinkling behaviour in the design of very large flexible floating structures?
Is a post-buckling calculation adequate to research wrinkling behaviour of very large flexible offshore solar platforms?
By which indicators can the wrinkling behaviour of a membrane be approximated?

By the use of the developed research method, also a framework for the design of wrinkle structures is developed. Rules of thumb were formulated by answering the following research questions:

How should holes be chosen such that wrinkling behaviour can be minimised?
In a membrane?
In a very large flexible floating solar platform?

The remainder of this chapter will summarise all conclusions which form the answers to these research questions.

7.1. Modelling an offshore solar power plant as a wrinkling membrane

A literature review was performed to review the state-of-the art in the design of very large floating offshore solar power plants and to review literature on wrinkling behaviour of membranes (chapter 2). Floating solar platforms are design so that the mooring installation holds the platform in place by tension load. Furthermore it became clear that membranes are susceptible to wrinkling due to different loads: torsion, shear and tension. The influence of the dimensions of a membrane on the wrinkling behaviour is extensively researched for rectangular membranes subjected to uniaxial tension.
Therefore, the flexible solar power plant will be modelled as such a rectangular membrane subjected to uniaxial tension. Holes will be added to this membrane to study the influence of permeability on the wrinkling behaviour of the flexible solar power plant.

7.2. Framework to research the wrinkling behaviour of very large flexible floating structures

A non-linear buckling calculation was set up to be able to research the wrinkling behaviour of membranes. By a non-linear buckling calculation, all details on the wrinkled geometry can be calculated: the number of wrinkles, the wrinkle amplitude, the wrinkle wave length, the lower and upper critical strain in between which wrinkling occurs and the region of the membrane which wrinkles. The model was verified and validated by comparison to experimental and simulation results from literature.
Problems occurred when using the non-linear buckling calculation to research the wrinkling behaviour of membranes with different geometries. The first buckling mode is used in the model as the initial perturbation of the membrane for the post-buckling calculation. For some of the geometries, it appeared that this first buckling mode could not be found. Other methods were investigated to perturbate the membrane: using the second or thirth buckling mode, using the first buckling mode under compression load or using a initial deformation constructed by unbalancing forces. From this investigation it became clear that the result of the post-buckling behaviour is highly dependent on the initial perturbation which is used. The dependency on this user-defined input leads to the fact that the results of the post-buckling calculation are subjective. This uncertainty on the results as well as the fact that for some of the geometries no buckling mode can be found and the computational costs of a non-linear buckling calculation lead to the conclusion that this type of calculation is not adequate to investigate the wrinkling behaviour of (permeable) very large floating structures.

An alternative method was found in studying the second principal stress distribution in membranes. If no compressive stresses are present in a membrane, the membrane will not be susceptible to wrinkling. Searching for wrinkle free membranes can thus be done by searching for membranes which are free of compressive stresses. This method is objective and furthermore computationally cheap compared to the non-linear buckling calculation.
Next to the binary criterion which separates wrinkle free membranes from membranes which are susceptible to wrinkling, three other indicators were found by which details on the wrinkling behaviour can be approximated:

- The distribution of the compressive stresses in a membrane is an indicator for the distribution of the wrinkling regions in the membrane.
- The size of the region in which compressive stresses occur is an indicator by which the wrinkle amplitude can be approximated: the larger this area, the larger the wrinkle amplitude and vice versa.
- The magnitude of the compressive stresses is an indicator for the critical strains of the membrane.

7.3. Framework for the design of very large flexible floating structures with minimal wrinkling behaviour

It became clear that the effect of permeability on the wrinkling behaviour of a membrane depends on the compressive stress distribution in the non-permeable membrane. The distribution of compressive stresses in non-permeable membranes depends on the aspect ratio of the membrane. Three categories can be identified: membranes with small aspect ratios ($\alpha \leq 1.5$), intermediate aspect ratios ($1.5 < \alpha < 4$) and large aspect ratios ($4 \geq \alpha$). Having no compressive stress region, one compressive stress region and two compressive stress regions in their non-permeable configuration respectively. For every category of membranes observations were made on how to minimise the wrinkling behaviour by lowering the strain for which restabilization will take place or by minimising the area of the negative compressive stress region:

- In membranes of small aspect ratios, holes will lead to wrinkling while the non-permeable configurations will not be susceptible to wrinkling. If wrinkling should be avoided, holes should thus be avoided as well. If, due to practicals reasons, a holes is necessary, it should be placed at the clamped edge to have minimal effect on the wrinkling behaviour.
- Wrinkling behaviour of membranes with intermediate aspect ratios can be minimised or even be completely avoided by influencing the two causes of wrinkling: the contraction of the membrane in the width direction and the restraining effect of the clamped edges. This can be done by adding a hole at the clamped edge of the membrane or by shaping the sides of the membranes parabolically instead of straight. Furthermore, by adding a long but small hole in the middle of the membrane, the membrane will act like two separate membranes of double the aspect ratio. Membranes with high aspect ratios are less susceptible to wrinkling, so this will lead to a minimisation of the wrinkling behaviour of the membrane.
- For membranes with large aspect ratios, no wrinkle free configurations were found. But localisation of the wrinkle region can be obtained by adding a hole at the clamped edge of the membrane. This will lead to a configuration in which only the middle of the membrane is susceptible to wrinkling, while in the non-permeable membrane two regions are susceptible to wrinkling.

By combining all observations on the influence of holes of different sizes, shapes and at different locations, on membranes of different sizes, two design rules were derived. To eliminate wrinkles in membranes, holes should be added which comply to both of these design rules:

1. Holes should be chosen so that when the membrane is strained, they deform in a way so that they bring tension in the regions of the membrane which are subjected to negative second principal stress in the non-permeable configuration.
2. Holes should be chosen such that load paths in the membrane are not interrupted

7.4. Practical implications of the framework to research and design very large flexible floating structures

To study the practical implications of the framework to research and design very large flexible floating structures which was set up in this thesis, it was applied to eliminate wrinkles from a flexible membrane with a stiff solar panel mounted on top. From this application it was observed that multiple regions can be distinguished in the reinforced membranes. In regions with a free edge, it was proven that the framework which was developed in this thesis is applicable to minimise or even eliminate negative second principal stresses, and thus wrinkling. The free edge can be the free edge of the membrane or platform, but can also be created by adding a long cut which will act like a free edge. Furthermore, from this application, it could be seen that there is a need for a second set of design rules, one which is applicable in regions subjected to shear load.

8

Recommendations

This chapter will discuss recommendations for further research. Recommendations on three aspects of the research are presented. First, suggestions to improve the analysis of the wrinkling behaviour of a membrane by studying the second principal stress distribution in the membrane. Secondly, recommendations are presented to extend the design rules which were developed in this thesis. Finally, further research on the development of very large flexible floating solar platforms will be discussed.

8.1. Further development of wrinkling indicators

In this thesis, wrinkling behaviour of a membrane was investigated by researching the presence of compressive stresses in the membrane. If no negative second principal stresses are present in the membrane, the membrane will not wrinkle. If negative second principal stresses are present in the membrane, the membrane *can* wrinkle. Literature [16, 44] suggested that a membrane in which negative second principal stress is present will not wrinkle when the wrinkle region is small or when the magnitude of compressive stress is small. It has never been research before how small the region should be, and how small the magnitude of the negative second principal stress should be to prevent for wrinkling. But this might be of interest to be able to asses the susceptibility of a membrane with a small region of second principal stress and with low magnitudes of second principal stress more precisely. Another improvement on the calculation of the wrinkling behaviour of a membrane can be obtained by researching new wrinkling indicators. An example would be researching the relation between the orientation of the principal stress in a membrane and the wrinkle orientation. The work of Liu [34] can be used as an inspiration here. They have researched the wrinkle direction in orthotropic membranes by studying the direction of the principal stresses. To validate the wrinkling indicators, more experiments on wrinkle behaviour of membranes are suggested. Especially experiments on the wrinkling behaviour of membranes with holes.
Furthermore, further research on buckling calculations might lead to a method for the calculation of the first buckling mode which leads to a result for all possible geometries. To develop a method by which a bifurcation point can be approximated, the work of Wriggers [49] might be used as an inspiration.

8.2. Extension of design rules

This thesis focused on minimising wrinkling behaviour of membranes by removing material. In maritime engineering it is common practice to localise buckling behaviour by adding material: by adding stiffeners to the structure. Adding stiffeners to a membrane might also lead to wrinkling minimisation or localisation in membranes. From section 6.1 the potential of this technique can already be observed. By the addition of an infinitely stiff region in the middle of the membrane, the membrane acts as multiple membranes with effective aspect ratios. However some questions are still open, an investigation of the influence of the stiffeners and dimensions of the stiffeners for example. Therefore the investigation of these mechanisms are recommended for future research. This analysis can be carried out by a study on the influence on the distribution of the second principal stresses.

Furthermore, sections 6.1 and 6.2 pointed out the necessity to research wrinkling due to other loads. As discussed in section 2.2.1, literature on the wrinkling phenomenon focuses on wrinkling due to tension, shear and torsion load. The design rules derived in this thesis can be extended by also investigating the effect of permeability and stiffeners in configurations other than the rectangular membrane subjected to uniaxial tension.

8.3. Recommended research on practical considerations

In section 2.1 mooring systems of floating solar platforms were discussed. Figures 8.1a and 8.1b give a schematic overview of the mooring systems of the solar platform by Floating Solar BV [15] and the concept by DNV GL [62] respectively. The solar platform of Floating Solar BV is moored by different buoys. The very large solar platform concept published by DNV GL consists of different solar panels which are connected to each other and moored to the seabed from one central point. In both systems, the solar panels are connected through horizontal cables to other solar panels or buoys and only indirectly to the seabed. Figure 8.1c shows a sketch of a mooring system in which the solar panel is moored directly to the seabed. While the mooring systems in figures 8.1a and 8.1b keep the solar platform in position by tension force, the platform in figure 8.1c will experience forces in the direction perpendicular to the platform. Different mooring systems will lead to different loads in the platform, therefore wrinkling should be kept in mind when choosing the mooring system. The mooring system should be chosen such that a framework for the research of or for the design of wrinkling for the resulting loads exists. Next to the mooring loads, the platform will experience other loads, from waves, currents, the wind, green water et cetera. To design of very large flexible floating solar platforms, quantification of these loads would be necessary.

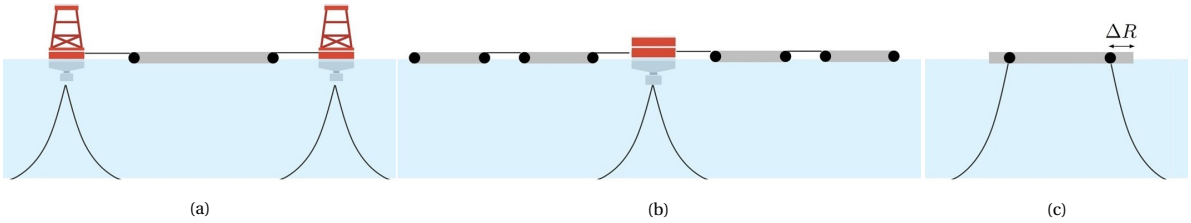

Figure 8.1: Schematic overview of mooring systems of very large flexible (floating solar) platforms, (a) based on the floating solar platform of Floating Solar BV [15], (b) on the concept of DNV GL [62] and (c) an alternative construction.

A

Mesh convergence

All results of numerical calculations which are shown in this report are obtained with a mesh consisting of 9800 elements. This appendix will discuss the influence of number of elements on the non-linear buckling calculation and the calculation of the second principal stress field. To show the influence of the element size on the non-linear buckling calculation, its influence on the calculation of buckling modes and on the post-buckling calculation are shown separately. Five different meshes are used for the mesh convergence study. The number of elements and the number of nodes is listed for every mesh in table A.1.

Table A.1: Overview of the number of elements and the number of nodes in the five meshes used for the mesh convergence study

Mesh	Nr. of elements	Nr. of elements in length and width direction	Nr. of nodes
Very Coarse	1225	25 x 49	1300
Coarse	2450	35 x 70	2556
Intermediate	4950	50 x 99	5100
Fine	9800	70 x 140	10011
Very Fine	19602	99 x 198	19900

A.1. Calculation of the buckling modes

The influence of the number of elements on the first buckling mode is shown in figures A.1a, A.1b and A.2. The different meshes which are compared with each other exist of 1225, 2450, 4950, 9800 and 19602 elements. The out-of-plane displacement of the first buckling mode along the symmetry axis of the membrane in width direction is shown in figure A.1a and a detail of this graph is shown in figure A.1b. In these figures it can be seen that the location of the maximal and minimal out-of-plane displacement are located more towards the free edge when the calculation is performed with a coarse mesh compared to a fine mesh. Furthermore, the curve of the out-of-plane displacement does not look smooth for the coarse mesh while is does look smooth for the fine meshes. The same can be seen in figure A.2, which shows the out-of-plane displacement for the different meshes in contour plots.

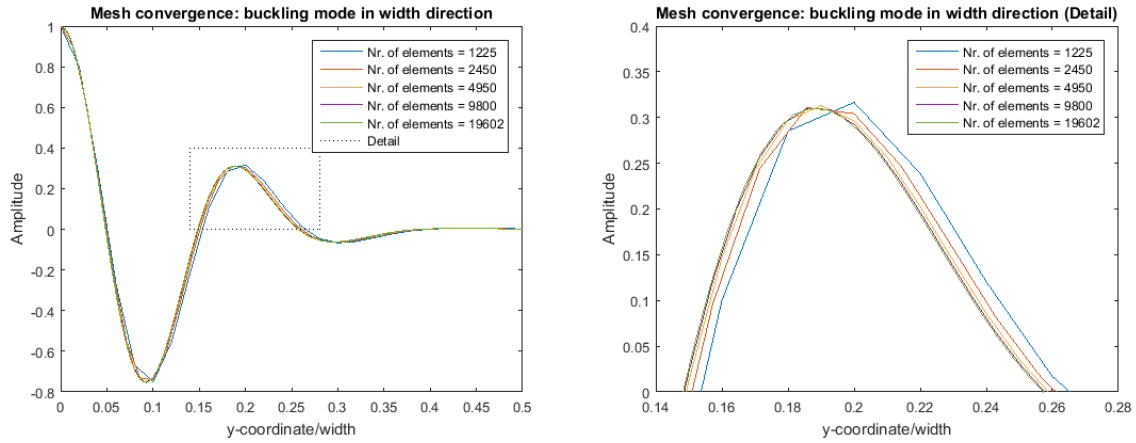

(a) (b)

Figure A.1: (a) Out-of-plane displacement as a function of the normalised width coordinate for the first buckling mode, calculated with five different meshes. All for a membrane of aspect ratio $\alpha = 2$, with a thickness of $\beta = 1000$ and a Neo-Hookean material model. (b) Detail of figure A.1a.

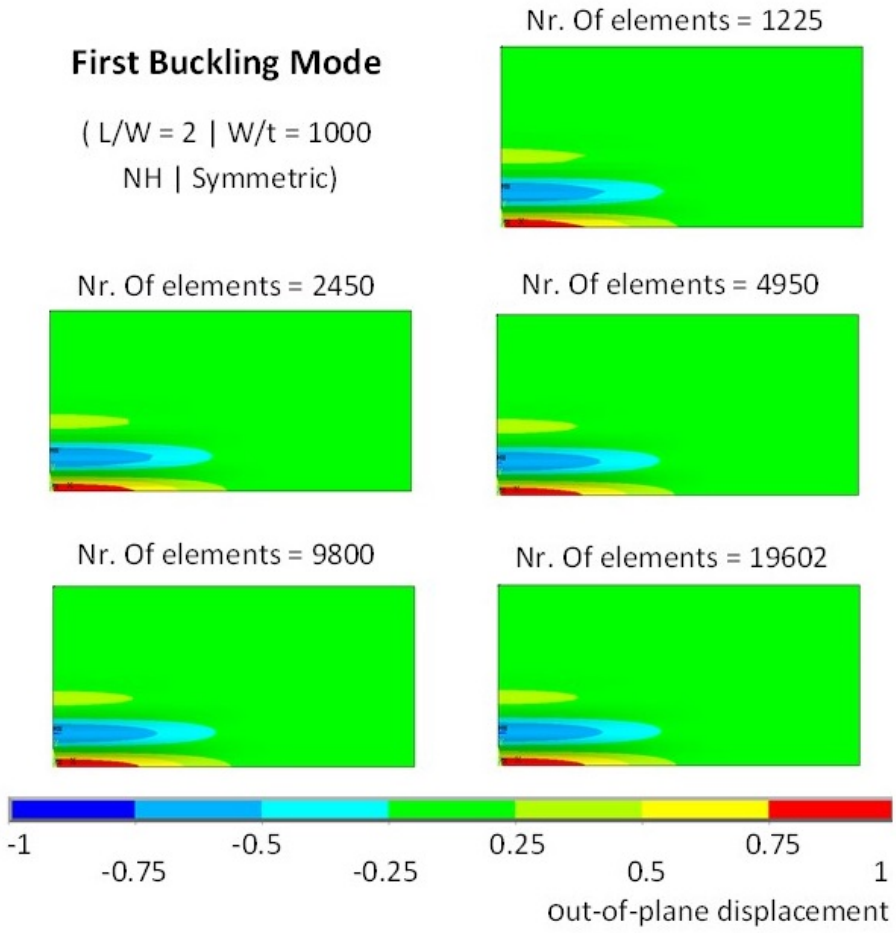

Figure A.2: Contour plot of the out-of-plane displacement of the first buckling mode, calculated with five different meshes. For a membrane of aspect ratio $\alpha = 2$, with a thickness of $\beta = 1000$ and a Neo-Hookean material model.

.

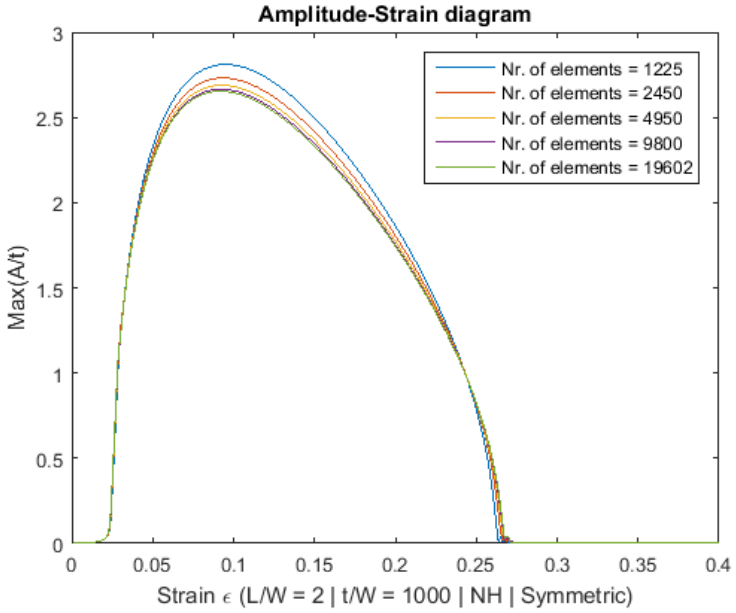

Figure A.3: Amplitude-strain diagram of a membrane of aspect ratio $\alpha = 2$, a thickness of $\beta = 1000$ and a Neo-Hookean material, calculated with five different meshes.

A.2. Post-buckling calculation

Grid convergence for the post-buckling calculation is shown in table A.2 and figure A.3. Figure A.3 shows the amplitude-strain diagram obtained for the different meshes. From this diagram it can be seen that the maximal amplitude is overestimated when for a coarse mesh and the strain for which restabilisation takes place is underestimated. For the fine meshes, mesh convergence can be seen. The same is illustrated in table A.2 in which convergence is shown by researching the maximal amplitude obtained from different meshes. This table confirms that a mesh with 9800 elements leads to valid results.

Table A.2: Comparison of the maximal wrinkle amplitude obtained with meshes consisting of different numbers of elements. The convergence is calculated by the ratio of the maximal amplitude of a coarser mesh to the amplitude obtained by a finer mesh

Mesh	**Nr. of elements**	**Convergence**
Very Coarse	1225	-
Coarse	2450	0.971
Intermediate	4950	0.984
Fine	9800	0.991
Very Fine	19602	1.000

A.3. Calculation of the second principal stress field

The influence of the number of elements on the distribution of the second principal stresses in the membrane are shown in figure A.4 for meshes consisting of 28 elements up to 19602 elements. Previously it was shown that 9800 elements were required to obtain mesh convergence for a post-buckling calculation. From figure A.4 it can be seen that less elements are needed to investigate the presence and the distribution of negative second principal stress. This is one of the reasons why the computational cost of investigating the wrinkling behaviour of a membrane by a study of the second principal stresses is lower than the computational cost of a fully non-linear post-buckling calculation.

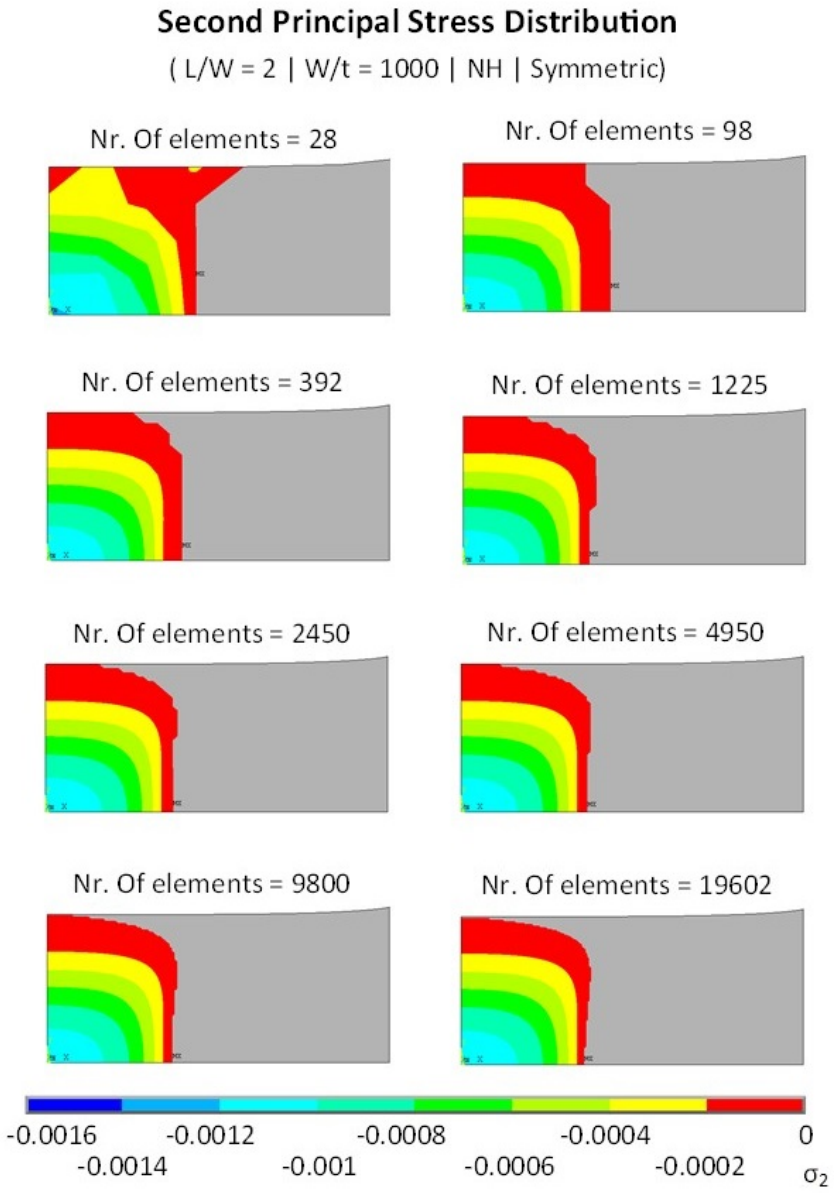

Figure A.4: Contour plot of negative second principal stress distribution, calculated with five different meshes. For a membrane of aspect ratio $\alpha = 2$ and a Neo-Hookean material model.

B

Isolated Plate Model

In section 4.3 the isolated plate model is mentioned as a method to approximate the critical strains for a wrinkling membrane. The main conclusions from applying the isolated plate model are the confirmation of the importance of the geometry of the membrane. The geometry influences the compressive stress distribution which causes wrinkling. Furthermore, the influence of the thickness of the membrane and the magnitude of the compressive stresses as suggested in literature is confirmed by this model [16, 34, 44, 71]. However, the applicability of this model is limited to membranes in which the compressive stress region is one clearly defined zone. This appendix will give a more detailed description on the isolated plate model and how it is applied.

Friedl [16] and Nayyar [44] both suggest to investigate a wrinkled membrane by modelling it as a simply supported rectagular plate subjected to a uniform biaxial stress. Friedl suggest to model the full membrane as such a plate, Nayyar however suggests to model the compressive stress region as an isolated plate. The suggestion of Nayyar will be worked out in this section. Figure B.1a gives an impression of how the compressive stress region is modelled as an isolated plate.

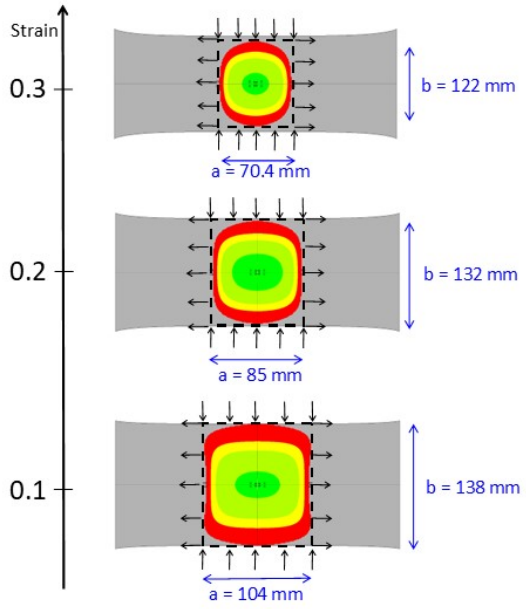

(a)

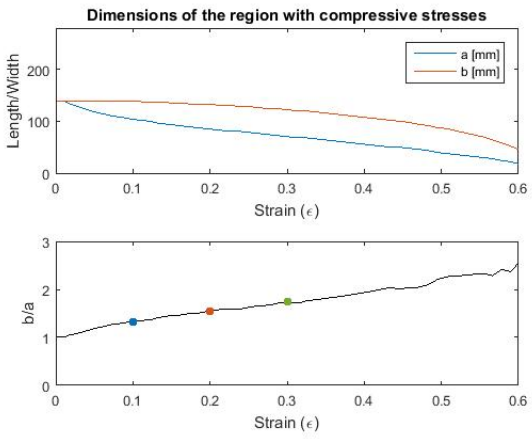

(b)

Figure B.1: (a) Uniaxially stretched membrane of aspect ratio $\alpha = 2$ and at strains $\varepsilon = 0.1$, $\varepsilon = 0.2$ and $\varepsilon = 0.3$. The coloured region in the membrane marks the region of the membrane subjected to negative second principal stress. Nayyar [44] proposes to model this part of the membrane as an isolated plate. This plate model is indicated in black. (b) Dimensions of the region with compressive stress in a membrane with aspect ratio $\alpha = 2$ as a function of the strain. a and b as defined in figure B.1a.

For a simply supported rectangular plate subjected to biaxial stress, the critical stress can analytically be estimated by formula B.1. For a plate, this leads to a constant value of the critical stress. However, when modelling the compressive stress region of a membrane as an isolated plate, the following parameters depend on the strain: the dimensions of the plate a and b, the Youngs modulus E and the proportionality factor C. To illustrate how to calculate the critical strain which is dependent of the strain, the calculation is illustrated specifically for a plate of aspect ratio $\alpha = 2$, for three strains: $\varepsilon = 0.1$, $\varepsilon = 0.2$ and $\varepsilon = 0.3$. For these three strains the results are indicated in every graph by a blue, red and green dot respectively and all intermediate results are summarised in table B.1.

$$\sigma_{x,c} = \frac{\pi^2 E}{12(1-\nu^2)}\left(\frac{t}{b}\right)^2\left[\frac{n^4(\frac{a}{b})^4 + 2m^2n^2(\frac{b}{a})^2 + m^4}{-Cm^2 + n^2(\frac{b}{a})^2}\right] \tag{B.1}$$

$$\text{With } C = \frac{\sigma_y}{\sigma_x} \tag{B.2}$$

with:

$\sigma_{x,c}$	The critical stress in the tension direction
σ_x	The stress in the tension direction
σ_y	The stress in the compression direction
C	The proportionality factor
E	The Youngs modulus
ν	The Poisson ratio
t	The thickness of the membrane
a	The length of the isolated plate (as indicated in figure B.1a)
b	The width of the isolated plate (as indicated in figure B.1a)
m	The number of half waves in the width direction of the isolated plate
n	The number of half waves in the length direction of the isolated plate

The dimensions of the plate a and b are calculated for every strain by the use of the numerical model. The dependency of a and b on the strain for a plate of aspect ratio $\alpha = 2$ is illustrated in figure B.1b. The derivative of the stress-strain curve at every strain is used as the Youngs modulus at every strain. This is illustrated in figure B.2.

In the model, the stress at the membranes clamped boundary is chosen as tensional load and the most negative second principal stress is chosen as the compressive stress because that will be the governing load to cause buckling. σ_x, σ_y and the proportionality factor C are shown as a function fo the strain in figure B.2.

Table B.1: Intermediate results to make an analytical estimation of the critical strains. All intermediate results are displayed for a memrbane of aspect ratio $\alpha = 2$

		$\varepsilon = 0.1$	$\varepsilon = 0.2$	$\varepsilon = 0.3$
a	[mm]	103.7	85.0	70.4
$\frac{b}{a}$	[-]	1.331	1.553	1.739
σ_x	[MPa]	0.00539	0.0994	0.139
$\sigma_{2,max}$	[MPa]	-0.001119	-0.001321	-0.00144
E	[MPa]	0.9945	0.8512	0.7482
C	[-]	-0.0208	-0.0133	-0.0082
$\sigma_{x,crit,Non-dim}$	[-]	9441	22920	59992
$\sigma_{x,crit}$ voor $\beta = 1000$	[MPa]	0.0187	0.0579	0.195
$\sigma_{x,crit}$ voor $\beta = 2000$	[MPa]	0.00467	0.0169	0.0647

Now that the dimensions of the isolated plate a and b, Youngs modulus E and the proportionality factor C are known for every strain, the last two parameters which are needed to calculate the critical strain are the number of waves in length direction n and the number of waves in with direction m. The number of waves in length direction is set to one $n = 1$. m is chosen such that it results in the minimal value of the critical strain σ_{crit}. This is illustrated in figure B.3a.

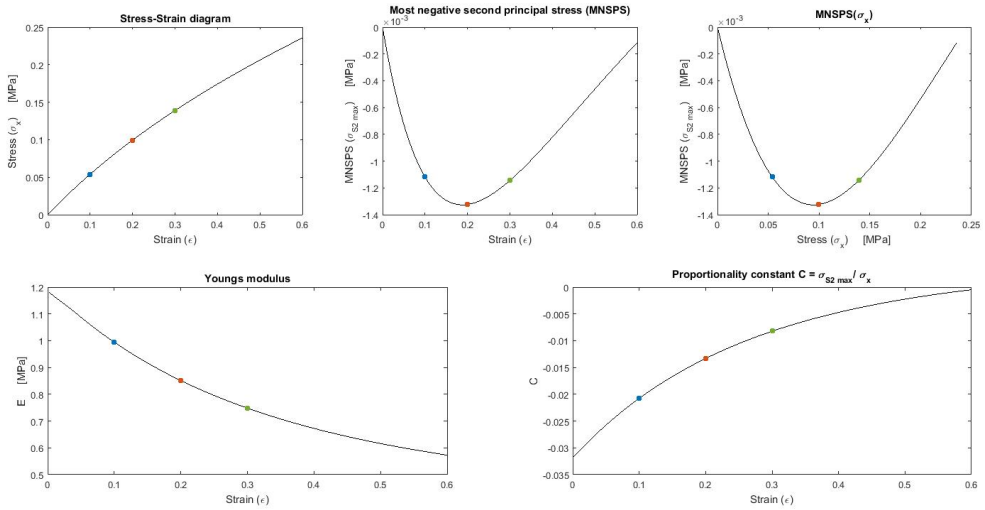

Figure B.2: Results on the stresses in a rectangular membrane of aspect ratio $\alpha = 2$ which is uniaxially stretched. These results will be used as input values to make an analytical estimation of the lower and upper critical strains in between which wrinkling of the membrane occurs.

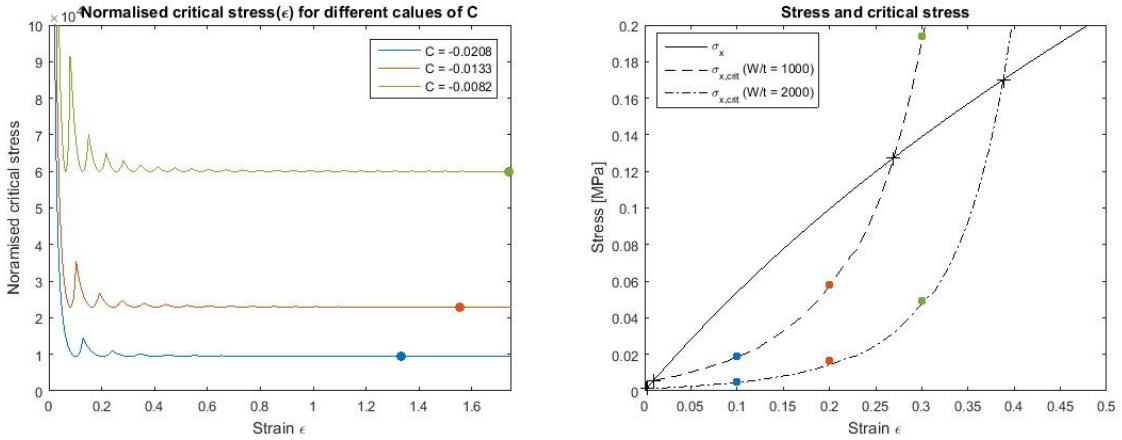

(a) (b)

Figure B.3: (a) Normalised critical stress as a function of strain for $C = -0.0208$, $C = -0.0133$ and $C = -0.0082$. The critical stress is normalised by $\frac{\pi^2 E}{12(1-\nu^2)}(\frac{t}{b})^2$ (b) Stress strain diagram and critical stress as a function of strain for $\beta = 1000$ and $\beta = 2000$ for a membrane of aspect ratio $\alpha = 2$. At a certain strain the membrane will wrinkle if the stress σ_x is higher than the critical stress $\sigma_{x,crit}$.

From the previous calculations, the critical stress is known as a function of the strain. The isolated plate will be susceptible for wrinkling at all strains for which the stress is larger than the critical stress. Figure B.3b shows the actual stress and the critical stress for two membranes, both having aspect ratio $\alpha = 2$ but having two different thickness aspect ratios: $\beta = 1000$ and $\beta = 2000$. For both membranes, the stress and critical stress curve cross two times: at the strain at which wrinkles start to form, and at the strain at which the wrinkles decay: the critical strains

The isolated plate model was illustrated for a memnbrane of aspect ratio $\alpha = 2$. It is repeated for membranes of other aspect ratios for thicknesses $\beta = 1000$ and $\beta = 2000$. The upper critical strains which were found for all aspect ratios are displayed in figures B.4a and B.4b together with stability boundaries from literature [33, 44, 71]. Good agreement is found for membranes for which a clear compressive stress can be isolated (phase C in figure 4.5). When this region is more irregular in shape, the isolated plate model cannot be applied or will lead to inaccurate results.

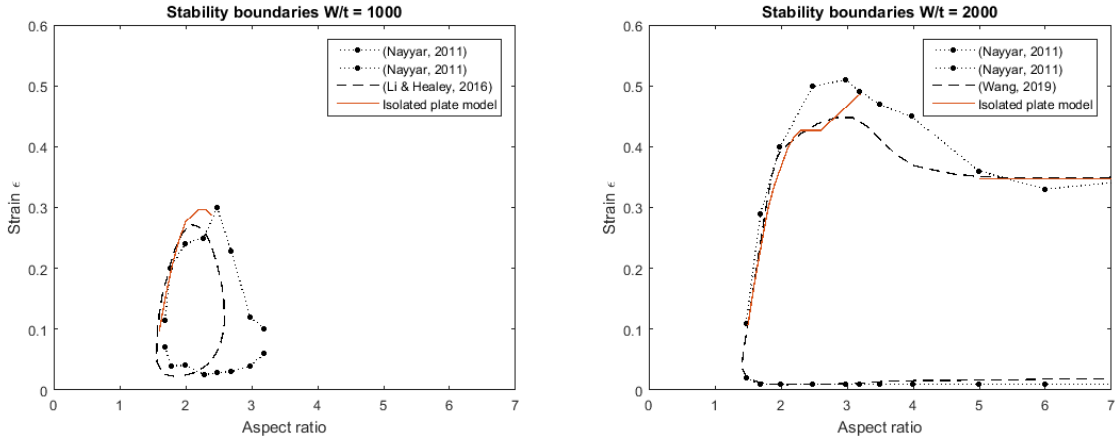

(a) (b)

Figure B.4: Stability boundaries for membranes of thickness aspect ratio $\beta = 1000$ (a) and $\beta = 2000$ (b) from literature [33, 44, 71] together with the critical strain approximated by the isolated plate model for a limit number of aspect ratios.

Bibliography

[1] Aaron L. Adler, Martin M. Mikulas, and John M. Hedgepeth. Static and dynamic analysis of partially wrinkled membrane structures. *Collection of Technical Papers - AIAA/ASME/ASCE/AHS/ASC Structures, Structural Dynamics and Materials Conference*, 4:158–171, 2000. ISSN 02734508. doi: 10.2514/6.2000-1810.

[2] Martin Philip Bendsøe and Noboru Kikuchi. Generating optimal topologies in structural design using a homogenization method. *Computer Methods in Applied Mechanics and Engineering*, 71(2):197–224, 1988. ISSN 00457825. doi: 10.1016/0045-7825(88)90086-2.

[3] Joseph R. Blandino, John D. Johnston, and Urmil K. Dharamsi. Corner wrinkling of a square membrane due to symmetric mechanical loads. *Journal of Spacecraft and Rockets*, 39(5):717–724, 2002. ISSN 00224650. doi: 10.2514/2.3870.

[4] E. Cerda and L. Mahadevan. Geometry and Physics of Wrinkling. *Physical Review Letters*, 2003. ISSN 10797114. doi: 10.1103/PhysRevLett.90.074302.

[5] E. Cerda, K. Ravi-Chandar, and L. Mahadevan. Wrinkling of an elastic sheet under tension. *Nature*, 419(6907):579–580, oct 2002. ISSN 0028-0836. doi: 10.1038/419579b. URL `http://www.nature.com/articles/419579b`.

[6] Michael A. Champ. Preliminary review of the potential environment and social impacts from nearshore standing or very large floating platforms. *International workshop on very large floating structures*, 2: 463–470, 1996.

[7] C. D. Coman. On the applicability of tension field theory to a wrinkling instability problem. *Acta Mechanica*, 190(1-4):57–72, 2007. ISSN 00015970. doi: 10.1007/s00707-006-0395-7.

[8] C. D. Coman and D. M. Haughton. Localized wrinkling instabilities in radially stretched annular thin films. *Acta Mechanica*, 185(3-4):179–200, 2006. ISSN 00015970. doi: 10.1007/s00707-005-0307-2.

[9] Ciprian D. Coman and Andrew P. Bassom. Wrinkling of pre-stressed annular thin films under azimuthal shearing. *Mathematics and Mechanics of Solids*, 13(6):513–531, 2008. ISSN 10812865. doi: 10.1177/1081286507077107.

[10] R. De Rooij and M. M. Abdalla. A finite element interior-point implementation of tension field theory. *Computers and Structures*, 151:30–41, 2015. ISSN 00457949. doi: 10.1016/j.compstruc.2015.01.007. URL `http://dx.doi.org/10.1016/j.compstruc.2015.01.007`.

[11] H.M. Verhelst M. Möller H. den Besten A. Mantzaflaris M. Kaminski. Stretch-Based Hyperelastic Material Formulations for Isogeometric Kirchhoff-Love Shells. 2020. doi: hal-02890963.

[12] Urmil K. Dharamsi, Daniel M. Evanchik, and Joseph R. Blandino. Comparing photogrammetry with a conventional displacement measurement technique on a 0.5m square Kapton® membrane. *Collection of Technical Papers - AIAA/ASME/ASCE/AHS/ASC Structures, Structural Dynamics and Materials Conference*, 1(April):463–472, 2002. ISSN 02734508. doi: 10.2514/6.2002-1258.

[13] DNV-GL. Energy transition outlook 2018. Technical report, 2018.

[14] Emiliano Bellini. Japan's largest floating PV plant catches fire after typhoon Faxai iimpact, 2019. URL `https://www.pv-magazine.com/2019/09/09/japans-largest-floating-pv-plant-catches-fire-after-typhoon-faxai-impact/`.

[15] Floating Solar BV. Drijvende zonnepanelen van Floating Solar BV, 2020. URL `https://floatingsolar.nl/`.

[16] N. Friedl, F. G. Rammerstorfer, and F. D. Fischer. Buckling of stretched strips. *Computers and Structures*, 78(1):185–190, 2000. ISSN 00457949. doi: 10.1016/S0045-7949(00)00072-9.

[17] E. Friel, D., Karimirad, M., Whittaker, T., Doran, W.J., Howlin. A review of floating photovoltaic design concepts and installed variations. *International conference on offshore renewable energy*, 4, 2019.

[18] C. Fu, T. Wang, F. Xu, Y. Huo, and M. Potier-Ferry. A modeling and resolution framework for wrinkling in hyperelastic sheets at finite membrane strain. *Journal of the Mechanics and Physics of Solids*, 124:446–470, mar 2019. ISSN 0022-5096. doi: 10.1016/J.JMPS.2018.11.005. URL https://www-sciencedirect-com.tudelft.idm.oclc.org/science/article/pii/S0022509618307026.

[19] Timothy J. Healey, Qingdu Li, and Ron-Bin Cheng. Wrinkling Behavior of Highly Stretched Rectangular Elastic Films via Parametric Global Bifurcation. *Journal of Nonlinear Science*, 23(5):777–805, oct 2013. ISSN 0938-8974. doi: 10.1007/s00332-013-9168-3. URL http://link.springer.com/10.1007/s00332-013-9168-3.

[20] T. Iwasa, M. C. Natori, and K. Higuchi. Evaluation of tension field theory for wrinkling analysis with respect to the post-buckling study. *Journal of Applied Mechanics, Transactions ASME*, 71(4):532–540, 2004. ISSN 00218936. doi: 10.1115/1.1767171.

[21] Nicolas Jacques and Michel Potier-Ferry. On mode localisation in tensile plate buckling. *Comptes Rendus Mécanique*, 333(11):804–809, nov 2005. ISSN 1631-0721. doi: 10.1016/J.CRME.2005.10.013. URL https://www.sciencedirect.com/science/article/pii/S1631072105001920.

[22] C. H. Jenkins, F. Haugen, and W. H. Spicher. Experimental measurement of wrinkling in membranes undergoing planar deformation. *Experimental Mechanics*, 38(2):147–152, 1998. ISSN 00144851. doi: 10.1007/BF02321658.

[23] Amulya Karavadi and Robert S. Balog. Novel non-flat photovoltaic module geometries and implications to power conversion. *IEEE Energy Conversion Congress and Exposition: Energy Conversion Innovation for a Clean Energy Future, ECCE 2011, Proceedings*, pages 7–13, 2011. doi: 10.1109/ECCE.2011.6063742.

[24] Madjid Karimirad and Trevor Whittaker. The integration of existing photovoltaic technologies with floatation systems has realised The technology , initially installed to offset land usage and dependence on conventional energy sources in agricultural sectors , has seen substantial developments . 2019.

[25] Siham Khalil, Youssef Belaasilia, Abdellah Hamdaoui, Bouazza Braikat, Mohammad Jamal, Noureddine Damil, and Zitouni Azari. ANM analysis of a wrinkled elastic thin membrane. *Comptes Rendus - Mecanique*, 347(10):701–709, 2019. ISSN 16310721. doi: 10.1016/j.crme.2019.10.001.

[26] Munehiro Kon, Yoshiharu, Yoshida, Atsunori, Hoshi. An examination of introducting Japan's mitigation style into Mega-Float. *International workshop on very large floating structures*, 2:451 – 456, 1996.

[27] Toshimitsu Kondo, Kazou, Iai, Takeshi, Moriguti, Sigeiti, Marasaki. Tension field theory. *Memoirs of the unifying study of the basic problems in engineering sciences by means of geometry*, 1:61–85, 1954.

[28] Y. Kyozuka, S. Kato, and H. Nakagawa. A numerical study on environmental impact assessment of mega-float of Japan. *Marine Structures*, 14(1-2):147–161, 2001. ISSN 09518339. doi: 10.1016/s0951-8339(00)00039-3.

[29] Hiroyuki Kyozuka, Yusaky, Hasemi. An ecohydrodynamic model for environmental assessment of Mega-Float in a bay. pages 427 – 434, 1996.

[30] J. Leifer and W. K. Belvin. Prediction of wrinkle amplitudes in thin film membranes using finite element modeling. *Collection of Technical Papers - AIAA/ASME/ASCE/AHS/ASC Structures, Structural Dynamics and Materials Conference*, 7(April):5319–5324, 2003. ISSN 02734508. doi: 10.2514/6.2003-1983.

[31] Ming Li, Yangjun Luo, Hua Ping Wu, Kai Zhu, Yanzhuang Niu, Tengfei Zhao, Jian Xing, and Zhan Kang. A Prenecking Strategy Makes Stretched Membranes With Clamped Ends Wrinkle-Free. *Journal of Applied Mechanics, Transactions ASME*, 84(6), 2017. ISSN 15289036. doi: 10.1115/1.4036416.

[32] Ming Li, Yanzhuang Niu, Huaping Wu, Xiaopeng Zhang, Yangjun Luo, and Zhan Kang. Wrinkling and wrinkling-suppression in graphene membranes with frozen zone. *Thin Solid Films*, 638:345–353, 2017. ISSN 00406090. doi: 10.1016/j.tsf.2017.08.009. URL http://dx.doi.org/10.1016/j.tsf.2017.08.009.

[33] Qingdu Li and Timothy J. Healey. Stability boundaries for wrinkling in highly stretched elastic sheets. *Journal of the Mechanics and Physics of Solids*, 97:260–274, 2016. ISSN 00225096. doi: 10.1016/j.jmps.2015.12.001.

[34] Fei Liu, Fan Xu, and Chenbo Fu. Orientable wrinkles in stretched orthotropic films. *Extreme Mechanics Letters*, 33:100579, nov 2019. ISSN 2352-4316. doi: 10.1016/J.EML.2019.100579. URL https://www.sciencedirect.com/science/article/pii/S2352431619302470{#}fig1.

[35] Haohui Liu, Vijay Krishna, Jason Lun Leung, Thomas Reindl, and Lu Zhao. Field experience and performance analysis of floating PV technologies in the tropics. *Progress in Photovoltaics: Research and Applications*, 26(12):957–967, 2018. ISSN 1099159X. doi: 10.1002/pip.3039.

[36] Xinxiang Liu, Christopher H. Jenkins, and Willi W. Schur. Large deflection analysis of pneumatic envelopes using a penalty parameter modified material model. *Finite elements in analysis and design*, 37 (3):233–251, 2001. ISSN 0168874X. doi: 10.1016/S0168-874X(00)00040-8.

[37] Yangjun Luo, Jian Xing, Yanzhuang Niu, Ming Li, and Zhan Kang. Wrinkle-free design of thin membrane structures using stress-based topology optimization. *Journal of the Mechanics and Physics of Solids*, 102: 277–293, 2017. ISSN 00225096. doi: 10.1016/j.jmps.2017.02.003.

[38] Takeshi Maeda, Hisaalki, Horigome, Takashi, Hiruma. Development of Renewable Energy Park on Oceans. *International work*, 2:53–60, 1996.

[39] E.H. Mansfield. Load transfer via a wrinkled membrane. *Proceedings of the Royal Society of London. A. Mathematical and Physical Sciences*, 316(1525):269–289, 1970. ISSN 2053-9169. doi: 10.1098/rspa.1970.0079.

[40] Martin M Mikulas. Behavior of a Flat Stretched Membrane Wrinkled by the Rotation of an Attached Hub. *Nasa technical note*, (September), 1964.

[41] Tomoshi Miyamura. Wrinkling on stretched circular membrane under in-plane torsion: Bifurcation analyses and experiments. *Engineering Structures*, 22(11):1407–1425, 2000. ISSN 01410296. doi: 10.1016/S0141-0296(99)00101-7.

[42] L Mule' Stagno. Floating Photovoltaics - Technological Issues, Cost and Practical Implications. *SUSTAINABLE ENERGY 2014: THE ISE ANNUAL CONFERENCE*, (March), 2014. URL http://www.windpowerengineering.com/design/mechanical/u.

[43] Kazuo Murakami. Study on environmental impacts assessment of huge floating structure. *International workshop on very large floating structures*, 2:435 – 442, 1996.

[44] Vishal Nayyar, K. Ravi-Chandar, and Rui Huang. Stretch-induced stress patterns and wrinkles in hyperelastic thin sheets. *International Journal of Solids and Structures*, 48(25-26): 3471–3483, dec 2011. ISSN 0020-7683. doi: 10.1016/J.IJSOLSTR.2011.09.004. URL https://www.sciencedirect.com/science/article/pii/S0020768311003040{#}f0005https://www.sciencedirect.com/science/article/pii/S0020768311003040.

[45] NOS. Drijvend zonnepark Nij Beets losgeraakt door noodweer, 2020. URL https://nos.nl/artikel/2344923-drijvend-zonnepark-nij-beets-losgeraakt-door-noodweer.html.

[46] Ocean Sun AS. Ocean Sun, 2020. URL https://oceansun.no/.

[47] Oceans of Energy. Oceans of Energy installeert eerste drijvende zonnefarm-systeem op zee ter wereld, 2019. URL https://oceansofenergy.blue/2019/12/10/nederland-heeft-wereldprimeur-met-eerste-offshore-zonnefarm-systeem/.

[48] Oceans of Energy. Oceans of Energy verdubbelt aantal zonnepanelen van drijvend zonnepark op Noordzee, 2020. URL https://oceansofenergy.blue/2020/01/29/oceans-of-energy-verdubbelt-aantal-zonnepanelen-van-drijvend-zonnepark-op-noordzee-29-01-202

[49] C. Miehe P. Wriggers, W. Wagner. A quadratically convergent procedure for the calculation of stability points in finite element analysis. *Computer methods in applied mechanics and engineering*, (70), 1988.

[50] Andreea Panaitescu, Meng Xin, Benny Davidovitch, Julien Chopin, and Arshad Kudrolli. Birth and decay of tensional wrinkles in hyperelastic sheets. jun 2019. URL http://arxiv.org/abs/1906.10054.

[51] Bruce D. Patterson, Frode Mo, Andreas Borgschulte, Magne Hillestad, Fortunat Joos, Trygve Kristiansen, Svein Sunde, and Jeroen A. van Bokhoven. Renewable CO2 recycling and synthetic fuel production in a marine environment. *Proceedings of the National Academy of Sciences of the United States of America*, 116(25):12212–12219, 2019. ISSN 10916490. doi: 10.1073/pnas.1902335116.

[52] Luka Pocivavsek, Robert Dellsy, Andrew Kern, Sebastián Johnson, Binhua Lin, Ka Yee C. Lee, and Enrique Cerda. Stress and fold localization in thin elastic membranes. *Science*, 2008. ISSN 00368075. doi: 10.1126/science.1154069.

[53] Eric Puntel, Luca Deseri, and Eliot Fried. Wrinkling of a Stretched Thin Sheet. *Journal of Elasticity*, 105(1-2):137–170, nov 2011. ISSN 0374-3535. doi: 10.1007/s10659-010-9290-5. URL http://link.springer.com/10.1007/s10659-010-9290-5.

[54] P. Ray. Renewable energy and sustainability. *Clean Technologies and Environmental Policy*, 21(8):1517–1533, 2019. ISSN 16189558. doi: 10.1007/s10098-019-01739-4.

[55] Marco Rivetti and Sébastien Neukirch. The mode branching route to localization of the finite-length floating elastica. *Journal of the Mechanics and Physics of Solids*, 69:143–155, sep 2014. ISSN 0022-5096. doi: 10.1016/J.JMPS.2014.05.004. URL https://www.sciencedirect.com/science/article/pii/S0022509614000878.

[56] Dennis G. Roddeman. Finite-element analysis of wrinkling membranes. *Communications in Applied Numerical Methods*, 7(4):299–307, 1991. ISSN 07488025. doi: 10.1002/cnm.1630070408.

[57] Wilfried van Sark S. Zahra Golroodbari. Simulation of performance differences between offshore and land-based photovoltaic systems. *Progress in Photovoltaics: Research and Applications*, 28(9):873–886, 2020. doi: 10.1002/pip.3276.

[58] K Sahu, Alok, Yadav, Neha, Sudhakar. Floating photovoltaic power plant: a review. *Renewable and sustainable energy reviews*, 66:815 – 824, 2016.

[59] Nuno Silvestre. Wrinkling of stretched thin sheets: Is restrained Poisson's effect the sole cause? *Engineering Structures*, 106:195–208, 2016. ISSN 18737323. doi: 10.1016/j.engstruct.2015.09.035. URL http://dx.doi.org/10.1016/j.engstruct.2015.09.035.

[60] András A. Sipos and Eszter Fehér. Disappearance of stretch-induced wrinkles of thin sheets: A study of orthotropic films. *International Journal of Solids and Structures*, 97-98:275–283, oct 2016. ISSN 0020-7683. doi: 10.1016/J.IJSOLSTR.2016.07.021. URL https://www-sciencedirect-com.tudelft.idm.oclc.org/science/article/pii/S0020768316301834.

[61] David J. Steigmann. Two-dimensional models for the combined bending and stretching of plates and shells based on three-dimensional linear elasticity. *International Journal of Engineering Science*, 46(7):654–676, 2008. ISSN 00207225. doi: 10.1016/j.ijengsci.2008.01.015.

[62] Stuart D. Brewer. Forum: DNV unveils its SUNdy floating solar field concept, 2012.

[63] Akio Takata, Jun, Isozaki, Soichiro, Hikai. An experimental research on environmental assessment of mega-float - current pattern & ecological system. *International workshop on very large floating structures*, 2:419–426, 1996.

[64] Alexander Tessler, David W. Sleight, and John T. Wang. Effective modeling and nonlinear shell analysis of thin membranes exhibiting structural wrinkling. *Journal of Spacecraft and Rockets*, 42(2):287–298, 2005. ISSN 00224650. doi: 10.2514/1.3915.

[65] Y. Tomita and A. Shindo. Onset and growth of wrinkles in thin square plates subjected to diagonal tension. *International Journal of Mechanical Sciences*, 30(12):921–931, 1988. ISSN 00207403. doi: 10.1016/0020-7403(88)90074-4.

[66] Migual Redon Trapani, Kim, Santafe. A review of floating photovoltaic installations: 2007-2013. *Progress in Photovoltaics: Research and Applications*, 23:524–532, 2015.

[67] Herbert Wagner. Flat sheet metal girders with very thin metal web Part I: General theories and assumptions. *National advisory committee for aeronautics*, (604), 1929.

[68] Herbert Wagner. Flat sheet metal girders with very thin metal web: Part II: Sheet metlab girders with sparce resistance to bending - oblique uprights - stiffness. *National advisory committee for aeronautics*, 1931.

[69] Herbert Wagner. Flat sheet metal girders with very thin metal web: Part III: Sheet metal firders with spars resistant to bending - the stress in uprights - diagonal tension fields. *National advisory committee for aeronautics*, 1931.

[70] C.G. Wang, H.F. Tan, X.W. Du, and Z.M. Wan. Wrinkling prediction of rectangular shell-membrane under transverse in-plane displacement. *International Journal of Solids and Structures*, 44(20):6507–6516, oct 2007. ISSN 0020-7683. doi: 10.1016/J.IJSOLSTR.2007.02.036. URL https://www.sciencedirect.com/science/article/pii/S0020768307001059{#}bib7.

[71] T. Wang, C. Fu, F. Xu, Y. Huo, and M. Potier-Ferry. On the wrinkling and restabilization of highly stretched sheets. *International Journal of Engineering Science*, 136:1–16, mar 2019. ISSN 0020-7225. doi: 10.1016/J.IJENGSCI.2018.12.002. URL https://www-sciencedirect-com.tudelft.idm.oclc.org/science/article/pii/S0020722518323085.

[72] Wesley Wong and Sergio Pellegrino. Wrinkled membranes I: experiments. *Journal of Mechanics of Materials and Structures*, 1(1):3–25, may 2006. ISSN 1559-3959. doi: 10.2140/jomms.2006.1.3. URL http://msp.org/jomms/2006/1-1/p02.xhtml.

[73] Wesley Wong and Sergio Pellegrino. Wrinkled membranes II: analytical models. *Journal of Mechanics of Materials and Structures*, 1(1):27–61, may 2006. ISSN 1559-3959. doi: 10.2140/jomms.2006.1.27. URL http://msp.org/jomms/2006/1-1/p03.xhtml.

[74] Wesley Wong and Sergio Pellegrino. Wrinkled membranes III: numerical simulations. *Journal of Mechanics of Materials and Structures*, 1(1):63–95, may 2006. ISSN 1559-3959. doi: 10.2140/jomms.2006.1.63. URL http://msp.org/jomms/2006/1-1/p04.xhtml.

[75] Y Wong, Sergio Pellegrino, and K Park. Prediction of winkle amplitudes in square solar sails. In *44th AIAA/ASME/ASCE/AHS/ASC Structures, Structural Dynamics, and Materials Conference*, page 1982, 2003.

[76] Y. W. Wong and S. Pellegrino. Amplitude of Wrinkles in Thin Membranes. pages 257–270. Springer, Dordrecht, 2002. doi: 10.1007/978-94-015-9930-6_21. URL http://link.springer.com/10.1007/978-94-015-9930-6{_}21.

[77] Y W Wong and Sergio Pellegrino. Computation of wrinkle amplitudes in thin membrane. In *43rd AIAA/ASME/ASCE/AHS/ASC Structures, Structural Dynamics, and Materials Conference*, page 1369, 2002.

[78] Dong Yan, Kai Zhang, Fujun Peng, and Gengkai Hu. Tailoring the wrinkle pattern of a microstructured membrane. *Applied Physics Letters*, 105(7):3–6, 2014. ISSN 00036951. doi: 10.1063/1.4893596.

[79] Dong Yan, Dongzhen Huangfu, Kai Zhang, and Gengkai Hu. Wrinkling of the membrane with square rigid elements. *EPL*, 116(2):1–7, 2016. ISSN 12864854. doi: 10.1209/0295-5075/116/24005.

[80] Li Yunliang, Tan Huifeng, Wang Changguo, and Lu Ming Yu. Membrane Buckling Patterns and Secondary Buckling Analysis. *International Journal of Space Structures*, 23(3):183–191, sep 2008. ISSN 0266-3511. doi: 10.1260/026635108786260965. URL http://journals.sagepub.com/doi/10.1260/026635108786260965.

[81] Ling Zheng. Wrinkling of Dielectric Elastomer Membranes. Technical report, 2009. URL https://search.proquest.com/openview/860d207036c60bc329678880067b71ad/1?cbl=18750{&}diss=y{&}pq-origsite=gscholarhttps://thesis.library.caltech.edu/3701/.